Fourth ESoA Course on

Compressive Sensing in Electromagnetics

Trento, Italy

October 23-27, 2023

NDE/NDT Methodologies and Applications

Mats Gustafsson

Department of Electrical and Information Technology, Lund University, Sweden

Day 3: Inverse Problems and Imaging with CS

October 25th, 2023

Outline

Non-destructive testing and inverse source problems

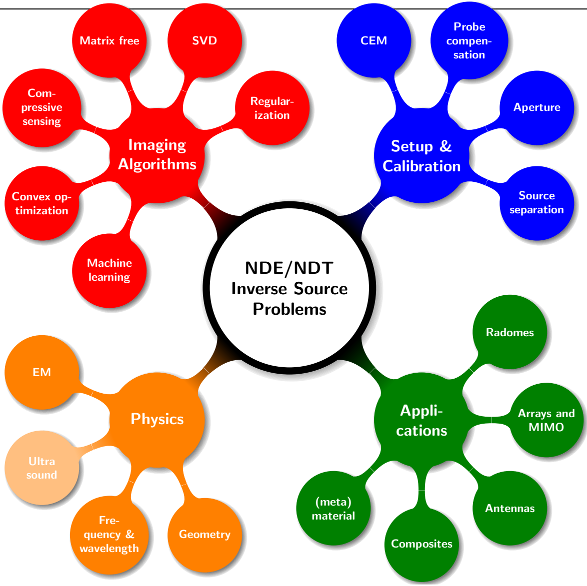

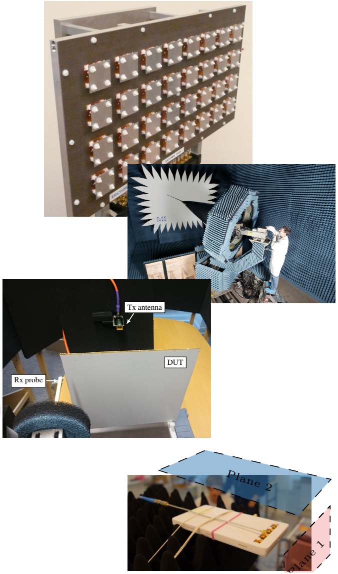

- Use physics that is sensitive to the desired properties or parameters
- Insensitive to environmental disturbances
- EM fields are sensitive to EM properties
- Sometimes but not always sensitive to mechanical properties, *e.g.*, strain can effect resistance but cracks can be hard to detect
- Ultrasound is often used
- Important to use the correct field and frequency range
- Geometrical setup to increase sensitivity and reduce errors

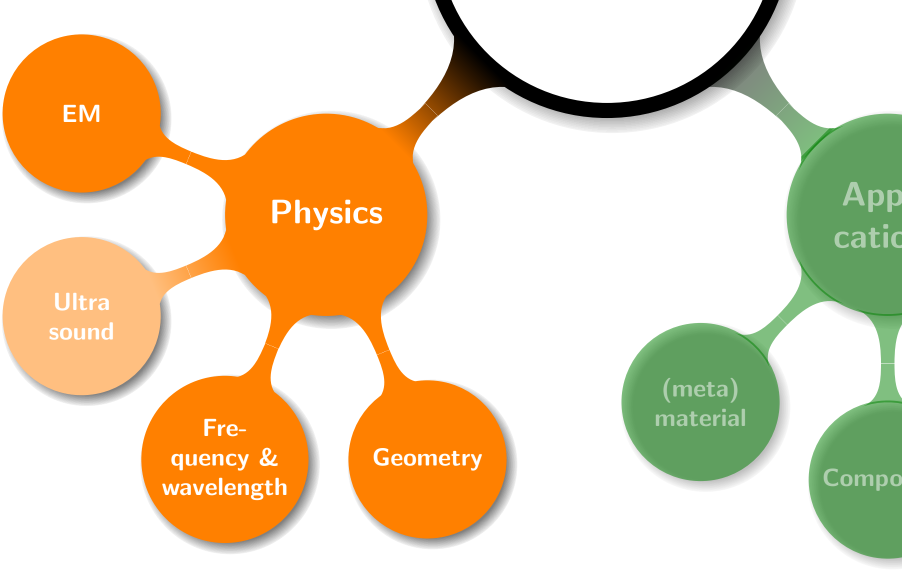

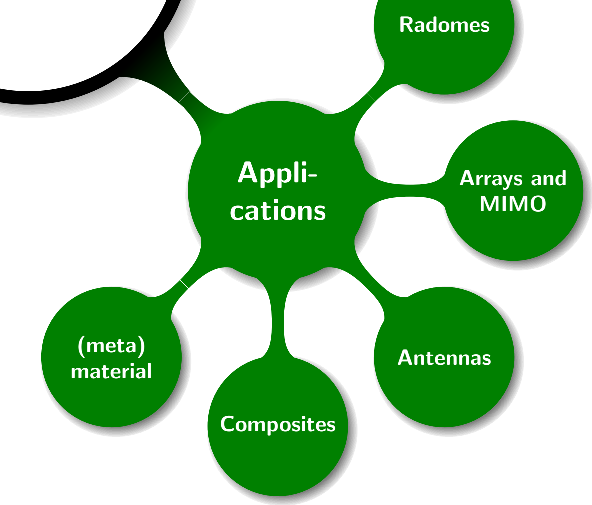

- Production testing of material or manufacturing errors
- Malfunctioning array elements
- Detect errors and localize them spatially, *e.g.*, faulty array element
- Undesired radiation and scattering from cables and support structures
- Complyings testing of power levels and EMF

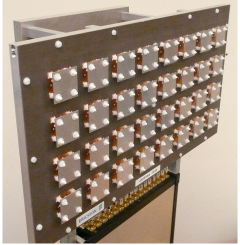

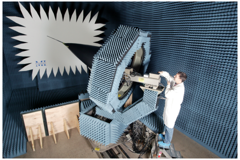

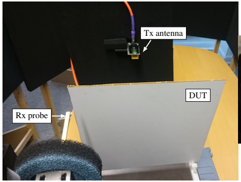

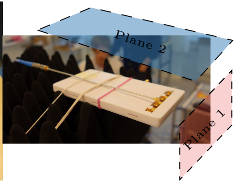

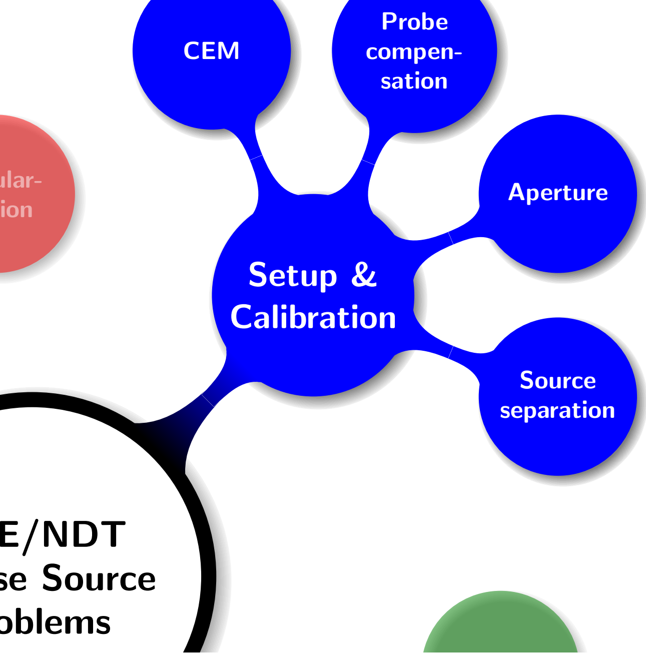

- Use a setup that is sensitive to desired properties and insensitive to other defects
- Calibration to reduce errors
- Probe calibration to compensate for probe pattern, *i.e.*, to transform measured (voltage) signals to EM field values at some point
- Combine with CEM for calibration of setup and numerical code
- Examples with aperture and source separation
- Aperture to position DUT and calibrate CEM with setup
- Source separation to remove illumination from knowledge of its physical location

- Inverse source problems are linear but illposed, *i.e.*, small measurement errors and cause large errors
- Need regularization to stabilize the inversion, *i.e.*, to reduce deteriorating effects from unresolved components
- Incorporate prior information (knowledge, assumption) *e.g.*, smoothness or number of defects
- Matrix free formulation for computational efficiency
- Computational efficiency vs generality vs robustness

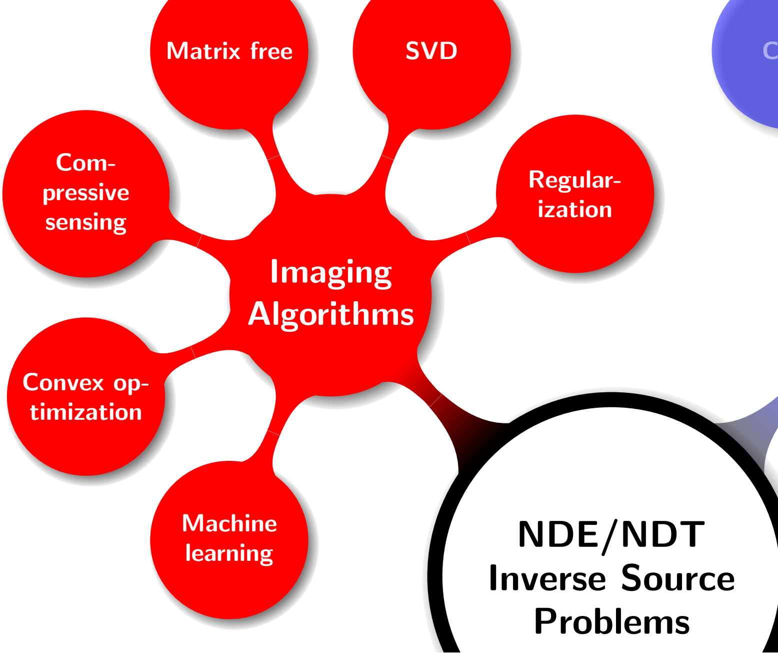

Non-destructive testing and inverse source problems

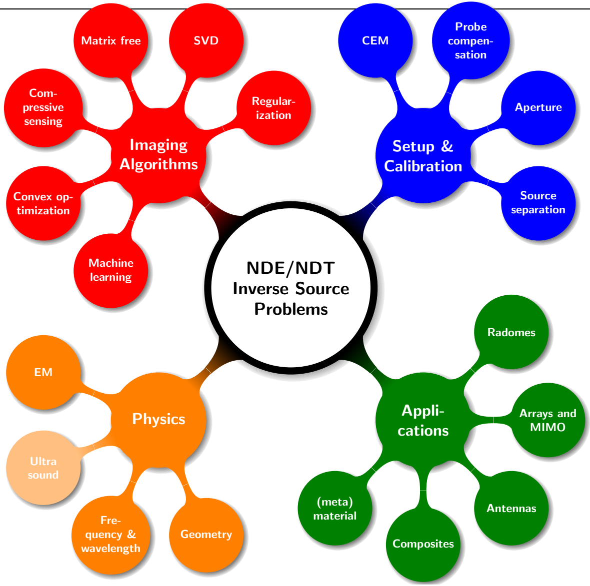

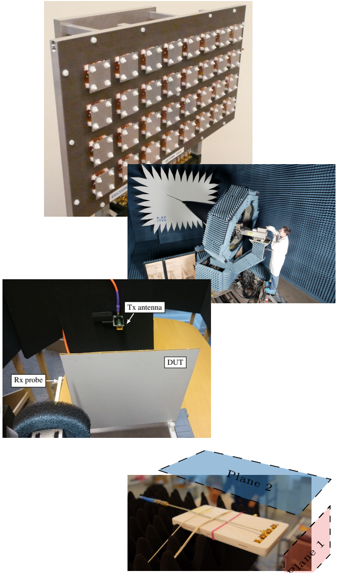

Non-Destructive Testing and near-field imaging

Non-destructive testing (NDT):
The science and practice of evaluating various properties of a DUT without compromising its utility and usefulness

Non-Destructive Testing and near-field imaging

Non-destructive testing (NDT):
The science and practice of evaluating various properties of a DUT without compromising its utility and usefulness

Used to evaluate materials and components:

- Save money and time in product evaluation and troubleshooting
- Ultrasonic testing, radiographic testing, and laser testing, microwave and millimeter wave imaging, *etc.*

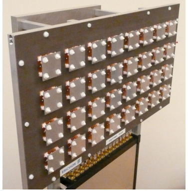

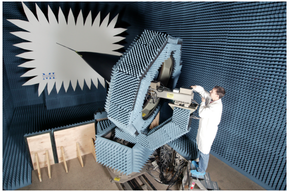

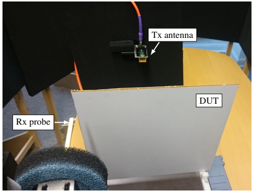

Abou-Khousa et al., "Comparison of X-Ray, Millimeter Wave, Shearography and Through-Transmission Ultrasonic Methods for Inspection of Honeycomb Composites", 2007; Ahmed et al., "Advanced Microwave imaging", 2012; Blitz, *Electrical and Magnetic Methods of Non-Destructive*

Antennas

- Antennas radiate (or receive) electromagnetic waves.
- Usually characterized by the impedance (S-parameters) and radiation pattern (gain, realized gain, cross polarization,...).
- Defects (*e.g.*, malfunctioning elements) affect these parameters in a complex way.
- Near field and/or equivalent currents can localize defects.
- EMF exposure level from near-field measurements.

Radomes

- A radome encloses an antenna to protect it from, *e.g.*, environmental influences
- Airplane and car radar system
- Ideally electrically transparent. FSS for frequency filters
- Often reduces gain and increases side-lobe levels
- Flash (image) lobes from reflections of the radome wall.

Composite panels

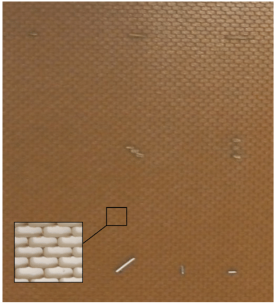

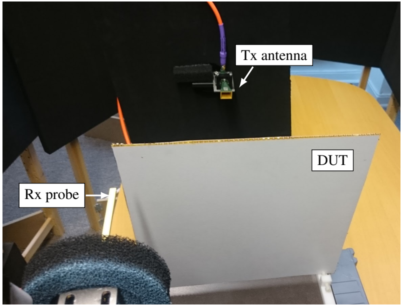

- Aircraft structural components are often composite-based
- Multilayer structure with low and high permittivity materials
- Distinguish between regions with varying resistivities (inhomogeneities, delaminations, dielectric inclusions)

Outline

Localization of defects

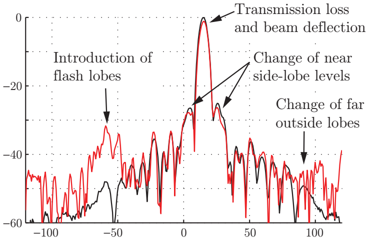

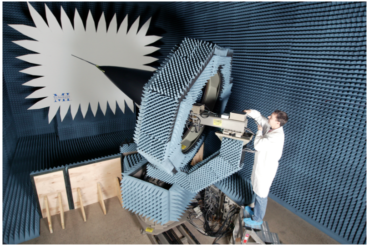

- Defects in antennas (in elements, feed structure) and radomes affect the impedance and radiated field in a complex manner.
- The small localized defect can perturb the radiation pattern (for all angles). Can be difficult to correlate with the location of the defect.
- Near field and/or equivalent currents can localize defects.

Inverse source problems

Inverse problem

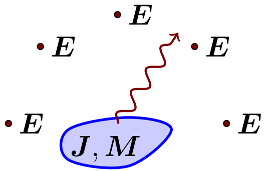

Inverse source problem. Determine the sources $(\boldsymbol{J}, \boldsymbol{M})$ in a region from observation of the field $\boldsymbol{E}$ in some points.

Inverse source problems

Inverse problem

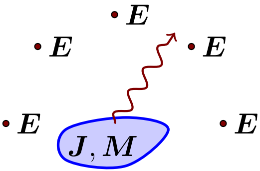

Inverse source problem. Determine the sources $(\boldsymbol{J}, \boldsymbol{M})$ in a region from observation of the field $\boldsymbol{E}$ in some points.

Back propagation

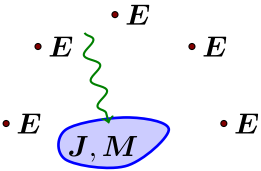

Use the data as sources and retransmit the field (time reversal or phase conjugation). Robust classical approach.

Inverse source problems

Inverse problem

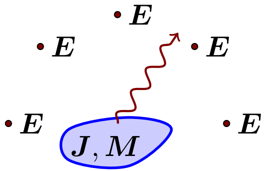

Inverse source problem. Determine the sources $(\boldsymbol{J}, \boldsymbol{M})$ in a region from observation of the field $\boldsymbol{E}$ in some points.

Back propagation

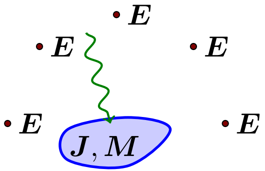

Use the data as sources and retransmit the field (time reversal or phase conjugation). Robust classical approach.

Inversion

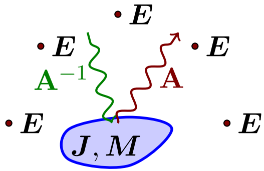

Find the source distribution from the linear system

$$\mathbf{A}\mathbf{x} = \mathbf{b}$$

with

- $\mathbf{x}$ as $\boldsymbol{J}, \boldsymbol{M}$
- $\mathbf{b}$ as $\boldsymbol{E}, \boldsymbol{H}$

Inverse source problems

Inverse problem

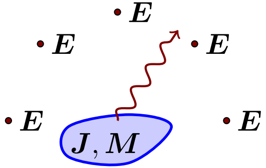

Inverse source problem. Determine the sources $(\boldsymbol{J}, \boldsymbol{M})$ in a region from observation of the field $\boldsymbol{E}$ in some points.

Back propagation

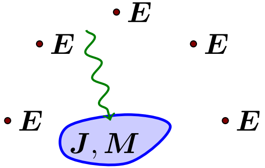

Use the data as sources and retransmit the field (time reversal or phase conjugation). Robust classical approach.

Inversion

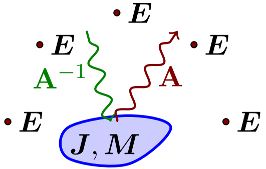

Find the source distribution from the linear system

$$\mathbf{A}\mathbf{x} = \mathbf{b}$$

with

- $\mathbf{x}$ as $\boldsymbol{J}, \boldsymbol{M}$
- $\mathbf{b}$ as $\boldsymbol{E}, \boldsymbol{H}$

- Inverse source problems are linear inverse problems
- Inverse scattering problems (*e.g.*, to determine material parameters) are non-linear inverse problems
- Both types of inverse problems are difficult in their own way

Inverse source problems

Determine the current distribution from measurements of the radiated field

Volume currents

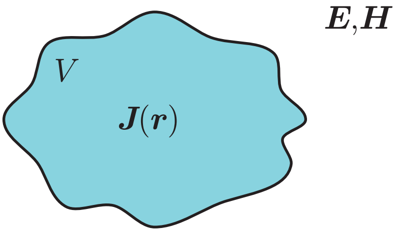

- Electric current density $\boldsymbol{J}(\boldsymbol{r})$ in the volume V. (Also magnetic currents.)
- Non-unique.
- Non-radiating currents.
- Ill-posed.

Inverse source problems

Determine the current distribution from measurements of the radiated field

Volume currents

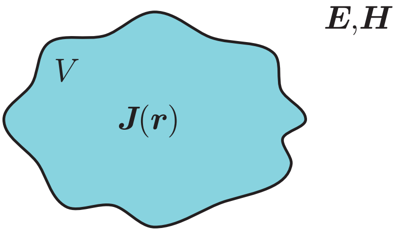

- Electric current density $\boldsymbol{J}(\boldsymbol{r})$ in the volume V. (Also magnetic currents.)
- Non-unique.
- Non-radiating currents.
- Ill-posed.

Equivalent surface currents

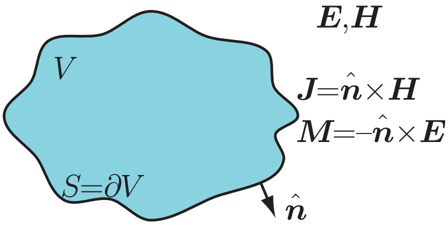

- Equivalent electric and magnetic surface current densities $\boldsymbol{J}, \boldsymbol{M}$ on the surface $S = \partial V$.
- Non-unique.
- Equivalence principle.
- Ill-posed.

Inverse source problem: far-field data

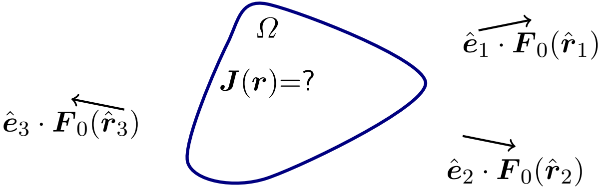

Consider for simplicity an example with

- Far-field $\hat{\boldsymbol{e}}_m \cdot \boldsymbol{F}_0(\hat{\boldsymbol{r}}_m)$, $m = 1, \dots, M$ data in directions $\hat{\boldsymbol{r}}_m$ and polarizations $\hat{\boldsymbol{e}}_m$

Inverse source problem: far-field data

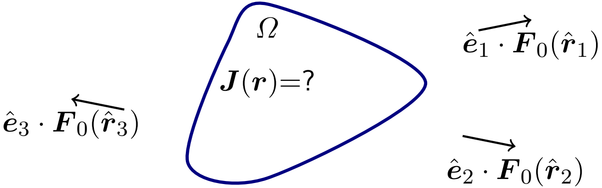

Consider for simplicity an example with

- Far-field $\hat{\boldsymbol{e}}_m \cdot \boldsymbol{F}_0(\hat{\boldsymbol{r}}_m)$, $m = 1, \dots, M$ data in directions $\hat{\boldsymbol{r}}_m$ and polarizations $\hat{\boldsymbol{e}}_m$
- Electric current density $\boldsymbol{J}(\boldsymbol{r}) = \sum_{n=1}^{N} I_n \boldsymbol{\psi}_n(\boldsymbol{r})$ in basis functions $\boldsymbol{\psi}_n(\boldsymbol{r})$

Inverse source problem: far-field data

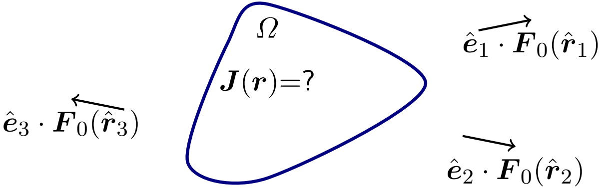

Consider for simplicity an example with

- Far-field $\hat{\boldsymbol{e}}_m \cdot \boldsymbol{F}_0(\hat{\boldsymbol{r}}_m)$, $m = 1, \dots, M$ data in directions $\hat{\boldsymbol{r}}_m$ and polarizations $\hat{\boldsymbol{e}}_m$
- Electric current density $\boldsymbol{J}(\boldsymbol{r}) = \sum_{n=1}^{N} I_n \boldsymbol{\psi}_n(\boldsymbol{r})$ in basis functions $\boldsymbol{\psi}_n(\boldsymbol{r})$
- Radiated far field

$$\hat{\boldsymbol{e}}_m \cdot \boldsymbol{F}_0(\hat{\boldsymbol{r}}_m) = \sum_{n=1}^{N} \left(\frac{-\mathrm{j}k\eta_0}{4\pi} \int_{\Omega} \mathrm{e}^{\mathrm{j}k\hat{\boldsymbol{r}}_m \cdot \boldsymbol{r}} \hat{\boldsymbol{e}}_m \cdot \boldsymbol{\psi}_n(\boldsymbol{r}) \, \mathrm{dV} \right) I_n \approx \sum_{n=1}^{N} F_{mn} I_n$$

Inverse source problem: far-field data

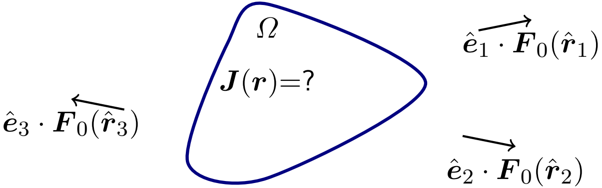

Consider for simplicity an example with

- Far-field $\hat{\boldsymbol{e}}_m \cdot \boldsymbol{F}_0(\hat{\boldsymbol{r}}_m)$, $m = 1, ..., M$ data in directions $\hat{\boldsymbol{r}}_m$ and polarizations $\hat{\boldsymbol{e}}_m$
- Electric current density $\boldsymbol{J}(\boldsymbol{r}) = \sum_{n=1}^{N} I_n \boldsymbol{\psi}_n(\boldsymbol{r})$ in basis functions $\boldsymbol{\psi}_n(\boldsymbol{r})$
- Radiated far field

$$\hat{\boldsymbol{e}}_m \cdot \boldsymbol{F}_0(\hat{\boldsymbol{r}}_m) = \sum_{n=1}^{N} \left(\frac{-\mathrm{j}k\eta_0}{4\pi} \int_{\Omega} \mathrm{e}^{\mathrm{j}k\hat{\boldsymbol{r}}_m \cdot \boldsymbol{r}} \hat{\boldsymbol{e}}_m \cdot \boldsymbol{\psi}_n(\boldsymbol{r}) \, \mathrm{dV} \right) I_n \approx \sum_{n=1}^{N} F_{mn} I_n$$

- In matrix notation $\mathbf{F}\mathbf{I} = \mathbf{F}_0$

Inverse source problem: far-field data

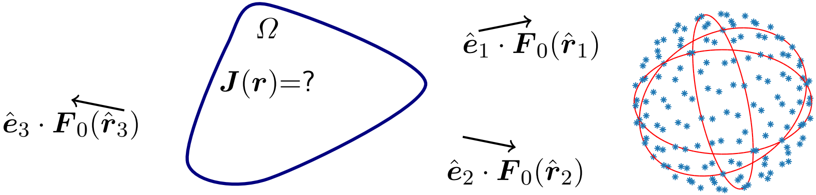

Consider for simplicity an example with

- Far-field $\hat{\boldsymbol{e}}_m \cdot \boldsymbol{F}_0(\hat{\boldsymbol{r}}_m)$, $m = 1, ..., M$ data in directions $\hat{\boldsymbol{r}}_m$ and polarizations $\hat{\boldsymbol{e}}_m$
- Electric current density $\boldsymbol{J}(\boldsymbol{r}) = \sum_{n=1}^{N} I_n \boldsymbol{\psi}_n(\boldsymbol{r})$ in basis functions $\boldsymbol{\psi}_n(\boldsymbol{r})$
- Radiated far field

$$\hat{\boldsymbol{e}}_m \cdot \boldsymbol{F}_0(\hat{\boldsymbol{r}}_m) = \sum_{n=1}^{N} \left(\frac{-\mathrm{j}k\eta_0}{4\pi} \int_{\Omega} \mathrm{e}^{\mathrm{j}k\hat{\boldsymbol{r}}_m\cdot\boldsymbol{r}} \hat{\boldsymbol{e}}_m \cdot \boldsymbol{\psi}_n(\boldsymbol{r}) \,\mathrm{dV} \right) I_n \approx \sum_{n=1}^{N} F_{mn} I_n$$

- In matrix notation $\mathbf{F}\mathbf{I} = \mathbf{F}_0$
- Lebedev points for uniform sampling over the sphere

Inverse source problem: far-field data

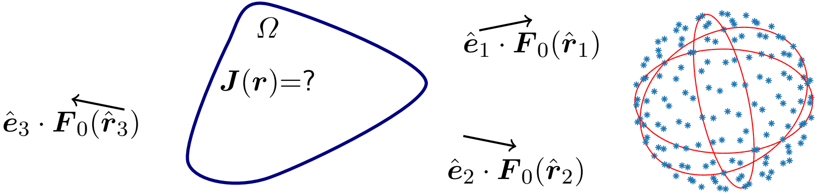

Consider for simplicity an example with

- Far-field $\hat{\boldsymbol{e}}_m \cdot \boldsymbol{F}_0(\hat{\boldsymbol{r}}_m)$, $m = 1, \dots, M$ data in directions $\hat{\boldsymbol{r}}_m$ and polarizations $\hat{\boldsymbol{e}}_m$
- Electric current density $\boldsymbol{J}(\boldsymbol{r}) = \sum_{n=1}^{N} I_n \boldsymbol{\psi}_n(\boldsymbol{r})$ in basis functions $\boldsymbol{\psi}_n(\boldsymbol{r})$
- Radiated far field

$$\hat{\boldsymbol{e}}_m \cdot \boldsymbol{F}_0(\hat{\boldsymbol{r}}_m) = \sum_{n=1}^{N} \left(\frac{-\mathrm{j}k\eta_0}{4\pi} \int_{\Omega} \mathrm{e}^{\mathrm{j}k\hat{\boldsymbol{r}}_m \cdot \boldsymbol{r}} \hat{\boldsymbol{e}}_m \cdot \boldsymbol{\psi}_n(\boldsymbol{r}) \, \mathrm{dV} \right) I_n \approx \sum_{n=1}^{N} F_{mn} I_n$$

- In matrix notation $\mathbf{F}\mathbf{I} = \mathbf{F}_0$
- Lebedev points for uniform sampling over the sphere
- Similar for near-field measurements but need probe calibration

Some background

Antenna/radome diagnostics are intimately tied to the development of measurement technology and can be characterized by the measurement geometry, computational method, and purpose. Inverse source problem with analysis of non-radiating currents and regularization.

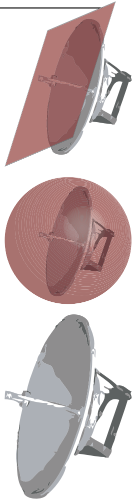

- **Measurement geometry:** near- and far-field, planar (rectangular, polar, bi-polar), cylindrical, and spherical.
- **Method:** field expansion (plane waves, cylindrical, spherical), back propagation (phase conjugation/time reversal, microwave holography), and inversion (integral representation).
- **Purpose:** diagnostics and/or near- to far-field transformation.

Some references:

- Barrett & Barnes, Automatic antenna wavefront plotter, 1952.
- Bleistein & Cohen, Nonuniqueness in the inverse source problem in acoustics and electromagnetics, 1977.
- Rahmat-Samii, Surface diagnosis of large reflector antennas using microwave holographic metrology, 1984.
- Yaghjian, An Overview of Near-Field Antenna Measurements, 1986.
- Hansen, Spherical near-field antenna measurements, 1988.
- Slater, Near-Field Antenna Measurements, 1991.
- Rahmat-Samii *etal*, The UCLA Bi-Polar Planar Near Field Antenna Measurement and Diagnostics Range, 1995.
- Sarkar & Taaghol, Near-field to near/far-field transformation for arbitrary near-field geometry, utilizing an equivalent magnetic current, 1996.
- Hansen, Discrete Inverse Problems: Insight and Algorithms, 2010.
- Devaney, Mathematical foundations of imaging, tomography and wavefield inversion, 2012.

Inverse source problems/diagnostics background

- Plane wave spectrum at least 1950 Barrett & Barnes, see also *e.g.*, Devany, Joy, Hansen, Yaghijian, Wang, Sarkar, Rahmat-Samii, ...
- Modal expansion (spherical, cylindrical) at least 70's, see *e.g.*, Devany, Hansen, Guler, Joy, Sten, Marengo, Ziyyat,Cappellin, Breinbjerg, Frandsen,...
- Integral representation (MoM)
  - 2001 Laurin *etal*: $\boldsymbol{M}$ *on planar structures for N2FF.*
  - 2005 Persson & Gustafsson: *BoR using the (Love) extinction theorem for radome applications.*
  - 2006 Las-Heras *etal*: $\boldsymbol{J}$ *and* $\boldsymbol{M}$ *on antennas without the extinction theorem*.
  - 2009 Eibert *etal*: *Fast multipole and higher order basis functions.*
  - 2009 Araque Quijano & Vecchi: *3D structures with Love extinction theorem.*
  - 2010 Jögensen *etal*: antenna diagnostics.
  - 2011 Araque Quijano *etal*: *post-processing to remove disturbances.*
  - 2011 *Commercial packages:* by TICRA and MVG.

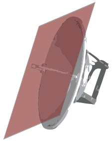

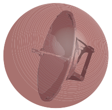

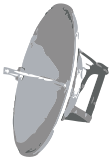

CEM part of the inversion algorithm (outline of the derivation) I

Compute a matrix that models the transformation from currents $(\boldsymbol{J}, \boldsymbol{M})$ to sampled fields $(\boldsymbol{E}, \boldsymbol{H})$, note follows from linearity.

CEM part of the inversion algorithm (outline of the derivation) I

Compute a matrix that models the transformation from currents $(\boldsymbol{J}, \boldsymbol{M})$ to sampled fields $(\boldsymbol{E}, \boldsymbol{H})$, note follows from linearity.

The electric fields at the position $\boldsymbol{r}$ from the electric surface current $\boldsymbol{J}$ on $S = \partial\Omega$ is

$$\boldsymbol{E}(\boldsymbol{r}) = -\mathcal{L}\left(\eta_0 \boldsymbol{J}\right)(\boldsymbol{r})$$

were (free space Green's function $G = \mathrm{e}^{-\mathrm{j}k|\boldsymbol{r}-\boldsymbol{r}'|}/(4\pi|\boldsymbol{r}-\boldsymbol{r}'|)$

$$\mathcal{L}(\boldsymbol{X})(\boldsymbol{r}) = \mathrm{j}k \int_S G(\boldsymbol{r}-\boldsymbol{r}')\boldsymbol{X}(\boldsymbol{r}') - \frac{1}{k^2}\,\nabla' G(\boldsymbol{r}-\boldsymbol{r}')\nabla'_{\mathrm{S}} \cdot \boldsymbol{X}(\boldsymbol{r}')\,\mathrm{dS}'$$

CEM part of the inversion algorithm (outline of the derivation) I

Compute a matrix that models the transformation from currents $(\boldsymbol{J}, \boldsymbol{M})$ to sampled fields $(\boldsymbol{E}, \boldsymbol{H})$, note follows from linearity.

The electric fields at the position $\boldsymbol{r}$ from the electric surface current $\boldsymbol{J}$ on $S = \partial\Omega$ is

$$\boldsymbol{E}(\boldsymbol{r}) = -\mathcal{L}\left(\eta_0 \boldsymbol{J}\right)(\boldsymbol{r})$$

were (free space Green's function $G = \mathrm{e}^{-\mathrm{j}k|\boldsymbol{r}-\boldsymbol{r}'|}/(4\pi|\boldsymbol{r}-\boldsymbol{r}'|)$)

$$\mathcal{L}(\boldsymbol{X})(\boldsymbol{r}) = \mathrm{j}k \int_S G(\boldsymbol{r}-\boldsymbol{r}')\boldsymbol{X}(\boldsymbol{r}') - \frac{1}{k^2}\,\nabla' G(\boldsymbol{r}-\boldsymbol{r}')\nabla'_{\mathrm{S}} \cdot \boldsymbol{X}(\boldsymbol{r}')\,\mathrm{dS}'$$

and from the magnetic surface current $\boldsymbol{M}$ we have

$$\boldsymbol{E}(\boldsymbol{r}) = \mathcal{K}\left(\boldsymbol{M}\right)(\boldsymbol{r})$$

where

$$\mathcal{K}(\boldsymbol{X})(\boldsymbol{r}) = \int_S \nabla' G(\boldsymbol{r}-\boldsymbol{r}') \times \boldsymbol{X}(\boldsymbol{r}')\,\mathrm{dS}'$$

CEM part of the inversion algorithm (outline of the derivation) I

Compute a matrix that models the transformation from currents $(\boldsymbol{J}, \boldsymbol{M})$ to sampled fields $(\boldsymbol{E}, \boldsymbol{H})$, note follows from linearity.

The electric fields at the position $\boldsymbol{r}$ from the electric surface current $\boldsymbol{J}$ on $S = \partial\Omega$ is

$$\boldsymbol{E}(\boldsymbol{r}) = -\mathcal{L}\left(\eta_0\boldsymbol{J}\right)(\boldsymbol{r})$$

were (free space Green's function $G = \mathrm{e}^{-\mathrm{j}k|\boldsymbol{r}-\boldsymbol{r}'|}/(4\pi|\boldsymbol{r}-\boldsymbol{r}'|)$

$$\mathcal{L}(\boldsymbol{X})(\boldsymbol{r}) = \mathrm{j}k\int_S G(\boldsymbol{r}-\boldsymbol{r}')\boldsymbol{X}(\boldsymbol{r}') - \frac{1}{k^2}\,\nabla' G(\boldsymbol{r}-\boldsymbol{r}')\nabla'_{\mathrm{S}}\cdot\boldsymbol{X}(\boldsymbol{r}')\,\mathrm{dS}'$$

and from the magnetic surface current $\boldsymbol{M}$ we have

$$\boldsymbol{E}(\boldsymbol{r}) = \mathcal{K}\left(\boldsymbol{M}\right)(\boldsymbol{r})$$

where

$$\mathcal{K}(\boldsymbol{X})(\boldsymbol{r}) = \int_S \nabla' G(\boldsymbol{r}-\boldsymbol{r}')\times\boldsymbol{X}(\boldsymbol{r}')\,\mathrm{dS}'$$

Well-known integral operators used in standard MoM codes.

CEM part of the inversion algorithm (outline of the derivation) II

Consider a measured electric field, $\boldsymbol{E}_{\text{meas}}(\boldsymbol{r}_n)$, in the points $\boldsymbol{r}_n$ and the polarization $\hat{\boldsymbol{e}}_n$, where $n = 1, ..., N$ and N is the number of measurement points.

CEM part of the inversion algorithm (outline of the derivation) II

Consider a measured electric field, $\boldsymbol{E}_{\mathrm{meas}}(\boldsymbol{r}_n)$, in the points $\boldsymbol{r}_n$ and the polarization $\hat{\boldsymbol{e}}_n$, where $n = 1, ..., N$ and N is the number of measurement points.

The integral representation relates the surface currents to the measured fields

$$\hat{\boldsymbol{e}}_n \cdot \Big(-\mathcal{L}\left(\eta_0 \boldsymbol{J}\right)(\boldsymbol{r}_n) + \mathcal{K}\left(\boldsymbol{M}\right)(\boldsymbol{r}_n) \Big) = \hat{\boldsymbol{e}}_n \cdot \boldsymbol{E}_{\mathrm{meas}}(\boldsymbol{r}_n)$$

for all points $n = 1, ..., N$.

CEM part of the inversion algorithm (outline of the derivation) II

Consider a measured electric field, $\boldsymbol{E}_{\mathrm{meas}}(\boldsymbol{r}_n)$, in the points $\boldsymbol{r}_n$ and the polarization $\hat{\boldsymbol{e}}_n$, where $n = 1, ..., N$ and N is the number of measurement points.

The integral representation relates the surface currents to the measured fields

$$\hat{\boldsymbol{e}}_n \cdot \Big(-\mathcal{L}\left(\eta_0 \boldsymbol{J}\right)(\boldsymbol{r}_n) + \mathcal{K}\left(\boldsymbol{M}\right)(\boldsymbol{r}_n) \Big) = \hat{\boldsymbol{e}}_n \cdot \boldsymbol{E}_{\mathrm{meas}}(\boldsymbol{r}_n)$$

for all points $n = 1, ..., N$.

We can now expand the surface currents $\boldsymbol{J}, \boldsymbol{M}$ in basis functions (as in MoM) to get a linear system which can be solved to estimate $\boldsymbol{J}, \boldsymbol{M}$.

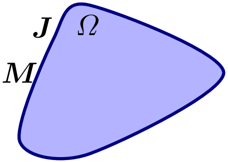

CEM part of the inversion algorithm (outline of the derivation) II

Consider a measured electric field, $\boldsymbol{E}_{\mathrm{meas}}(\boldsymbol{r}_n)$, in the points $\boldsymbol{r}_n$ and the polarization $\hat{\boldsymbol{e}}_n$, where $n = 1, ..., N$ and N is the number of measurement points.

The integral representation relates the surface currents to the measured fields

$$\hat{\boldsymbol{e}}_n \cdot \Big(-\mathcal{L}\left(\eta_0 \boldsymbol{J}\right)(\boldsymbol{r}_n) + \mathcal{K}\left(\boldsymbol{M}\right)(\boldsymbol{r}_n)\Big) = \hat{\boldsymbol{e}}_n \cdot \boldsymbol{E}_{\mathrm{meas}}(\boldsymbol{r}_n)$$

for all points $n = 1, ..., N$.

We can now expand the surface currents $\boldsymbol{J}, \boldsymbol{M}$ in basis functions (as in MoM) to get a linear system which can be solved to estimate $\boldsymbol{J}, \boldsymbol{M}$.

- We could also assume that $\boldsymbol{M} = \boldsymbol{0}$ and only solve for $\boldsymbol{J}$.

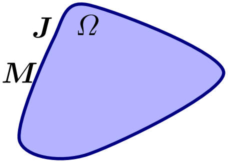

CEM part of the inversion algorithm (outline of the derivation) II

Consider a measured electric field, $\boldsymbol{E}_{\text{meas}}(\boldsymbol{r}_n)$, in the points $\boldsymbol{r}_n$ and the polarization $\hat{\boldsymbol{e}}_n$, where $n = 1, ..., N$ and N is the number of measurement points.

The integral representation relates the surface currents to the measured fields

$$\hat{\boldsymbol{e}}_n \cdot \Big(-\mathcal{L}\left(\eta_0 \boldsymbol{J}\right)(\boldsymbol{r}_n) + \mathcal{K}\left(\boldsymbol{M}\right)(\boldsymbol{r}_n)\Big) = \hat{\boldsymbol{e}}_n \cdot \boldsymbol{E}_{\text{meas}}(\boldsymbol{r}_n)$$

for all points $n = 1, ..., N$.

We can now expand the surface currents $\boldsymbol{J}, \boldsymbol{M}$ in basis functions (as in MoM) to get a linear system which can be solved to estimate $\boldsymbol{J}, \boldsymbol{M}$.

- We could also assume that $\boldsymbol{M} = \boldsymbol{0}$ and only solve for $\boldsymbol{J}$.
- Or any linear combination between $\boldsymbol{M}$ and $\boldsymbol{J}$.

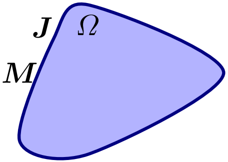

CEM part of the inversion algorithm (outline of the derivation) II

Consider a measured electric field, $\boldsymbol{E}_{\text{meas}}(\boldsymbol{r}_n)$, in the points $\boldsymbol{r}_n$ and the polarization $\hat{\boldsymbol{e}}_n$, where $n = 1, ..., N$ and N is the number of measurement points.

The integral representation relates the surface currents to the measured fields

$$\hat{\boldsymbol{e}}_n \cdot \Big(-\mathcal{L}\left(\eta_0 \boldsymbol{J}\right)(\boldsymbol{r}_n) + \mathcal{K}\left(\boldsymbol{M}\right)(\boldsymbol{r}_n) \Big) = \hat{\boldsymbol{e}}_n \cdot \boldsymbol{E}_{\text{meas}}(\boldsymbol{r}_n)$$

for all points $n = 1, ..., N$.

We can now expand the surface currents $\boldsymbol{J}, \boldsymbol{M}$ in basis functions (as in MoM) to get a linear system which can be solved to estimate $\boldsymbol{J}, \boldsymbol{M}$.

- We could also assume that $\boldsymbol{M} = \boldsymbol{0}$ and only solve for $\boldsymbol{J}$.
- Or any linear combination between $\boldsymbol{M}$ and $\boldsymbol{J}$.
- Can we do better?

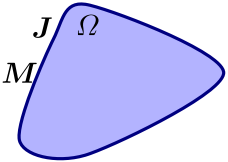

CEM part of the inversion algorithm (outline of the derivation) II

Consider a measured electric field, $\boldsymbol{E}_{\mathrm{meas}}(\boldsymbol{r}_n)$, in the points $\boldsymbol{r}_n$ and the polarization $\hat{\boldsymbol{e}}_n$, where $n = 1, \ldots, N$ and N is the number of measurement points.

The integral representation relates the surface currents to the measured fields

$$\hat{\boldsymbol{e}}_n \cdot \Big(-\mathcal{L}\left(\eta_0 \boldsymbol{J}\right)(\boldsymbol{r}_n) + \mathcal{K}\left(\boldsymbol{M}\right)(\boldsymbol{r}_n) \Big) = \hat{\boldsymbol{e}}_n \cdot \boldsymbol{E}_{\mathrm{meas}}(\boldsymbol{r}_n)$$

for all points $n = 1, \ldots, N$.

We can now expand the surface currents $\boldsymbol{J}, \boldsymbol{M}$ in basis functions (as in MoM) to get a linear system which can be solved to estimate $\boldsymbol{J}, \boldsymbol{M}$.

- We could also assume that $\boldsymbol{M} = \boldsymbol{0}$ and only solve for $\boldsymbol{J}$.
- Or any linear combination between $\boldsymbol{M}$ and $\boldsymbol{J}$.
- Can we do better?
- Radiating sources are inside Ω

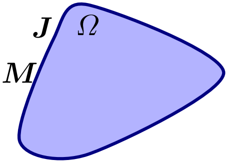

CEM part of the inversion algorithm (outline of the derivation) II

Consider a measured electric field, $\boldsymbol{E}_{\text{meas}}(\boldsymbol{r}_n)$, in the points $\boldsymbol{r}_n$ and the polarization $\hat{\boldsymbol{e}}_n$, where $n = 1, ..., N$ and N is the number of measurement points.

The integral representation relates the surface currents to the measured fields

$$\hat{\boldsymbol{e}}_n \cdot \Big(-\mathcal{L}\left(\eta_0 \boldsymbol{J}\right)(\boldsymbol{r}_n) + \mathcal{K}\left(\boldsymbol{M}\right)(\boldsymbol{r}_n)\Big) = \hat{\boldsymbol{e}}_n \cdot \boldsymbol{E}_{\text{meas}}(\boldsymbol{r}_n)$$

for all points $n = 1, ..., N$.

We can now expand the surface currents $\boldsymbol{J}, \boldsymbol{M}$ in basis functions (as in MoM) to get a linear system which can be solved to estimate $\boldsymbol{J}, \boldsymbol{M}$.

- We could also assume that $\boldsymbol{M} = \boldsymbol{0}$ and only solve for $\boldsymbol{J}$.
- Or any linear combination between $\boldsymbol{M}$ and $\boldsymbol{J}$.
- Can we do better?
- Radiating sources are inside Ω
- Equivalence theorem to relate $\boldsymbol{J}$ and $\boldsymbol{M}$

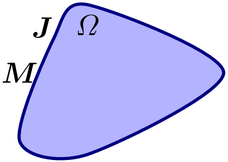

CEM part of the inversion algorithm (outline of the derivation) III

Assume a reconstruction surface S that surrounds the volume Ω and do not intersect $\partial\Omega$. This implies that the sources of the radiated field is inside of S.

CEM part of the inversion algorithm (outline of the derivation) III

Assume a reconstruction surface S that surrounds the volume Ω and do not intersect $\partial\Omega$. This implies that the sources of the radiated field is inside of S.

The electric $\boldsymbol{E}$ and magnetic $\boldsymbol{H}$ fields outside S can be represented with the equivalent currents $\boldsymbol{M} = -\hat{\boldsymbol{n}} \times \boldsymbol{E}$ and $\boldsymbol{J} = \hat{\boldsymbol{n}} \times \boldsymbol{H}$ on the surface $S = \partial\Omega$.

CEM part of the inversion algorithm (outline of the derivation) III

Assume a reconstruction surface S that surrounds the volume Ω and do not intersect $\partial\Omega$. This implies that the sources of the radiated field is inside of S.

The electric $\boldsymbol{E}$ and magnetic $\boldsymbol{H}$ fields outside S can be represented with the equivalent currents $\boldsymbol{M} = -\hat{\boldsymbol{n}} \times \boldsymbol{E}$ and $\boldsymbol{J} = \hat{\boldsymbol{n}} \times \boldsymbol{H}$ on the surface $S = \partial\Omega$.
Integral representation to relate the equivalent currents to the fields

$$-\mathcal{L}\left(\eta_0 \boldsymbol{J}\right)(\boldsymbol{r}) + \mathcal{K}\left(\boldsymbol{M}\right)(\boldsymbol{r}) = \begin{cases} \boldsymbol{E}(\boldsymbol{r}) & \boldsymbol{r} \text{ outside } S \\ \boldsymbol{0} & \boldsymbol{r} \text{ inside } S \end{cases}$$

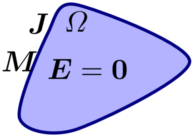

Also a corresponding representation for the magnetic field.

CEM part of the inversion algorithm (outline of the derivation) III

Assume a reconstruction surface S that surrounds the volume Ω and do not intersect $\partial\Omega$. This implies that the sources of the radiated field is inside of S.

The electric $\boldsymbol{E}$ and magnetic $\boldsymbol{H}$ fields outside S can be represented with the equivalent currents $\boldsymbol{M} = -\hat{\boldsymbol{n}} \times \boldsymbol{E}$ and $\boldsymbol{J} = \hat{\boldsymbol{n}} \times \boldsymbol{H}$ on the surface $S = \partial\Omega$.
Integral representation to relate the equivalent currents to the fields

$$-\mathcal{L}(\eta_0 \boldsymbol{J})(\boldsymbol{r}) + \mathcal{K}(\boldsymbol{M})(\boldsymbol{r}) = \begin{cases} \boldsymbol{E}(\boldsymbol{r}) & \boldsymbol{r} \text{ outside } S \\ \boldsymbol{0} & \boldsymbol{r} \text{ inside } S \end{cases}$$

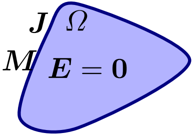

Also a corresponding representation for the magnetic field.

- first equation for the measured field.
- second equation to relate $\boldsymbol{J}$ and $\boldsymbol{M}$ at S.

Removes the ambiguity in $\boldsymbol{J}, \boldsymbol{M}$ and produces equivalent currents which correspond to the true $\boldsymbol{E}, \boldsymbol{H}$ fields outside S.

CEM part of the inversion algorithm (summary)

Integral equation EFIE (or MFIE, CFIE) on the reconstruction surface S with unit normal $\hat{\boldsymbol{n}}$

$$\hat{\boldsymbol{n}}(\boldsymbol{r}) \times \Big(\mathcal{L}\left(\eta_0 \boldsymbol{J}\right)(\boldsymbol{r}) - \mathcal{K}\left(\boldsymbol{M}\right)(\boldsymbol{r})\Big) = \frac{1}{2}\boldsymbol{M}(\boldsymbol{r}) \qquad \boldsymbol{r} \in S$$

and integral representation to relate equivalent currents to measured fields

$$\hat{\boldsymbol{e}}_n \cdot \Big(-\mathcal{L}\left(\eta_0 \boldsymbol{J}\right)(\boldsymbol{r}_n) + \mathcal{K}\left(\boldsymbol{M}\right)(\boldsymbol{r}_n)\Big) = \hat{\boldsymbol{e}}_n \cdot \boldsymbol{E}_{\mathrm{meas}}(\boldsymbol{r}_n)$$

for $n = 1, ..., N$ (number of measurement points), where (again)

$$\begin{cases} \mathcal{L}(\boldsymbol{X})(\boldsymbol{r}) = \mathrm{j}k \displaystyle\int_S G(\boldsymbol{r}', \boldsymbol{r})\boldsymbol{X}(\boldsymbol{r}') - \frac{1}{k^2}\,\nabla' G(\boldsymbol{r}', \boldsymbol{r})\nabla'_{\mathrm{S}} \cdot \boldsymbol{X}(\boldsymbol{r}')\,\mathrm{dS}' \\ \mathcal{K}(\boldsymbol{X})(\boldsymbol{r}) = \displaystyle\int_S \nabla' G(\boldsymbol{r}', \boldsymbol{r}) \times \boldsymbol{X}(\boldsymbol{r}')\,\mathrm{dS}' \end{cases}$$

Expand in basis functions to get a matrix equation $\mathbf{A}\mathbf{x} = \mathbf{b}$ (linearity).

Non-destructive testing and inverse source problems

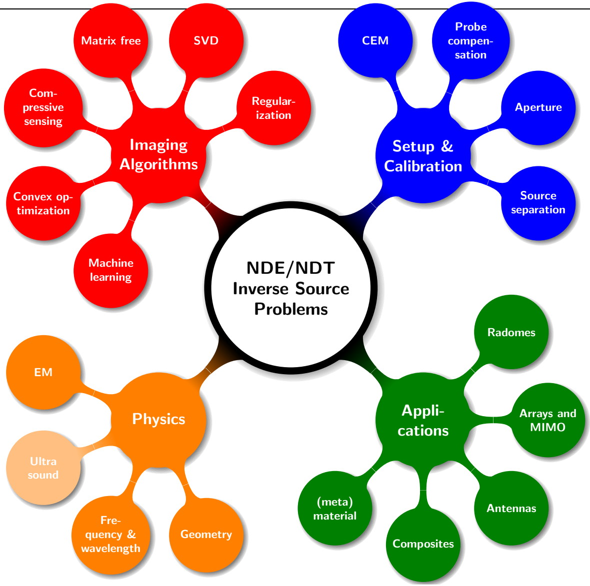

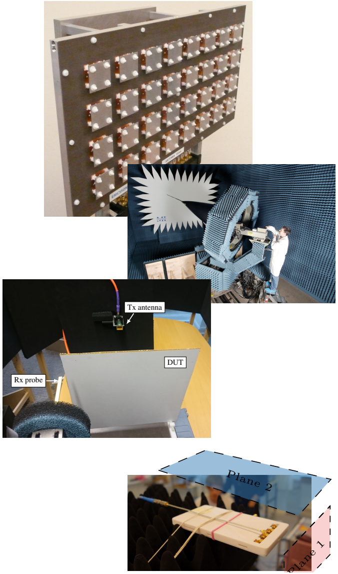

Radome diagnostics setup

Diagnostics to detect defects, *e.g.*, thickness variation in radome walls or FSS patterns

- Radomes are often planar to cover an aperture or curved to enclose a dish or an array

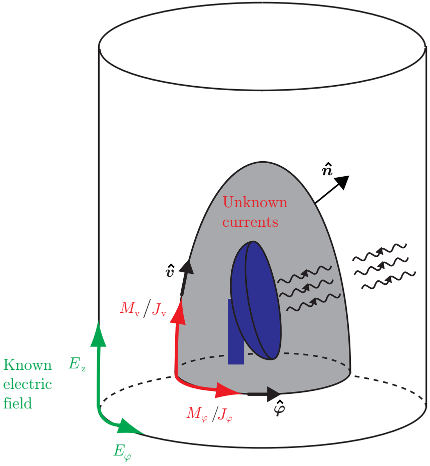

Radome diagnostics setup

Diagnostics to detect defects, *e.g.*, thickness variation in radome walls or FSS patterns

- Radomes are often planar to cover an aperture or curved to enclose a dish or an array
- NDT by measurements of radiated near/far field and comparison with desired field

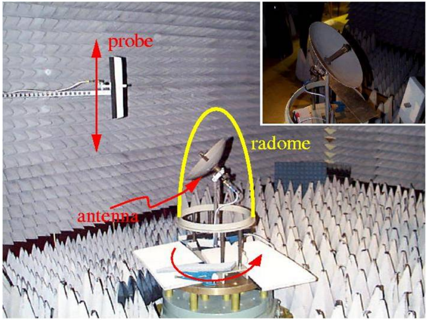

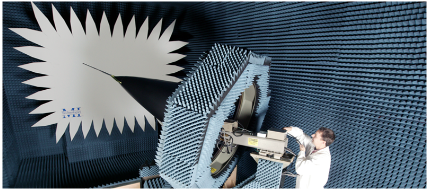

Radome diagnostics setup

Diagnostics to detect defects, *e.g.*, thickness variation in radome walls or FSS patterns

- Radomes are often planar to cover an aperture or curved to enclose a dish or an array
- NDT by measurements of radiated near/far field and comparison with desired field
- Reconstruction of fields (equivalent currents on radome surface) for localization of defects

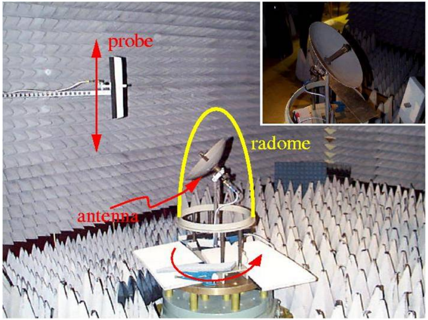

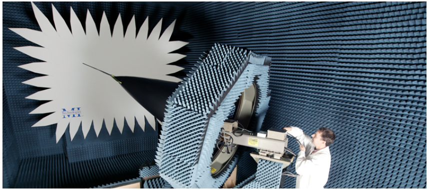

Radome diagnostics setup

Diagnostics to detect defects, *e.g.*, thickness variation in radome walls or FSS patterns

- Radomes are often planar to cover an aperture or curved to enclose a dish or an array
- NDT by measurements of radiated near/far field and comparison with desired field
- Reconstruction of fields (equivalent currents on radome surface) for localization of defects
- The electric field is measured (sampled) in a discrete set of points $\hat{e}_n \cdot \boldsymbol{E}_{\text{meas}}(\boldsymbol{r}_n)$

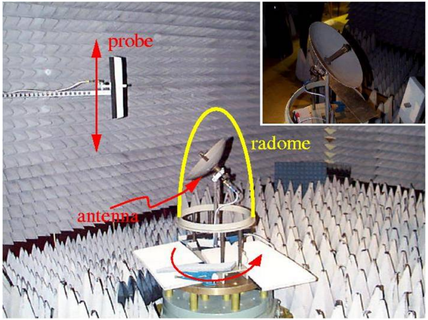

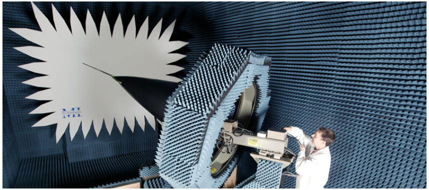

Radome diagnostics setup

Diagnostics to detect defects, *e.g.*, thickness variation in radome walls or FSS patterns

- Radomes are often planar to cover an aperture or curved to enclose a dish or an array
- NDT by measurements of radiated near/far field and comparison with desired field
- Reconstruction of fields (equivalent currents on radome surface) for localization of defects
- The electric field is measured (sampled) in a discrete set of points $\hat{\boldsymbol{e}}_n \cdot \boldsymbol{E}_{\mathrm{meas}}(\boldsymbol{r}_n)$
- Here, cylindrical near or spherical far-field

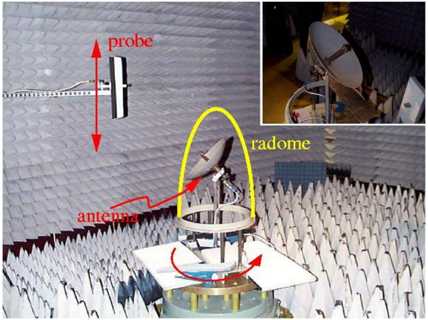

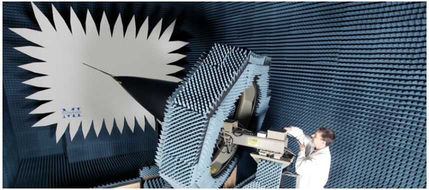

Radome diagnostics setup

Diagnostics to detect defects, *e.g.*, thickness variation in radome walls or FSS patterns

- Radomes are often planar to cover an aperture or curved to enclose a dish or an array
- NDT by measurements of radiated near/far field and comparison with desired field
- Reconstruction of fields (equivalent currents on radome surface) for localization of defects
- The electric field is measured (sampled) in a discrete set of points $\hat{\boldsymbol{e}}_n \cdot \boldsymbol{E}_{\mathrm{meas}}(\boldsymbol{r}_n)$
- Here, cylindrical near or spherical far-field
- Probe compensation is not needed for far-fields

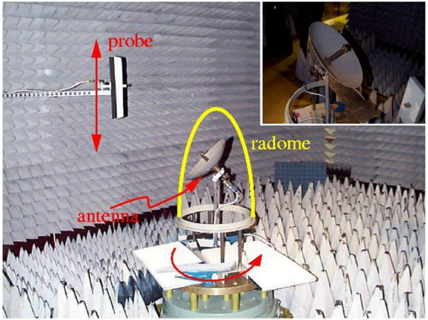

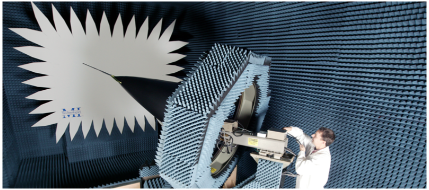

Radome diagnostics setup

Diagnostics to detect defects, *e.g.*, thickness variation in radome walls or FSS patterns

- Radomes are often planar to cover an aperture or curved to enclose a dish or an array
- NDT by measurements of radiated near/far field and comparison with desired field
- Reconstruction of fields (equivalent currents on radome surface) for localization of defects
- The electric field is measured (sampled) in a discrete set of points $\hat{\boldsymbol{e}}_n \cdot \boldsymbol{E}_{\text{meas}}(\boldsymbol{r}_n)$
- Here, cylindrical near or spherical far-field
- Probe compensation is not needed for far-fields
- Estimate the field (equivalent currents) on the radome surface

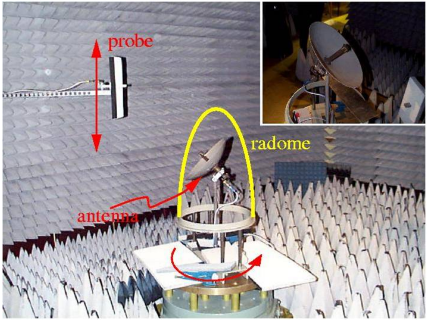

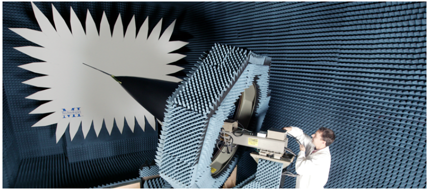

Imaging of dielectric tape on a radome

Radome

Amplitude

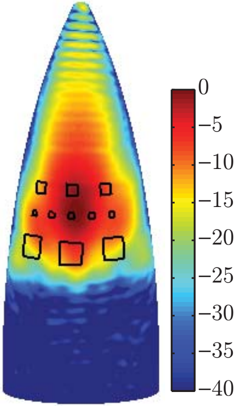

Phase

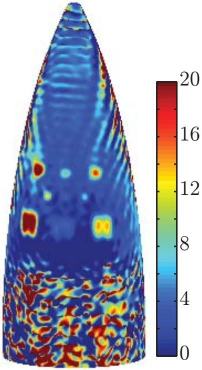

(Persson et al., "Radome diagnostics — source reconstruction of phase objects with an equivalent currents approach", 2014)

Imaging of dielectric tape on a radome

1 to 8 layers of tape

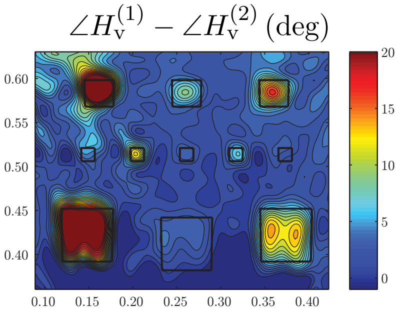

- Scotch Glass Cloth Electrical Tape 69-1 with thickness $\approx 0.15\,\mathrm{mm}$, $\epsilon_{\mathrm{r}} \approx 4.1$, and phase shift 1° to 2° (used to trim dielectric radomes).
- Squares with sides of $\{15, 30, 60\}\,\mathrm{mm}$. 1 to 8 layers.
- Measurements at $10\,\mathrm{GHz}$, $\lambda \approx 30\,\mathrm{mm}$.

Phase difference is sensitive to thin dielectric layers

FSS radome

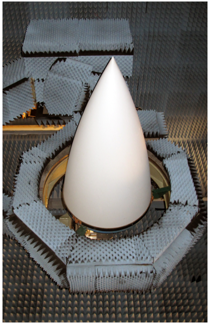

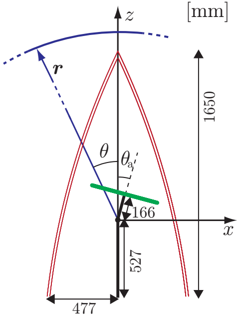

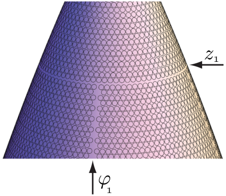

- Frequency selective radome with a passband around $9\,\mathrm{GHz}$
- Disturbances in the lattice due to the double curvature of the radome surface
- Here, line defects on a radome with height $1.65\,\mathrm{m} \approx 51\lambda$ at $9.35\,\mathrm{GHz}$
- Power flow to detect and image transmission errors

K. Persson et al. “Source reconstruction by far-field data for imaging of defects in frequency selective radomes”. *IEEE Antennas and Wireless*

FSS radome

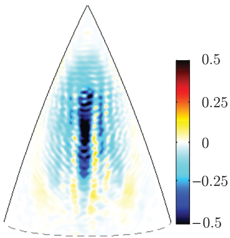

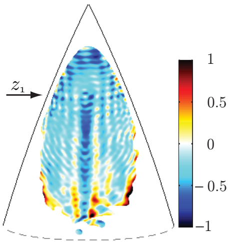

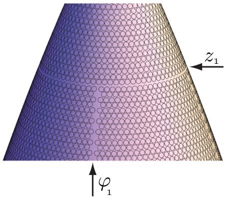

- Frequency selective radome with a passband around $9\,\mathrm{GHz}$
- Disturbances in the lattice due to the double curvature of the radome surface
- Here, line defects on a radome with height $1.65\,\mathrm{m} \approx 51\lambda$ at $9.35\,\mathrm{GHz}$
- Power flow to detect and image transmission errors

K. Persson et al. "Source reconstruction by far-field data for imaging of defects in frequency selective radomes". *IEEE Antennas and Wireless Propagation Letters* 12 (2013), pp. 480–483

Non-destructive testing and inverse source problems

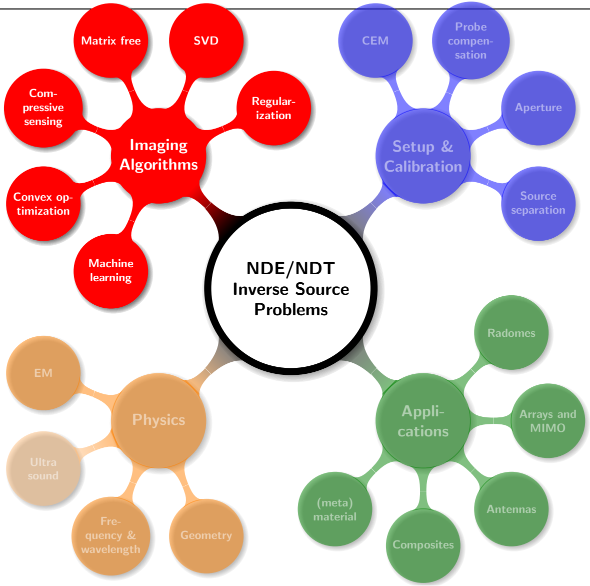

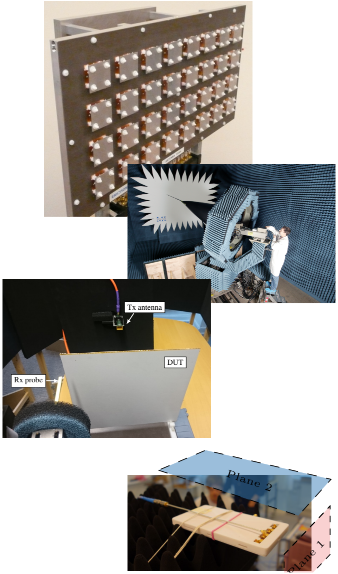

Inversion and regularization

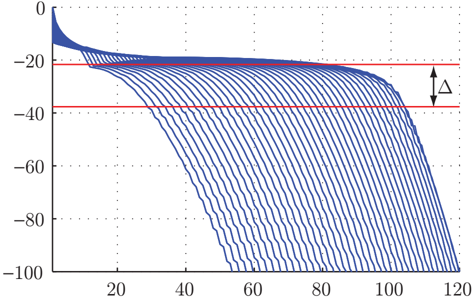

- The inverse source problem is ill-posed, *i.e.*, small errors in the data can produce large errors
- The approximate matrix equation is ill-conditioned
- Need regularization, *e.g.*, Tikhonov, SVD, randomized SVD, $\mathbf{L}^p$, …

We should not ask for more information than there exist in the data and prior information

Linear inverse problems

Would like to solve

$$\mathbf{A}\mathbf{x} = \mathbf{b}$$

with an $M \times N$ matrix $\mathbf{A}$. Simple to solve if $M = N$ and $\operatorname{cond}(\mathbf{A})$ not too large (compared with the errors and noise in $\mathbf{A}$ and $\mathbf{b}$).
Otherwise regularization:

- SVD: $\mathbf{A} = \mathbf{U}\boldsymbol{\Sigma}\mathbf{V}^{\mathsf{H}}$ with $\mathbf{U}^{\mathsf{H}}\mathbf{U} = \mathbf{1}$ and $\mathbf{V}^{\mathsf{H}}\mathbf{V} = \mathbf{1}$

S. P. Boyd and L. Vandenberghe. *Convex Optimization*. Cambridge Univ. Pr., 2004; P. C. Hansen. *Discrete inverse problems: insight and algorithms*. Vol. 7. Society for Industrial & Applied Mathematics, 2010; A. Massa, P. Rocca, and G. Oliveri. "Compressive Sensing in Electromagnetics-A Review". *IEEE Antennas Propag. Mag.* 57.1 (2015), pp. 224–238

Singular value decomposition (SVD)

$$\mathbf{A} = \mathbf{U}\boldsymbol{\Sigma}\mathbf{V}^{\mathsf{H}} \quad \text{with } \mathbf{U}^{\mathsf{H}}\mathbf{U} = \mathbf{1} \quad \text{and } \mathbf{V}^{\mathsf{H}}\mathbf{V} = \mathbf{1}$$

$\boldsymbol{\Sigma}$ is an $M \times N$ matrix with diagonal elements $\sigma_1, ..., \sigma_P$, where $P = \min\{M, N\}$

Singular value decomposition (SVD)

$$\mathbf{A} = \mathbf{U}\mathbf{\Sigma}\mathbf{V}^{\mathsf{H}} \quad \text{with } \mathbf{U}^{\mathsf{H}}\mathbf{U} = \mathbf{1} \quad \text{and } \mathbf{V}^{\mathsf{H}}\mathbf{V} = \mathbf{1}$$

$\mathbf{\Sigma}$ is an $M \times N$ matrix with diagonal elements $\sigma_1, ..., \sigma_P$, where $P = \min\{M, N\}$ to get

$$\mathbf{A}\mathbf{x} = \mathbf{U}\mathbf{\Sigma}\mathbf{V}^{\mathsf{H}}\mathbf{x} = \mathbf{b} \Rightarrow \mathbf{\Sigma}\mathbf{V}^{\mathsf{H}}\mathbf{x} = \mathbf{U}^{\mathsf{H}}\mathbf{b} \quad \text{or } \mathbf{\Sigma}\tilde{\mathbf{x}} = \tilde{\mathbf{b}}$$

Singular value decomposition (SVD)

$$\mathbf{A} = \mathbf{U}\boldsymbol{\Sigma}\mathbf{V}^{\mathsf{H}} \quad \text{with } \mathbf{U}^{\mathsf{H}}\mathbf{U} = \mathbf{1} \quad \text{and } \mathbf{V}^{\mathsf{H}}\mathbf{V} = \mathbf{1}$$

$\boldsymbol{\Sigma}$ is an $M \times N$ matrix with diagonal elements $\sigma_1, ..., \sigma_P$, where $P = \min\{M, N\}$ to get

$$\mathbf{A}\mathbf{x} = \mathbf{U}\boldsymbol{\Sigma}\mathbf{V}^{\mathsf{H}}\mathbf{x} = \mathbf{b} \Rightarrow \boldsymbol{\Sigma}\mathbf{V}^{\mathsf{H}}\mathbf{x} = \mathbf{U}^{\mathsf{H}}\mathbf{b} \quad \text{or } \boldsymbol{\Sigma}\tilde{\mathbf{x}} = \tilde{\mathbf{b}}$$

Have the solution

$$\tilde{\mathbf{x}} = \boldsymbol{\Sigma}^{-1}\tilde{\mathbf{b}} \quad \text{and } \mathbf{x} = \mathbf{V}\boldsymbol{\Sigma}^{-1}\mathbf{U}^{\mathsf{H}}\mathbf{b}$$

if $M = N$ and $\sigma_p > 0$ for $p = 1, ..., P$.

Singular value decomposition (SVD)

$$\mathbf{A} = \mathbf{U}\mathbf{\Sigma}\mathbf{V}^{\mathsf{H}} \quad \text{with } \mathbf{U}^{\mathsf{H}}\mathbf{U} = \mathbf{1} \quad \text{and } \mathbf{V}^{\mathsf{H}}\mathbf{V} = \mathbf{1}$$

$\mathbf{\Sigma}$ is an $M \times N$ matrix with diagonal elements $\sigma_1, ..., \sigma_P$, where $P = \min\{M, N\}$ to get

$$\mathbf{A}\mathbf{x} = \mathbf{U}\mathbf{\Sigma}\mathbf{V}^{\mathsf{H}}\mathbf{x} = \mathbf{b} \Rightarrow \mathbf{\Sigma}\mathbf{V}^{\mathsf{H}}\mathbf{x} = \mathbf{U}^{\mathsf{H}}\mathbf{b} \quad \text{or } \mathbf{\Sigma}\tilde{\mathbf{x}} = \tilde{\mathbf{b}}$$

Have the solution

$$\tilde{\mathbf{x}} = \mathbf{\Sigma}^{-1}\tilde{\mathbf{b}} \quad \text{and } \mathbf{x} = \mathbf{V}\mathbf{\Sigma}^{-1}\mathbf{U}^{\mathsf{H}}\mathbf{b}$$

if $M = N$ and $\sigma_p > 0$ for $p = 1, ..., P$. With additive noise

$$\tilde{\mathbf{x}} = \mathbf{\Sigma}^{-1}\tilde{\mathbf{b}} + \mathbf{\Sigma}^{-1}\tilde{\mathbf{n}}$$

so strong amplification if $\sigma_p < |\tilde{\mathbf{n}}|$. Set $\sigma_p^{-1} = 0$ if $\sigma_p < \epsilon$.

Singular value decomposition (SVD)

$$\mathbf{A} = \mathbf{U}\mathbf{\Sigma}\mathbf{V}^{\mathsf{H}} \quad \text{with } \mathbf{U}^{\mathsf{H}}\mathbf{U} = \mathbf{1} \quad \text{and } \mathbf{V}^{\mathsf{H}}\mathbf{V} = \mathbf{1}$$

$\mathbf{\Sigma}$ is an $M \times N$ matrix with diagonal elements $\sigma_1, ..., \sigma_P$, where $P = \min\{M, N\}$ to get

$$\mathbf{A}\mathbf{x} = \mathbf{U}\mathbf{\Sigma}\mathbf{V}^{\mathsf{H}}\mathbf{x} = \mathbf{b} \Rightarrow \mathbf{\Sigma}\mathbf{V}^{\mathsf{H}}\mathbf{x} = \mathbf{U}^{\mathsf{H}}\mathbf{b} \quad \text{or } \mathbf{\Sigma}\tilde{\mathbf{x}} = \tilde{\mathbf{b}}$$

Have the solution

$$\tilde{\mathbf{x}} = \mathbf{\Sigma}^{-1}\tilde{\mathbf{b}} \quad \text{and } \mathbf{x} = \mathbf{V}\mathbf{\Sigma}^{-1}\mathbf{U}^{\mathsf{H}}\mathbf{b}$$

if $M = N$ and $\sigma_p > 0$ for $p = 1, ..., P$. With additive noise

$$\tilde{\mathbf{x}} = \mathbf{\Sigma}^{-1}\tilde{\mathbf{b}} + \mathbf{\Sigma}^{-1}\tilde{\mathbf{n}}$$

so strong amplification if $\sigma_p < |\tilde{\mathbf{n}}|$. Set $\sigma_p^{-1} = 0$ if $\sigma_p < \epsilon$.

Classical robust solution similar to pseudoinverse and to the $\mathbf{L}^2$-solution.

Linear inverse problems

Would like to solve

$$\mathbf{Ax} = \mathbf{b}$$

with an $M \times N$ matrix $\mathbf{A}$. Simple to solve if $M = N$ and $\mathrm{cond}(\mathbf{A})$ not too large (compared with the errors and noise in $\mathbf{A}$ and $\mathbf{b}$).
Otherwise regularization:

- SVD: $\mathbf{A} = \mathbf{U\Sigma V}^{\mathsf{H}}$ with $\mathbf{U}^{\mathsf{H}}\mathbf{U} = \mathbf{1}$ and $\mathbf{V}^{\mathsf{H}}\mathbf{V} = \mathbf{1}$
- $\mathbf{L}^2$-minimization: $\|\mathbf{x}\|_2 = (\sum_{n=1}^{N} |x_n|^2)^{1/2}$ or with weight $\mathbf{x}^{\mathsf{H}}\mathbf{Wx}$

S. P. Boyd and L. Vandenberghe. *Convex Optimization*. Cambridge Univ. Pr., 2004; P. C. Hansen. *Discrete inverse problems: insight and algorithms*. Vol. 7. Society for Industrial & Applied Mathematics, 2010; A. Massa, P. Rocca, and G. Oliveri. "Compressive Sensing in Electromagnetics-A Review". *IEEE Antennas Propag. Mag.* 57.1 (2015), pp. 224–238

Linear inverse problems

Would like to solve

$$\mathbf{A}\mathbf{x} = \mathbf{b}$$

with an $M \times N$ matrix $\mathbf{A}$. Simple to solve if $M = N$ and cond$(\mathbf{A})$ not too large (compared with the errors and noise in $\mathbf{A}$ and $\mathbf{b}$).
Otherwise regularization:

- SVD: $\mathbf{A} = \mathbf{U}\mathbf{\Sigma}\mathbf{V}^{\mathsf{H}}$ with $\mathbf{U}^{\mathsf{H}}\mathbf{U} = \mathbf{1}$ and $\mathbf{V}^{\mathsf{H}}\mathbf{V} = \mathbf{1}$
- $\mathbf{L}^2$-minimization: $\|\mathbf{x}\|_2 = (\sum_{n=1}^{N} |x_n|^2)^{1/2}$ or with weight $\mathbf{x}^{\mathsf{H}}\mathbf{W}\mathbf{x}$
- $\mathbf{L}^1$-minimization: $\|\mathbf{x}\|_1 = \sum_{n=1}^{N} |x_n|$

S. P. Boyd and L. Vandenberghe. *Convex Optimization*. Cambridge Univ. Pr., 2004; P. C. Hansen. *Discrete inverse problems: insight and algorithms*. Vol. 7. Society for Industrial & Applied Mathematics, 2010; A. Massa, P. Rocca, and G. Oliveri. "Compressive Sensing in Electromagnetics-A Review". *IEEE Antennas Propag. Mag.* 57.1 (2015), pp. 224–238

Linear inverse problems

Would like to solve

$$\mathbf{Ax} = \mathbf{b}$$

with an $M \times N$ matrix $\mathbf{A}$. Simple to solve if $M = N$ and $\mathrm{cond}(\mathbf{A})$ not too large (compared with the errors and noise in $\mathbf{A}$ and $\mathbf{b}$).
Otherwise regularization:

- SVD: $\mathbf{A} = \mathbf{U\Sigma V}^{\mathsf{H}}$ with $\mathbf{U}^{\mathsf{H}}\mathbf{U} = \mathbf{1}$ and $\mathbf{V}^{\mathsf{H}}\mathbf{V} = \mathbf{1}$
- $\mathbf{L}^2$-minimization: $\|\mathbf{x}\|_2 = (\sum_{n=1}^{N} |x_n|^2)^{1/2}$ or with weight $\mathbf{x}^{\mathsf{H}}\mathbf{W}\mathbf{x}$
- $\mathbf{L}^1$-minimization: $\|\mathbf{x}\|_1 = \sum_{n=1}^{N} |x_n|$
- $\mathbf{L}^0$-minimization: the number of non-zero entries of $\mathbf{x}$. (not a norm)

S. P. Boyd and L. Vandenberghe. *Convex Optimization*. Cambridge Univ. Pr., 2004; P. C. Hansen. *Discrete inverse problems: insight and algorithms*. Vol. 7. Society for Industrial & Applied Mathematics, 2010; A. Massa, P. Rocca, and G. Oliveri. “Compressive Sensing in Electromagnetics-A Review”. *IEEE Antennas Propag. Mag.* 57.1 (2015), pp. 224–238

Linear inverse problems

Would like to solve

$$\mathbf{A}\mathbf{x} = \mathbf{b}$$

with an $M \times N$ matrix $\mathbf{A}$. Simple to solve if $M = N$ and $\mathrm{cond}(\mathbf{A})$ not too large (compared with the errors and noise in $\mathbf{A}$ and $\mathbf{b}$).
Otherwise regularization:

- SVD: $\mathbf{A} = \mathbf{U}\boldsymbol{\Sigma}\mathbf{V}^{\mathsf{H}}$ with $\mathbf{U}^{\mathsf{H}}\mathbf{U} = \mathbf{1}$ and $\mathbf{V}^{\mathsf{H}}\mathbf{V} = \mathbf{1}$
- $\mathbf{L}^2$-minimization: $\|\mathbf{x}\|_2 = (\sum_{n=1}^{N} |x_n|^2)^{1/2}$ or with weight $\mathbf{x}^{\mathsf{H}}\mathbf{W}\mathbf{x}$
- $\mathbf{L}^1$-minimization: $\|\mathbf{x}\|_1 = \sum_{n=1}^{N} |x_n|$
- $\mathbf{L}^0$-minimization: the number of non-zero entries of $\mathbf{x}$. (not a norm)
- Many choices of norms, weight functions, and (convex) optimization formulations

S. P. Boyd and L. Vandenberghe. *Convex Optimization*. Cambridge Univ. Pr., 2004; P. C. Hansen. *Discrete inverse problems: insight and algorithms*. Vol. 7. Society for Industrial & Applied Mathematics, 2010; A. Massa, P. Rocca, and G. Oliveri. “Compressive Sensing in Electromagnetics-A Review”. *IEEE Antennas Propag. Mag.* 57.1 (2015), pp. 224–238

Regularization

- $\mathbf{Ax} = \mathbf{b}$ with a matrix $\mathbf{A} \in \mathbb{C}^{M,N}$ having M rows (number of measurements) and N columns (number of basis functions) $\Rightarrow$ not invertible

Regularization

- $\mathbf{Ax} = \mathbf{b}$ with a matrix $\mathbf{A} \in \mathbb{C}^{M,N}$ having M rows (number of measurements) and N columns (number of basis functions) $\Rightarrow$ not invertible
- Not invertible and measurement noise $\Rightarrow$ optimization formulation

$$\underset{\mathbf{x}}{\text{minimize}}\ \|\mathbf{Ax} - \mathbf{b}\|_p.$$

Regularization

- $\mathbf{A}\mathbf{x} = \mathbf{b}$ with a matrix $\mathbf{A} \in \mathbb{C}^{M,N}$ having M rows (number of measurements) and N columns (number of basis functions) $\Rightarrow$ not invertible
- Not invertible and measurement noise $\Rightarrow$ optimization formulation

$$\underset{\mathbf{x}}{\text{minimize}} \; \|\mathbf{A}\mathbf{x} - \mathbf{b}\|_p.$$

- Often least-squares norm $p = 2$. Computational and analytic simplicity together with additive Gaussian noise (Kay, *Fundamentals of Statistical Signal Processing, Estimation Theory*, 1993; Tarantola, *Inverse problem theory and methods for model parameter estimation*, 2005)

Regularization

- $\mathbf{Ax} = \mathbf{b}$ with a matrix $\mathbf{A} \in \mathbb{C}^{M,N}$ having M rows (number of measurements) and N columns (number of basis functions) $\Rightarrow$ not invertible
- Not invertible and measurement noise $\Rightarrow$ optimization formulation

$$\underset{\mathbf{x}}{\text{minimize}}\ \|\mathbf{Ax} - \mathbf{b}\|_p.$$

- Often least-squares norm $p = 2$. Computational and analytic simplicity together with additive Gaussian noise (Kay, *Fundamentals of Statistical Signal Processing, Estimation Theory*, 1993; Tarantola, *Inverse problem theory and methods for model parameter estimation*, 2005)
- Regularization is necessary for solving (Hansen, *Discrete inverse problems: insight and algorithms*, 2010), *e.g.*, SVD or by reformulating it as (convex) optimization problems. Typically

$$\text{minimize}\ \|\mathbf{Ax} - \mathbf{b}\|_p^2 + \alpha\|\boldsymbol{\Upsilon}\mathbf{x}\|_q^2 \quad \text{or}$$

$$\text{minimize}\ \ \|\boldsymbol{\Upsilon}\mathbf{x}\|_q^2 \quad \text{subject to}\ \|\mathbf{Ax} - \mathbf{b}\|_p^2 \leq \delta,$$

where δ is related to the signal-to-noise ratio.

Non-destructive testing and inverse source problems

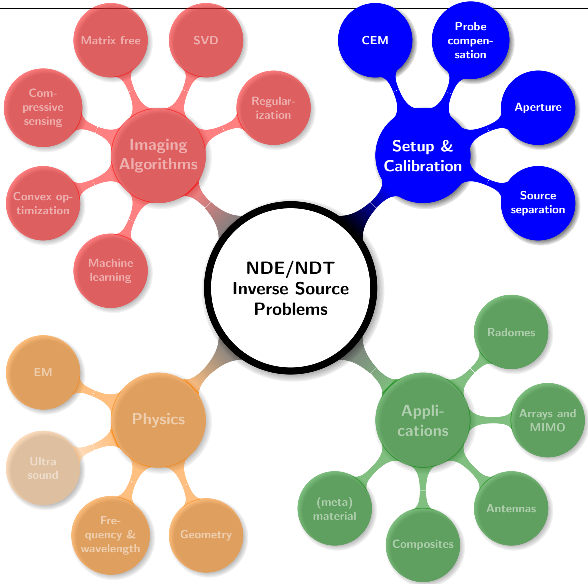

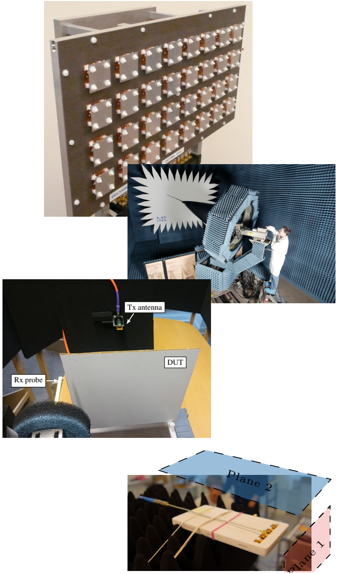

EMF and compliance testing of mm-wave devices

- mm-Waves: wavelength λ from 10 to $1\,\mathrm{mm}$ ($f \approx 30 - 300\,\mathrm{GHz}$) used and rapidly expanding in consumer electronics

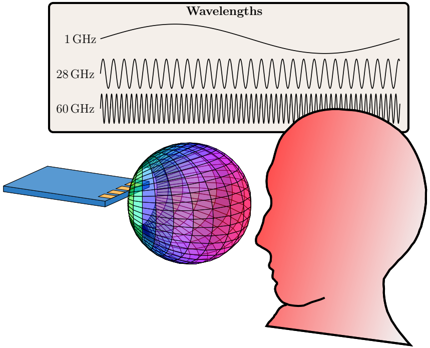

EMF and compliance testing of mm-wave devices

- mm-Waves: wavelength λ from 10 to $1\,\mathrm{mm}$ ($f \approx 30 - 300\,\mathrm{GHz}$) used and rapidly expanding in consumer electronics
- Frequencies above $24\,\mathrm{GHz}$ in 5G

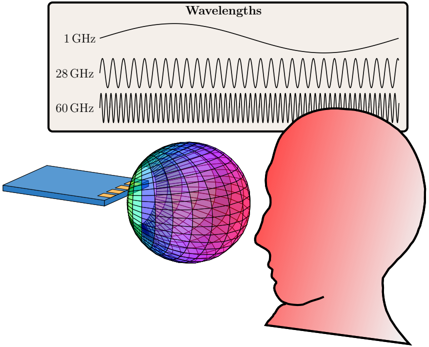

EMF and compliance testing of mm-wave devices

- mm-Waves: wavelength λ from 10 to $1\,\mathrm{mm}$ ($f \approx 30 - 300\,\mathrm{GHz}$) used and rapidly expanding in consumer electronics
- Frequencies above $24\,\mathrm{GHz}$ in 5G
- Arrays with beam steering in devices and base stations

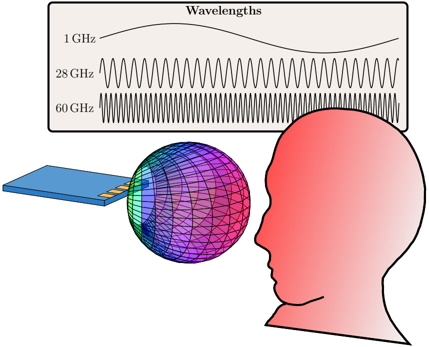

EMF and compliance testing of mm-wave devices

- mm-Waves: wavelength λ from 10 to $1\,\mathrm{mm}$ ($f \approx 30 - 300\,\mathrm{GHz}$) used and rapidly expanding in consumer electronics
- Frequencies above $24\,\mathrm{GHz}$ in 5G
- Arrays with beam steering in devices and base stations
- Often no need for miniaturized antennas ($\lambda/2 \approx 5\,\mathrm{mm}$ at $30\,\mathrm{GHz}$) and hence weak reactive near fields

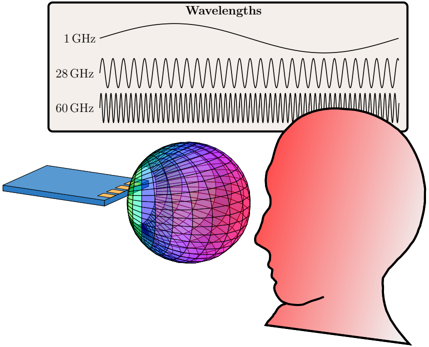

EMF and compliance testing of mm-wave devices

- mm-Waves: wavelength λ from 10 to $1\,\mathrm{mm}$ ($f \approx 30 - 300\,\mathrm{GHz}$) used and rapidly expanding in consumer electronics
- Frequencies above $24\,\mathrm{GHz}$ in 5G
- Arrays with beam steering in devices and base stations
- Often no need for miniaturized antennas ($\lambda/2 \approx 5\,\mathrm{mm}$ at $30\,\mathrm{GHz}$) and hence weak reactive near fields

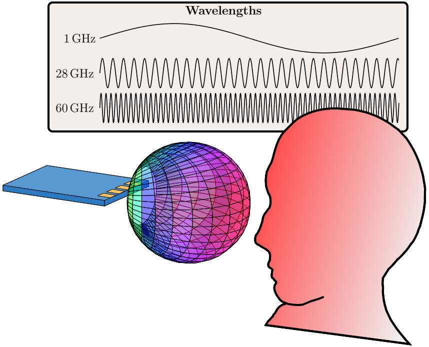

- Rapid attenuation in lossy bodies
- Absorption concentrated to surfaces
- EMF compliance through power density averaged over *e.g.*, $4\,\mathrm{cm}^2$

Measurement Technique: $28\,\mathrm{GHz}$ setup

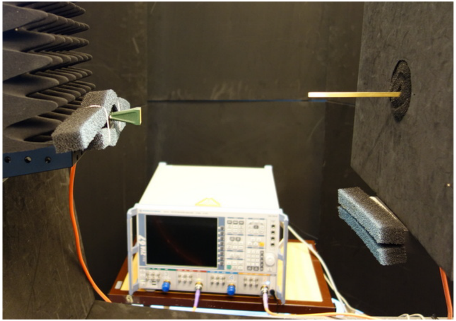

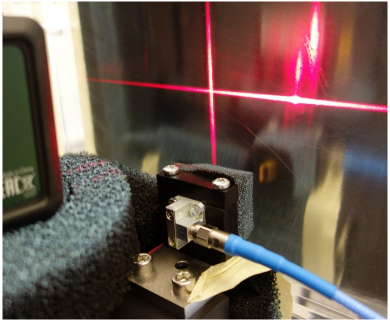

Determine the incident power flow close to the radiating DUT.

- $28\,\mathrm{GHz} \Rightarrow \lambda \approx 9\,\mathrm{mm} \approx 10\,\mathrm{mm} \Rightarrow 1\,\mathrm{mm}$ positioning error $\approx 36^\circ$ phase error and large amplitude

Measurement Technique: $28\,\mathrm{GHz}$ setup

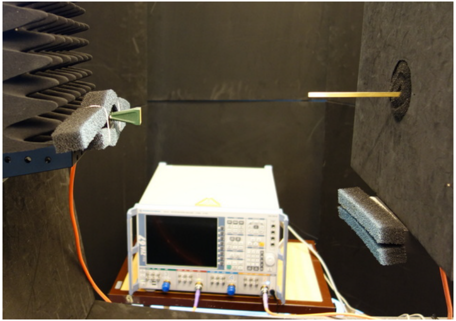

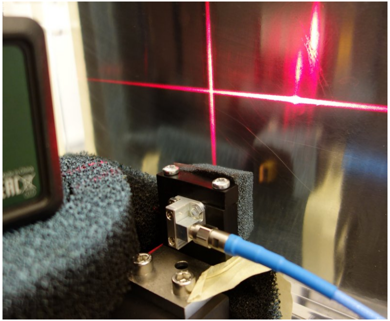

Determine the incident power flow close to the radiating DUT.

- $28\,\mathrm{GHz} \Rightarrow \lambda \approx 9\,\mathrm{mm} \approx 10\,\mathrm{mm} \Rightarrow 1\,\mathrm{mm}$ positioning error $\approx 36^\circ$ phase error and large amplitude
- Where is the field measured in the open wave guide?

Measurement Technique: $28\,\mathrm{GHz}$ setup

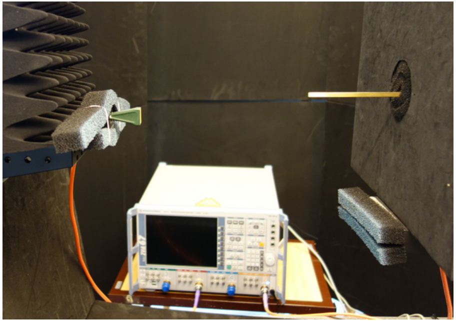
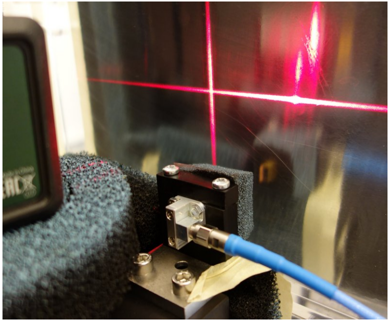

Determine the incident power flow close to the radiating DUT.

- $28\,\mathrm{GHz} \Rightarrow \lambda \approx 9\,\mathrm{mm} \approx 10\,\mathrm{mm} \Rightarrow 1\,\mathrm{mm}$ positioning error $\approx 36^\circ$ phase error and large amplitude
- Where is the field measured in the open wave guide?
- Probe calibration

Measurement Technique: $28\,\mathrm{GHz}$ setup

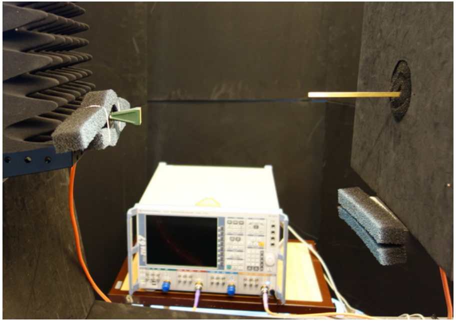

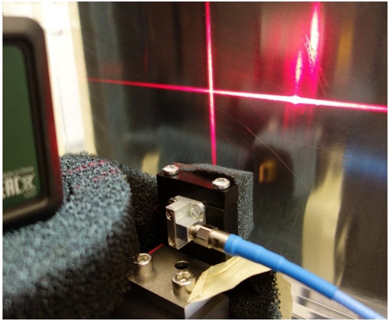

Determine the incident power flow close to the radiating DUT.

- $28\,\mathrm{GHz} \Rightarrow \lambda \approx 9\,\mathrm{mm} \approx 10\,\mathrm{mm} \Rightarrow 1\,\mathrm{mm}$ positioning error $\approx 36^\circ$ phase error and large amplitude
- Where is the field measured in the open wave guide?
- Probe calibration
- Need sub mm accuracy in positioning and measurement system

Measurement Technique: Setup

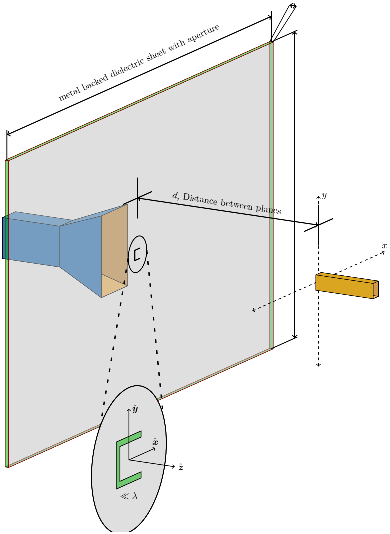

Aperture Sheet: Aperture cut out from metal backed dielectric.

- Well-defined radiation pattern.
- Independent of illumination.
- Self-resonant sub-wavelength.
- Also a closed object (box) with an aperture.

Illuminating Antenna: Situated behind aperture (any antenna will do) and excites aperture.

Distance: Scan plane to aperture distance is fixed and based on the DUT.

J. Lundgren et al. "A near-field measurement and calibration technique: Radio-frequency electromagnetic field exposure assessment of millimeter-wave 5G devices". *IEEE Antennas Propag. Mag.* 63.3 (2021), pp. 77–88

Measurement Technique: Calibration

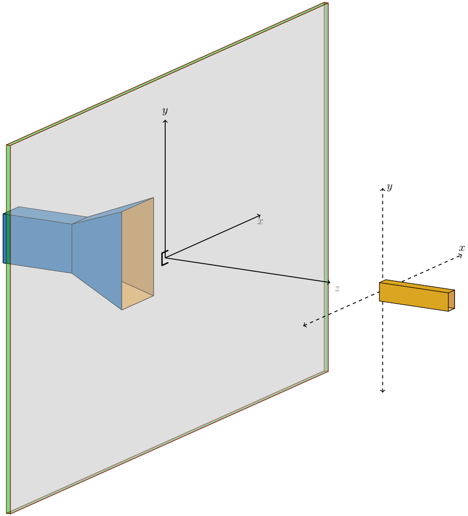

1. **Initiate**: Aperture radiates as a dipole.
2. **Measure**: Probe registers complex voltage value signals.
3. **Compare**: Comparison between registered and simulated aperture signals yields calibration.

Measurement Technique: Calibration

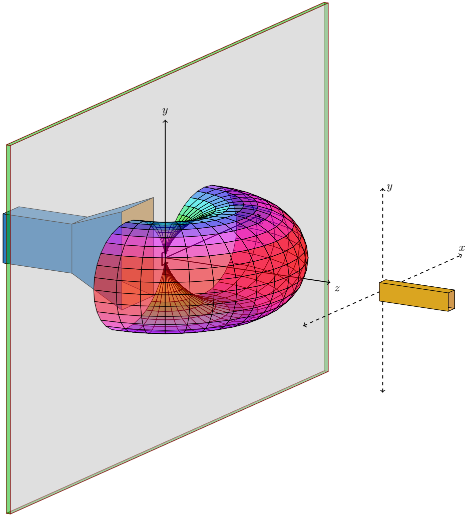

1. **Initiate**: Aperture radiates as a dipole.
2. **Measure**: Probe registers complex voltage value signals.
3. **Compare**: Comparison between registered and simulated aperture signals yields calibration.

Measurement Technique: Calibration

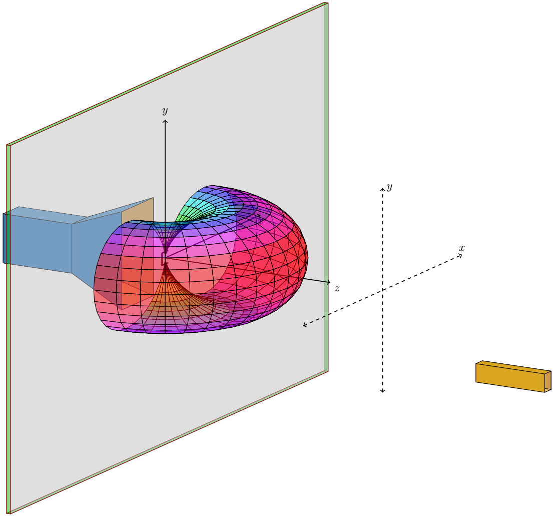

1. **Initiate**: Aperture radiates as a dipole.
2. **Measure**: Probe registers complex voltage value signals.
3. **Compare**: Comparison between registered and simulated aperture signals yields calibration.

Measurement Technique: Calibration

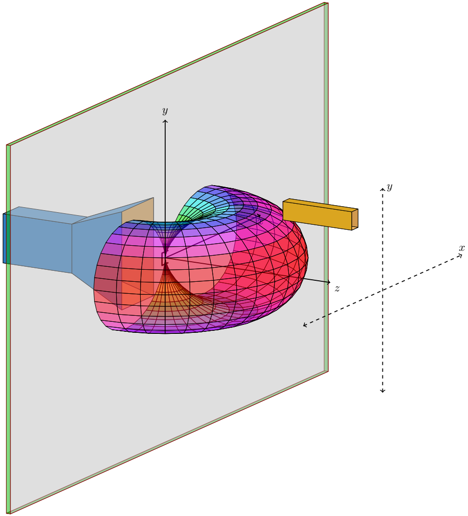

1. **Initiate**: Aperture radiates as a dipole.
2. **Measure**: Probe registers complex voltage value signals.
3. **Compare**: Comparison between registered and simulated aperture signals yields calibration.

Measurement Technique: Calibration

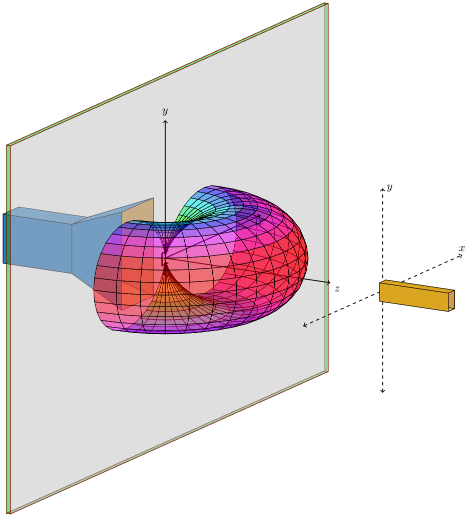

1. **Initiate**: Aperture radiates as a dipole.
2. **Measure**: Probe registers complex voltage value signals.
3. **Compare**: Comparison between registered and simulated aperture signals yields calibration.

Measurement Technique: DUT

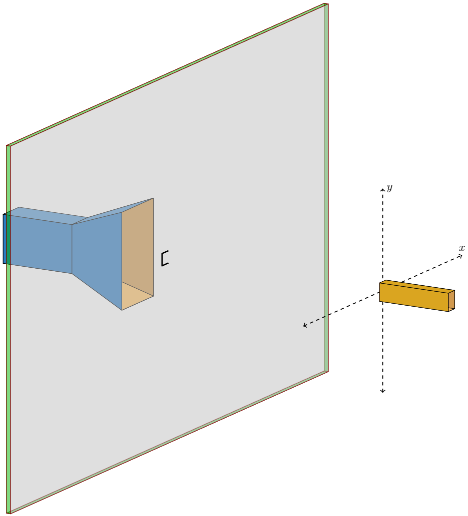

1. **Position the DUT**: Align with the aperture.
2. **Remove Aperture:** Lift out the aperture.
3. **Scan the DUT**: Scan the same region as the aperture was scanned.

Measurement Technique: DUT

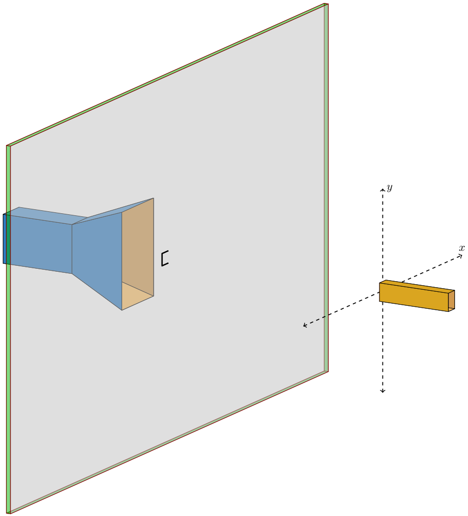

1. **Position the DUT**: Align with the aperture.
2. **Remove Aperture:** Lift out the aperture.
3. **Scan the DUT**: Scan the same region as the aperture was scanned.

Measurement Technique: DUT

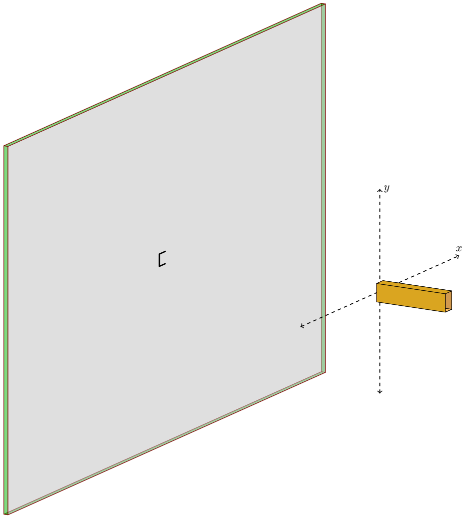

1. **Position the DUT**: Align with the aperture.
2. **Remove Aperture:** Lift out the aperture.
3. **Scan the DUT**: Scan the same region as the aperture was scanned.

Measurement Technique: DUT

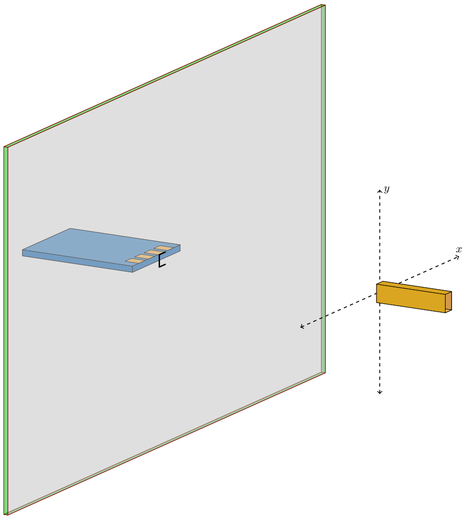

1. **Position the DUT**: Align with the aperture.
2. **Remove Aperture:** Lift out the aperture.
3. **Scan the DUT**: Scan the same region as the aperture was scanned.

Measurement Technique: DUT

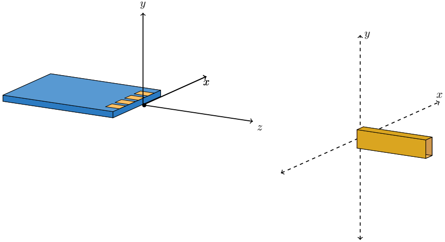

1. **Position the DUT**: Align with the aperture.
2. **Remove Aperture:** Lift out the aperture.
3. **Scan the DUT**: Scan the same region as the aperture was scanned.

Measurement Technique: DUT

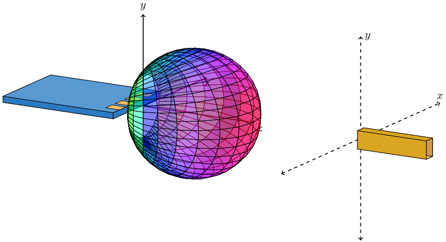

1. **Position the DUT**: Align with the aperture.
2. **Remove Aperture:** Lift out the aperture.
3. **Scan the DUT**: Scan the same region as the aperture was scanned.

Measurement Technique: DUT

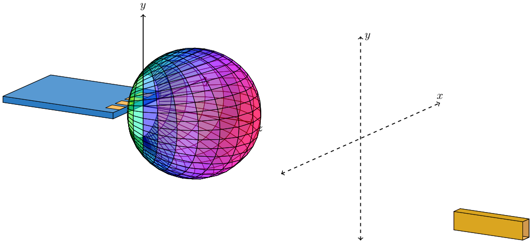

1. **Position the DUT**: Align with the aperture.
2. **Remove Aperture:** Lift out the aperture.
3. **Scan the DUT**: Scan the same region as the aperture was scanned.

Measurement Technique: DUT

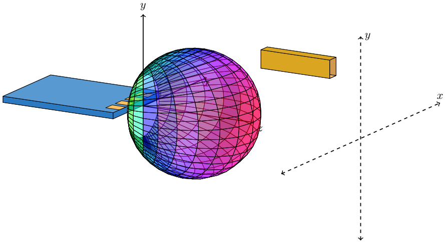

1. **Position the DUT**: Align with the aperture.
2. **Remove Aperture:** Lift out the aperture.
3. **Scan the DUT**: Scan the same region as the aperture was scanned.

Measurement Technique: DUT

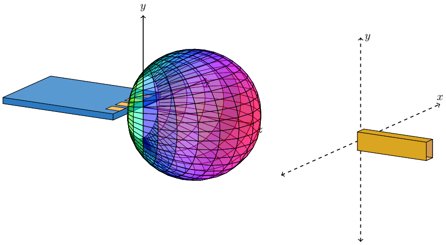

1. **Position the DUT**: Align with the aperture.
2. **Remove Aperture:** Lift out the aperture.
3. **Scan the DUT**: Scan the same region as the aperture was scanned.

Calibration

The measured complex voltage signals is compared with the probe calibrated field to obtain a corrected field corresponding to the actual field from the DUT.

Measurement Technique: MoM

Using method of moments to compute the currents on a plane at the DUT.

$$\boldsymbol{E}(\boldsymbol{r}) = \mathrm{j}k\eta_0 \int_S \boldsymbol{J}(\boldsymbol{r}')G(\boldsymbol{r}-\boldsymbol{r}') + \frac{1}{k^2}\nabla G(\boldsymbol{r}-\boldsymbol{r}')\nabla'\cdot\boldsymbol{J}(\boldsymbol{r}')\,\mathrm{dS}'$$

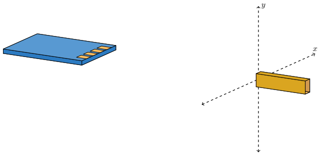

Measurement Technique: MoM

Using method of moments to relate the currents on a plane close to the DUT with the EM field

$$\boldsymbol{E} = \mathbf{N}^{\mathrm{e}} \boldsymbol{J}$$

- $\boldsymbol{E}$ is the electric field.
- $\boldsymbol{J}$ is the currents at the plane of the DUT.
- The matrix operator $\mathbf{N}^{\mathrm{e}}$ takes us from currents to the field.

Measured $\boldsymbol{E} \to \boldsymbol{J}$ at DUT plane $\to \boldsymbol{E}$ at other planes $\to$
Power density: $\frac{1}{2}\,\mathrm{Re}\{\boldsymbol{E} \times \boldsymbol{H}^*\} \cdot \hat{\boldsymbol{n}}$.

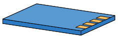

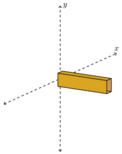

Measurement Technique: MoM

Using method of moments to compute the currents on a plane at the DUT.

$$\boldsymbol{E} = \mathbf{N}^{\mathrm{e}} \boldsymbol{J}$$

- $\boldsymbol{E}$ is the electric field.
- $\boldsymbol{J}$ is the currents at the plane of the DUT.
- The matrix operator $\mathbf{N}^{\mathrm{e}}$ takes us from currents to the field.

Measured $\boldsymbol{E} \rightarrow \boldsymbol{J}$ at DUT plane $\rightarrow \boldsymbol{E}$ at other planes.
Power density: $\frac{1}{2}\mathrm{Re}\{\boldsymbol{E} \times \boldsymbol{H}^*\} \cdot \hat{\boldsymbol{n}}$.

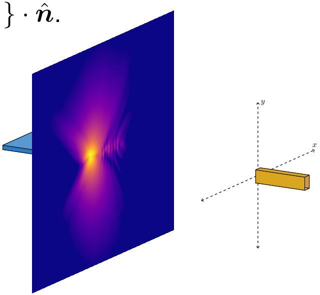

Measurement Technique: MoM

Using method of moments to compute the currents on a plane at the DUT.

$$\boldsymbol{E} = \mathbf{N}^{\mathrm{e}}\boldsymbol{J}$$

- $\boldsymbol{E}$ is the electric field.
- $\boldsymbol{J}$ is the currents at the plane of the DUT.
- The matrix operator $\mathbf{N}^{\mathrm{e}}$ takes us from currents to the field.

Measured $\boldsymbol{E} \to \boldsymbol{J}$ at DUT plane $\to \boldsymbol{E}$ at other planes.
Power density: $\frac{1}{2}\mathrm{Re}\{\boldsymbol{E} \times \boldsymbol{H}^*\} \cdot \hat{\boldsymbol{n}}$.

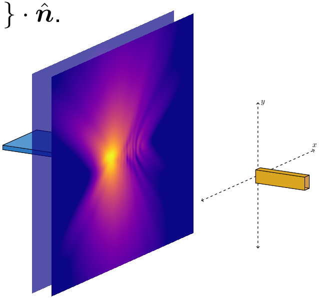

Measurement Technique: MoM

Using method of moments to compute the currents on a plane at the DUT.

$$\boldsymbol{E} = \mathbf{N}^{\mathrm{e}} \boldsymbol{J}$$

- $\boldsymbol{E}$ is the electric field.
- $\boldsymbol{J}$ is the currents at the plane of the DUT.
- The matrix operator $\mathbf{N}^{\mathrm{e}}$ takes us from currents to the field.

Measured $\boldsymbol{E} \rightarrow \boldsymbol{J}$ at DUT plane $\rightarrow \boldsymbol{E}$ at other planes.
Power density: $\frac{1}{2}\mathrm{Re}\{\boldsymbol{E} \times \boldsymbol{H}^*\} \cdot \hat{\boldsymbol{n}}$.

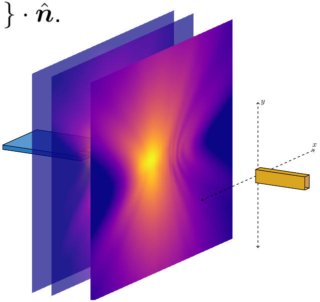

Mock Up Phone with four 28 GHz ports

- 4 ports $28\,\mathrm{GHz}$ with $\approx \lambda$ separation
- size $144 \times 72 \times 9.8\,\mathrm{mm}^3$
- plastic cover and PCB.
- 6 possible planes *e.g.*, front (plane 1) focus here and top (plane 2)

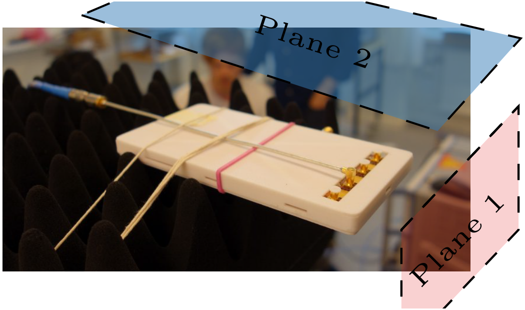

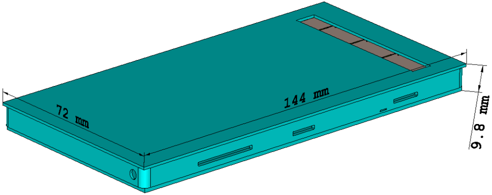

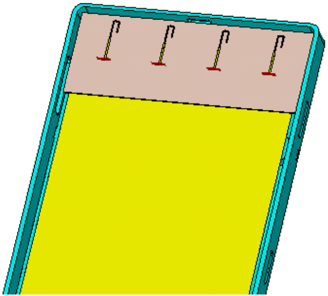

Results: Power Density, Mock Up Phone 28 GHz, Plane 1

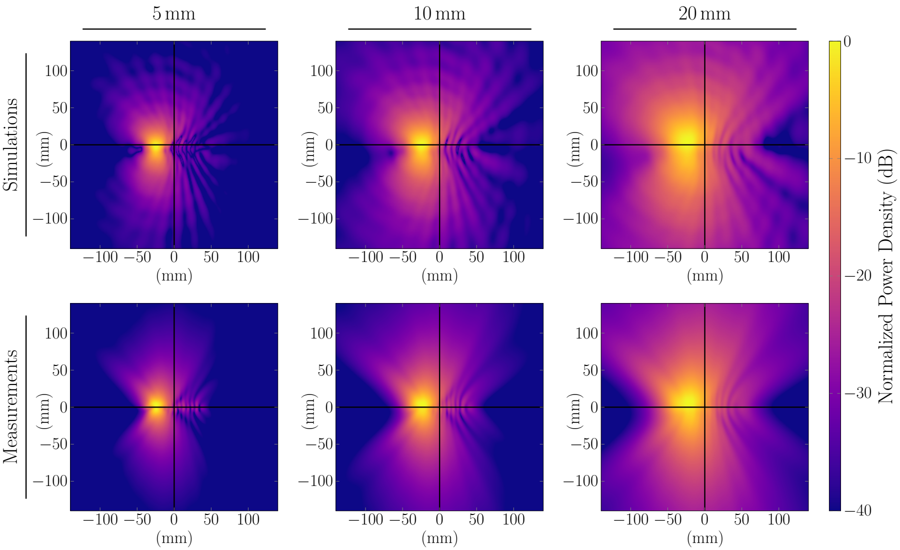

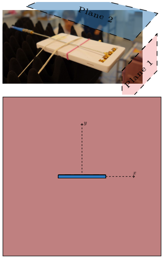

Planes: $284 \times 284\,\mathrm{mm}^2$.
Sampling: $8 \times 8\,\mathrm{mm}^2$, $3/4\lambda$.
Distance to DUT: 63 mm.

Results: Power Density, Mock Up Phone 28 GHz, Plane 1

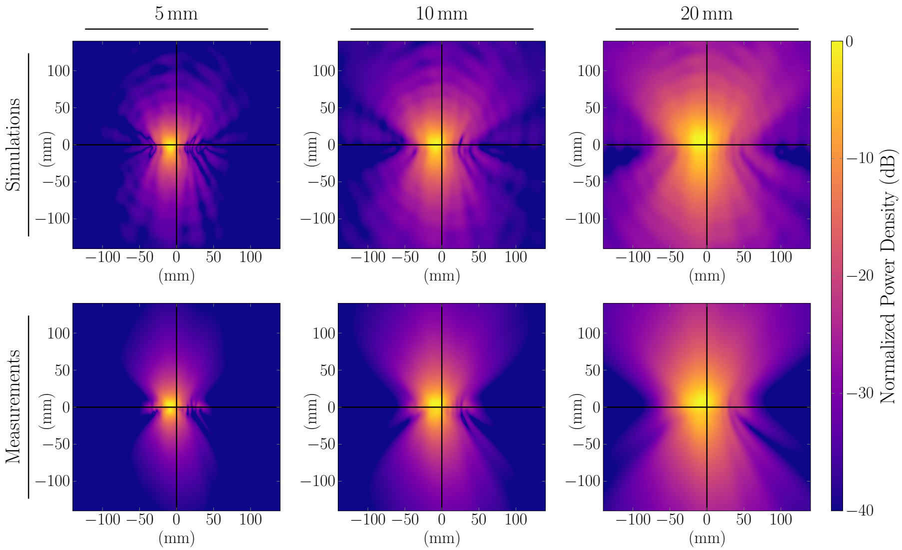

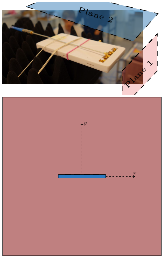

Planes:
$284 \times 284\,\mathrm{mm}^2$.
Sampling:
$8 \times 8\,\mathrm{mm}^2$, $3/4\lambda$.
Distance to DUT:
$63\,\mathrm{mm}$.

Results: Power Density, Mock Up Phone 28 GHz, Plane 1

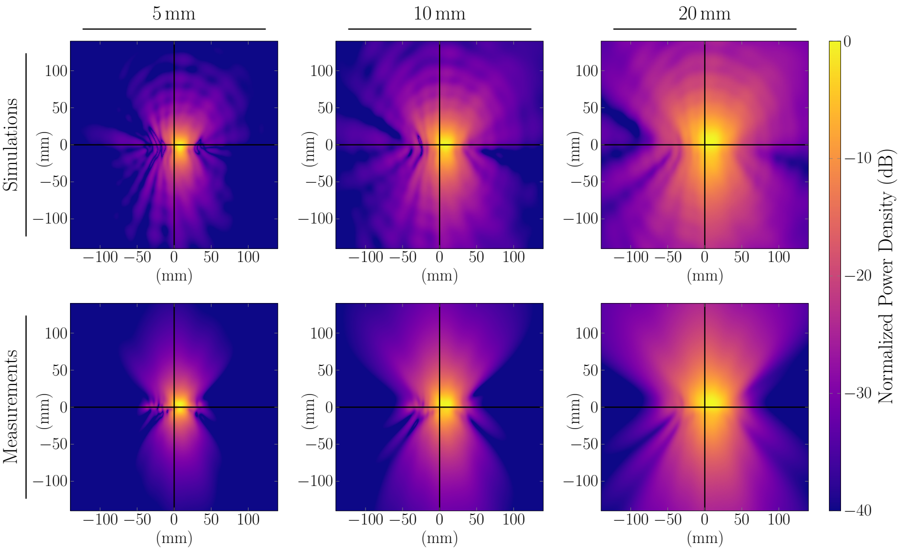

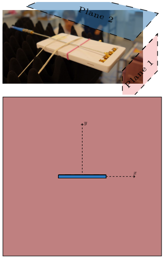

Planes:
$284 \times 284\,\mathrm{mm}^2$.
Sampling:
$8 \times 8\,\mathrm{mm}^2$, $3/4\lambda$.
Distance to DUT:
63 mm.

Results: Power Density, Mock Up Phone 28 GHz, Plane 1

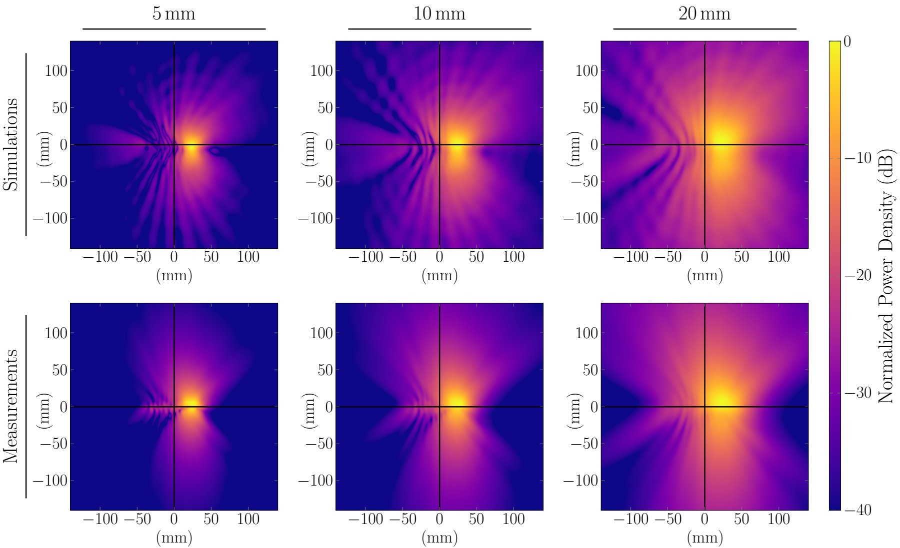

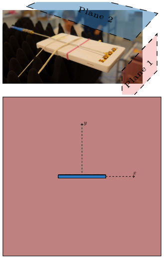

Planes:
$284 \times 284\,\mathrm{mm}^2$.
Sampling:
$8 \times 8\,\mathrm{mm}^2$, $3/4\lambda$.
Distance to DUT:
63 mm.

Non-destructive testing and compressive sensing

- Near field and/or equivalent currents can localize defects and estimate (EMF) exposure.

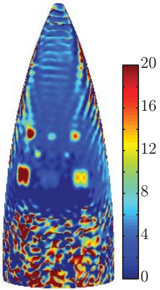

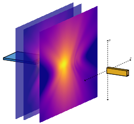

Non-destructive testing and compressive sensing

- Near field and/or equivalent currents can localize defects and estimate (EMF) exposure.
- Imaging of the fields and/or equivalent currents for understanding.

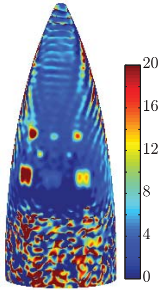

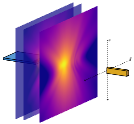

Non-destructive testing and compressive sensing

- Near field and/or equivalent currents can localize defects and estimate (EMF) exposure.
- Imaging of the fields and/or equivalent currents for understanding.
- Integral equations (similar to MoM).

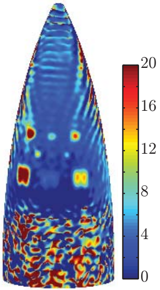

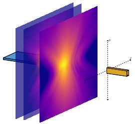

Non-destructive testing and compressive sensing

- Near field and/or equivalent currents can localize defects and estimate (EMF) exposure.
- Imaging of the fields and/or equivalent currents for understanding.
- Integral equations (similar to MoM).
- One drawback is the measurement time. Can take several hours to measure the near/far field around the structure.

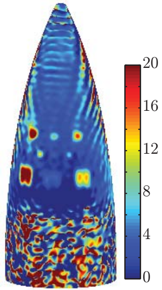

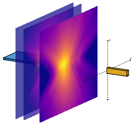

Non-destructive testing and compressive sensing

- Near field and/or equivalent currents can localize defects and estimate (EMF) exposure.
- Imaging of the fields and/or equivalent currents for understanding.
- Integral equations (similar to MoM).
- One drawback is the measurement time. Can take several hours to measure the near/far field around the structure.
- Defects are often localized and there are often only a few defects.

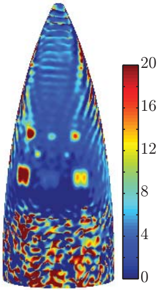

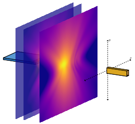

Non-destructive testing and compressive sensing

- Near field and/or equivalent currents can localize defects and estimate (EMF) exposure.
- Imaging of the fields and/or equivalent currents for understanding.
- Integral equations (similar to MoM).
- One drawback is the measurement time. Can take several hours to measure the near/far field around the structure.
- Defects are often localized and there are often only a few defects.
- Utilize the sparse image (few defects) to improve the image quality and reduce the measurement time.

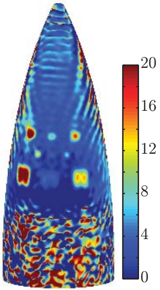

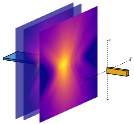

Non-destructive testing and compressive sensing

- Near field and/or equivalent currents can localize defects and estimate (EMF) exposure.
- Imaging of the fields and/or equivalent currents for understanding.
- Integral equations (similar to MoM).
- One drawback is the measurement time. Can take several hours to measure the near/far field around the structure.
- Defects are often localized and there are often only a few defects.
- Utilize the sparse image (few defects) to improve the image quality and reduce the measurement time.
- Compressive sensing.

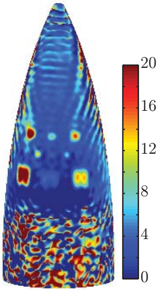

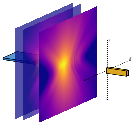

Outline

Non-destructive testing and inverse source problems

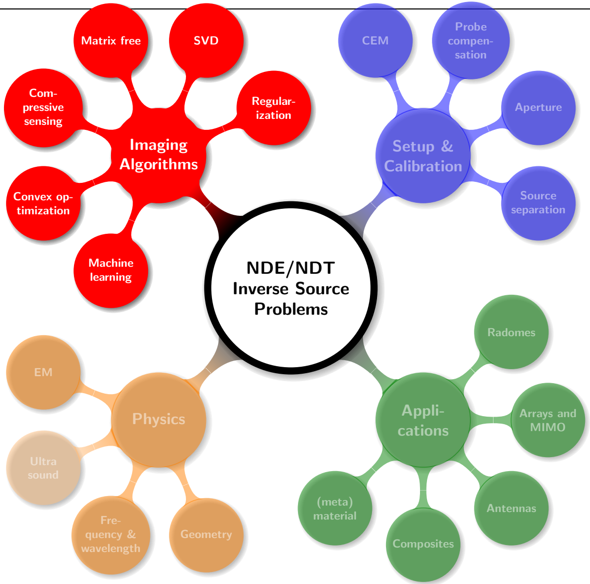

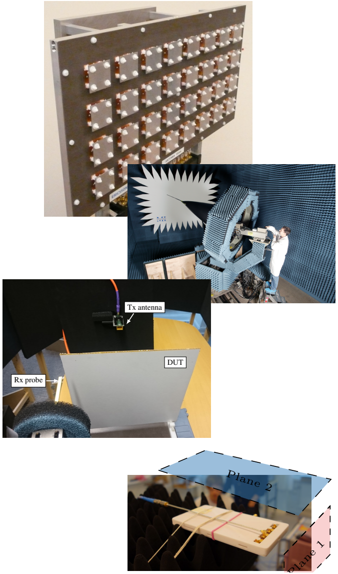

Linear inverse problems and regularization

Would like to solve

$$\mathbf{A}\mathbf{x} = \mathbf{b}$$

with an $M \times N$ matrix $\mathbf{A}$. Simple to solve if $M = N$ and cond$(\mathbf{A})$ not too large (compared with the errors and noise in $\mathbf{A}$ and $\mathbf{b}$).

Otherwise regularization:

- SVD: $\mathbf{A} = \mathbf{U}\boldsymbol{\Sigma}\mathbf{V}^{\mathsf{H}}$ with $\mathbf{U}^{\mathsf{H}}\mathbf{U} = \mathbf{1}$ and $\mathbf{V}^{\mathsf{H}}\mathbf{V} = \mathbf{1}$
- $\mathbf{L}^2$-minimization: $\|\mathbf{x}\|_2 = (\sum_{n=1}^{N} |x_n|^2)^{1/2}$ or with weight $\mathbf{x}^{\mathsf{H}}\mathbf{W}\mathbf{x}$
- $\mathbf{L}^1$-minimization: $\|\mathbf{x}\|_1 = \sum_{n=1}^{N} |x_n|$
- $\mathbf{L}^0$-minimization: the number of non-zero entries of $\mathbf{x}$. (not a norm)

Many choices of norms and weight functions

SVD and $\mathbf{L}^2$ have many similarities. Would like to use $\mathbf{L}^0$ in compressive sensing but approximate with $\mathbf{L}^1$ to form convex optimization problems. Can use CVX for small problems and dedicated solvers (TFOCS, spgl1,...) for larger size problems (matrix free).

$\mathbf{L}^1$-regularization

Changing the $\mathbf{L}^2$-regularization to $\mathbf{L}^1$ gives the (convex) optimization problem

$$\text{minimize} \|\mathbf{A}\mathbf{x} - \mathbf{b}\|_2 + \alpha \|\mathbf{x}\|_1$$

$\mathbf{L}^1$-regularization

Changing the $\mathbf{L}^2$-regularization to $\mathbf{L}^1$ gives the (convex) optimization problem

$$\text{minimize} \|\mathbf{Ax} - \mathbf{b}\|_2 + \alpha \|\mathbf{x}\|_1$$

Alternative related (convex) formulation

$$\begin{aligned} \text{minimize} \quad & \|\mathbf{x}\|_1 \\ \text{subject to} \quad & \|\mathbf{Ax} - \mathbf{b}\|_2 \leq \delta, \end{aligned}$$

where the parameter δ can be estimated from the SVD solution $\delta \approx \|\mathbf{Ax}_{\text{SVD}} - \mathbf{b}\|_2$. This formulation tries to produce a solution with similar fit to the data as the SVD ($\mathbf{L}^2$) but without the smoothing (a few dominant components).

$\mathbf{L}^1$-regularization

Changing the $\mathbf{L}^2$-regularization to $\mathbf{L}^1$ gives the (convex) optimization problem

$$\text{minimize} \|\mathbf{A}\mathbf{x} - \mathbf{b}\|_2 + \alpha\|\mathbf{x}\|_1$$

Alternative related (convex) formulation

$$\begin{aligned} \text{minimize} \quad & \|\mathbf{x}\|_1 \\ \text{subject to} \quad & \|\mathbf{A}\mathbf{x} - \mathbf{b}\|_2 \leq \delta, \end{aligned}$$

where the parameter δ can be estimated from the SVD solution $\delta \approx \|\mathbf{A}\mathbf{x}_{\mathrm{SVD}} - \mathbf{b}\|_2$. This formulation tries to produce a solution with similar fit to the data as the SVD ($\mathbf{L}^2$) but without the smoothing (a few dominant components).

$\mathbf{L}^2$ on the data term is often motivated by assuming Gaussian noise. $\mathbf{L}^1$ can be used and be better for cases with low SNR and outliers

(Tarantola, *Inverse problem theory and methods for model parameter estimation*, 2005)

$\mathbf{L}^2$ or $\mathbf{L}^1$?

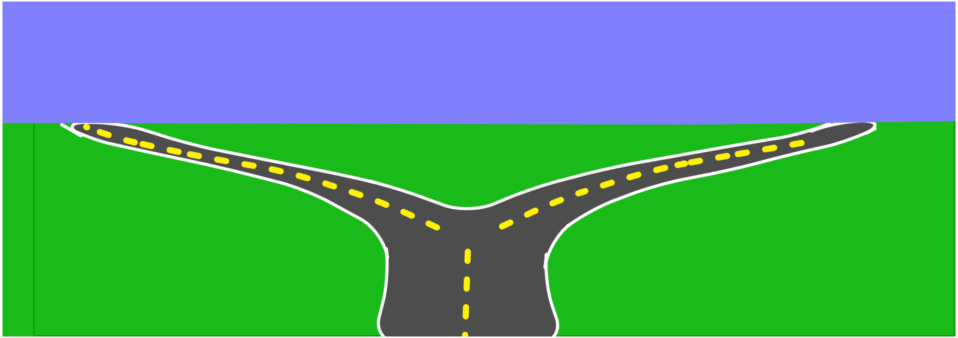

$\mathbf{L}^2$ or $\mathbf{L}^1$?

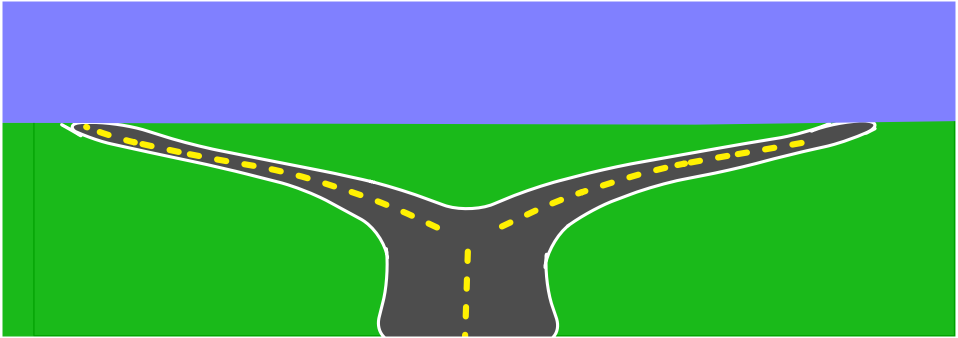

When a traveler reaches a fork in the road, the $\mathbf{L}^1$-norm tells him to take either one way or the other, but the $\mathbf{L}^2$-norm instructs him to head off into the bushes.

John F. Claerbout and Francis Muir, 1973

Small toy problem

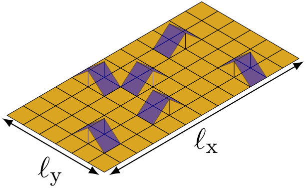

Consider a planar rectangle divided into $N_{\rm x} \times N_{\rm y}$ elements with a current density $\boldsymbol{J}(\boldsymbol{r})$ expanded in local basis functions $\boldsymbol{\psi}_m(\boldsymbol{r})$

$$\boldsymbol{J}(\boldsymbol{r}) = \sum_m I_m \boldsymbol{\psi}_m(\boldsymbol{r}) \quad \text{with } I_m \text{ collected in } \mathbf{x}$$

The radiated far field is expanded in spherical modes

$$\boldsymbol{F}(\hat{\boldsymbol{r}}) = \sum_{n=1}^{N} f_n \boldsymbol{A}_n(\boldsymbol{r}) \quad \text{with } f_n \text{ collected in } \mathbf{b}$$

Small toy problem

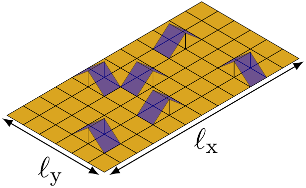

Consider a planar rectangle divided into $N_{\mathrm{x}} \times N_{\mathrm{y}}$ elements with a current density $\boldsymbol{J}(\boldsymbol{r})$ expanded in local basis functions $\boldsymbol{\psi}_m(\boldsymbol{r})$

$$\boldsymbol{J}(\boldsymbol{r}) = \sum_m I_m \boldsymbol{\psi}_m(\boldsymbol{r}) \quad \text{with } I_m \text{ collected in } \mathbf{x}$$

The radiated far field is expanded in spherical modes

$$\boldsymbol{F}(\hat{\boldsymbol{r}}) = \sum_{n=1}^{N} f_n \boldsymbol{A}_n(\boldsymbol{r}) \quad \text{with } f_n \text{ collected in } \mathbf{b}$$

Estimate the current density $\mathbf{x}$ from the far-field coefficients $\mathbf{b}$, where $\mathbf{b} = \mathbf{A}\mathbf{x}$.

SVD and $\mathbf{L}^1$-regularization

Use SVD and L^1-regularization to estimate the current density.

$$\begin{aligned} \text{minimize} \quad & \|\mathbf{x}\|_1 \\ \text{subject to} \quad & \|\mathbf{A}\mathbf{x} - \mathbf{b}\|_2 \leq \delta, \end{aligned}$$

The parameter δ is estimated from the SVD solution $\delta \sim \|\mathbf{A}\mathbf{x}_{\mathrm{SVD}} - \mathbf{b}\|_2$. This formulation tries to produce a solution with similar fit to the data as the SVD ($\mathbf{L}^2$) but without the smoothing (a few dominant components).
Here, we use SPGL1

```
x = spg_bpdn(A,b,d,opts);
```

$1\lambda \times 0.5\lambda$ rectangle with 2 sources

Current density: $\boldsymbol{J}_0$ SVD-current: $\boldsymbol{J}_2$ L^1-current: $\boldsymbol{J}_1$

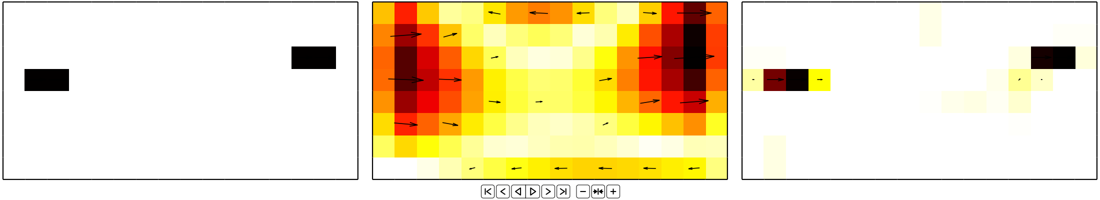

- $1\lambda \times 0.5\lambda$ rectangle divided into 16×8 elements.
- 232 current elements and 35 measurements (spherical modes).
- Additive noise from a random current density $0.01 \max |\boldsymbol{J}_0|$.
- Same mesh for data and reconstruction (inverse crime).

SVD (and L^2) regularization produces a smeared image to $\approx \lambda/4$ resolution. L^1 regularization recreates most cases even with sub $\lambda/4$ distance.

$2\lambda \times \lambda$ rectangle with 2 sources

Current density: $\boldsymbol{J}_0$ SVD-current: $\boldsymbol{J}_2$ L^1-current: $\boldsymbol{J}_1$

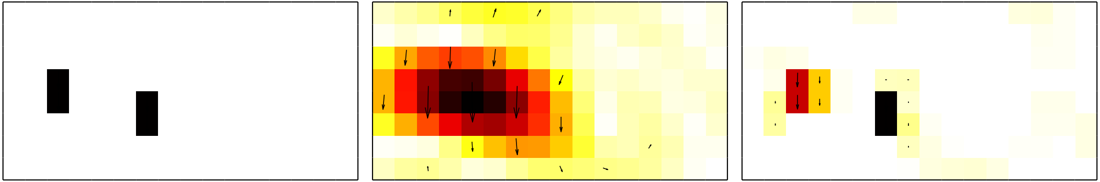

- $2\lambda \times \lambda$ rectangle divided into 16×8 elements.
- 232 current elements and 35 measurements (spherical modes).
- Additive noise from a random current density $0.01 \max |\boldsymbol{J}_0|$.
- Same mesh for data and reconstruction (inverse crime).

SVD (and L^2) regularization produces a smeared image to $\approx \lambda/4$ resolution. L^1 regularization recreates most cases even with sub $\lambda/4$ distance.

$2\lambda \times 1\lambda$ rectangle with 4 sources

Current density: $\boldsymbol{J}_0$ SVD-current: $\boldsymbol{J}_2$ L^1-current: $\boldsymbol{J}_1$

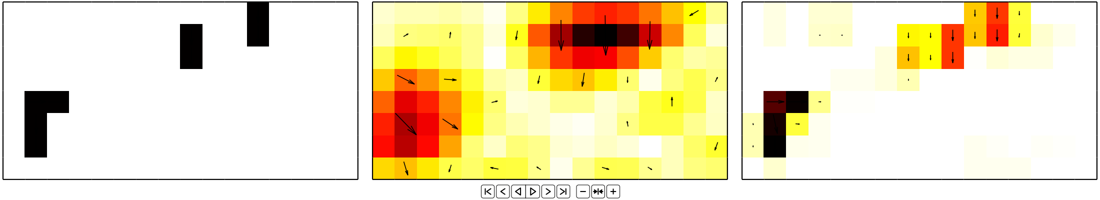

- $2\lambda \times \lambda$ rectangle divided into 16×8 elements.
- 232 current elements and 35 measurements (spherical modes).
- Additive noise from a random current density $0.01 \max |\boldsymbol{J}_0|$.
- Same mesh for data and reconstruction (inverse crime).

SVD (and L^2) regularization produces a smeared image to $\approx \lambda/4$ resolution. L^1 regularization recreates most cases but results deteriorate with increasing number of objects.

$2\lambda \times 1\lambda$ rectangle with 2 sources different mesh

Current density: $\boldsymbol{J}_0$

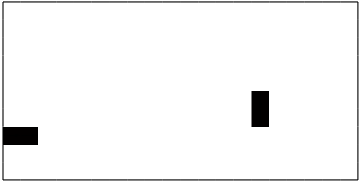

SVD-current: $\boldsymbol{J}_2$

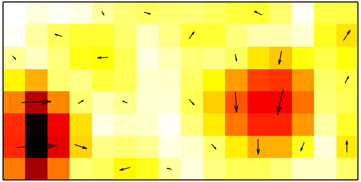

L^1-current: $\boldsymbol{J}_1$

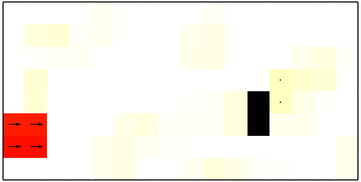

- $2\lambda \times \lambda$ rectangle divided into 16×8 elements.
- 232 current elements and 35 measurements (spherical modes).
- Additive noise from a random current density $0.01 \max |\boldsymbol{J}_0|$.
- Different mesh for data and reconstruction.

SVD (and L^2) regularization produces a smeared image to $\approx \lambda/4$ resolution. L^1 regularization recreates most cases but results deteriorate with increasing number of objects.

$2\lambda \times 1\lambda$ rectangle with 4 sources different mesh

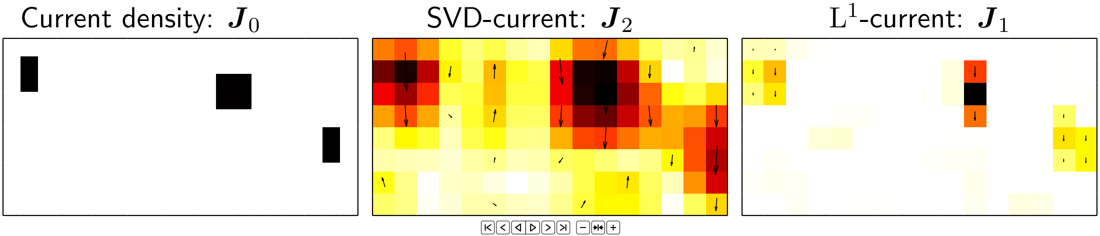

- $2\lambda \times \lambda$ rectangle divided into 16×8 elements.
- 232 current elements and 35 measurements (spherical modes).
- Additive noise from a random current density $0.01 \max |\boldsymbol{J}_0|$.
- Different mesh for data and reconstruction.

SVD (and L^2) regularization produces a smeared image to $\approx \lambda/4$ resolution. L^1 regularization recreates most cases but results deteriorate with increasing number of objects.

$2\lambda \times 1\lambda$ rectangle with 2 smooth sources

Current density: $\boldsymbol{J}_0$ SVD-current: $\boldsymbol{J}_2$ L^1-current: $\boldsymbol{J}_1$

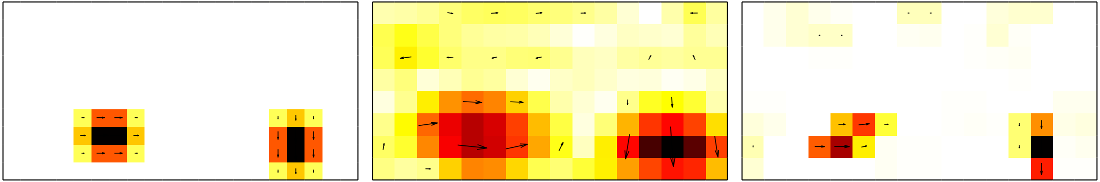

- $2\lambda \times \lambda$ rectangle divided into 16×8 elements.
- 232 current elements and 35 measurements (spherical modes).
- Additive noise from a random current density $0.01 \max |\boldsymbol{J}_0|$.
- Different mesh for data and reconstruction.

SVD (and L^2) regularization produces a smeared image to $\approx \lambda/4$ resolution. L^1 regularization recreates most cases but results deteriorate with increasing number of objects and smoothing.

$2\lambda \times 1\lambda$ rectangle with 4 smooth sources

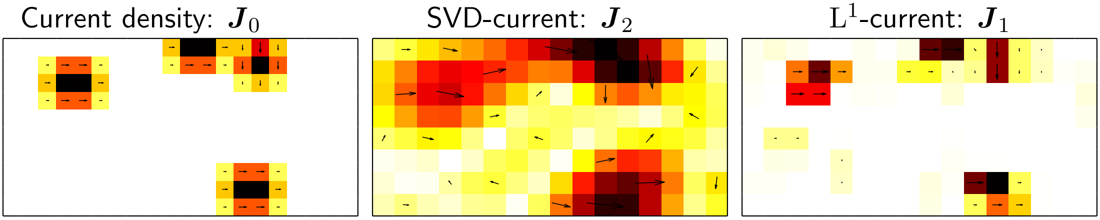

- $2\lambda \times \lambda$ rectangle divided into 16×8 elements.
- 232 current elements and 35 measurements (spherical modes).
- Additive noise from a random current density $0.01 \max |\boldsymbol{J}_0|$.
- Different mesh for data and reconstruction.

SVD (and L^2) regularization produces a smeared image to $\approx \lambda/4$ resolution. L^1 regularization recreates most cases but results deteriorate with increasing number of objects and smoothing.

$2\lambda \times 1\lambda$ rectangle with 4 smooth sources

Current density: $\boldsymbol{J}_0$ SVD-current: $\boldsymbol{J}_2$ L^1-current: $\boldsymbol{J}_1$

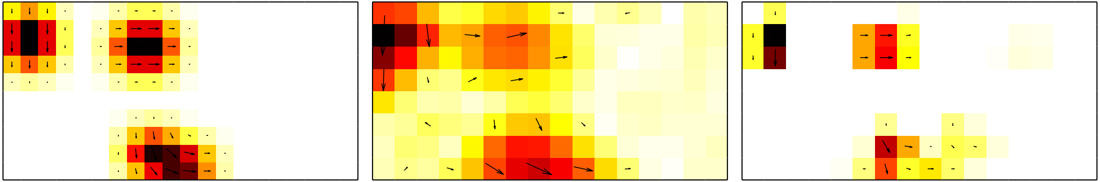

- $2\lambda \times \lambda$ rectangle divided into 16×8 elements.
- 232 current elements and 35 measurements (spherical modes).
- Additive noise from a random current density $0.01 \max |\boldsymbol{J}_0|$.
- Different mesh for data and reconstruction.

SVD (and L^2) regularization produces a smeared image to $\approx \lambda/4$ resolution. L^1 regularization recreates most cases but results deteriorate with increasing number of objects and smoothing.

$2\lambda \times 1\lambda$ rectangle with 4 smooth sources

Current density: $\boldsymbol{J}_0$ SVD-current: $\boldsymbol{J}_2$ L^1-current: $\boldsymbol{J}_1$

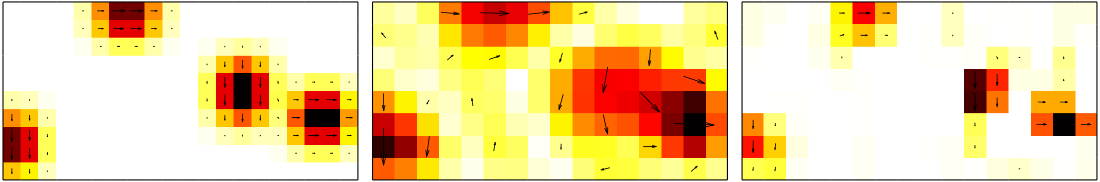

- $2\lambda \times \lambda$ rectangle divided into 16×8 elements.
- 232 current elements and 63 measurements (spherical modes).
- Additive noise from a random current density $0.01 \max |\boldsymbol{J}_0|$.
- Different mesh for data and reconstruction.

SVD (and L^2) regularization produces a smeared image to $\approx \lambda/4$ resolution. L^1 regularization recreates most cases but results deteriorate with increasing number of objects and smoothing.

Some observations from the toy problem

- SVD (L^2) regularization is robust and computationally efficient but smooth images to $\approx \lambda/4$ resolution.
- L^1-regularization is less robust and computationally more demanding.
  - potentially very efficient for imaging of small objects.
  - best for a few non-smooth objects (sparse).
  - important to use different approach to compute data and inversion (inverse crime).
- besides being computationally challenging L^0-regularization (sparsity) would preform worse than L^1 for most of these cases.

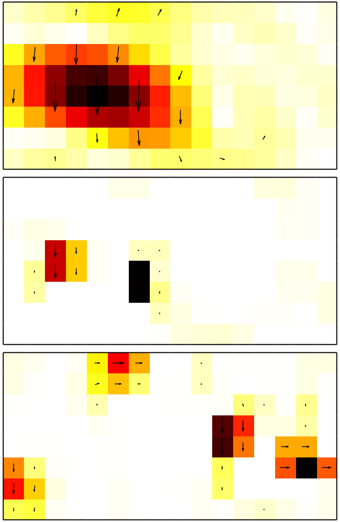

$\mathbf{L}^p$ for the unresolved components

$\mathbf{L}^2$ inversion indicates a resolution of the order $\lambda/4$ to $\lambda/2$. The resolved part can be determined from the observations $\mathbf{Ax} = \mathbf{b}$.
Regularization with just two components satisfying $x_1 + x_2 = 1$ (from $\mathbf{Ax} = \mathbf{b}$)

$$\min \|\mathbf{x}\|_2^2 = x_1^2 + x_2^2 = 0.5 \quad \text{for } x_1 = x_2 = 0.5$$

and

$$\min \|\mathbf{x}\|_1 = |x_1| + |x_2| = 1 \quad \text{for any } x_1, x_2 \geq 0$$

What happens if x_1 fits the data slightly better than x_2?

$\mathbf{L}^p$ for the unresolved components

$\mathbf{L}^2$ inversion indicates a resolution of the order $\lambda/4$ to $\lambda/2$. The resolved part can be determined from the observations $\mathbf{Ax} = \mathbf{b}$.

Regularization with just two components satisfying $x_1 + x_2 = 1$ (from $\mathbf{Ax} = \mathbf{b}$)

$$\min \|\mathbf{x}\|_2^2 = x_1^2 + x_2^2 = 0.5 \quad \text{for } x_1 = x_2 = 0.5$$

and

$$\min \|\mathbf{x}\|_1 = |x_1| + |x_2| = 1 \quad \text{for any } x_1, x_2 \geq 0$$

What happens if x_1 fits the data slightly better than x_2?

a) $\mathbf{L}^2$: $x_1 \approx x_2 \approx 0.5$ and $\mathbf{L}^1$: $x_1 \approx x_2 \approx 0.5$
b) $\mathbf{L}^2$: $x_1 \approx x_2 \approx 0.5$ and $\mathbf{L}^1$: $x_1 \approx 1$, $x_2 \approx 0$
c) $\mathbf{L}^2$: $x_1 \approx 1$, $x_2 \approx 0$ and $\mathbf{L}^1$: $x_1 \approx x_2 \approx 0.5$
d) $\mathbf{L}^2$: $x_1 \approx 1$, $x_2 \approx 0$ and $\mathbf{L}^1$: $x_1 \approx 1$, $x_2 \approx 0$

$\mathbf{L}^p$ for the unresolved components

$\mathbf{L}^2$ inversion indicates a resolution of the order $\lambda/4$ to $\lambda/2$. The resolved part can be determined from the observations $\mathbf{Ax} = \mathbf{b}$.
Regularization with just two components satisfying $x_1 + x_2 = 1$ (from $\mathbf{Ax} = \mathbf{b}$)

$$\min \|\mathbf{x}\|_2^2 = x_1^2 + x_2^2 = 0.5 \quad \text{for } x_1 = x_2 = 0.5$$

and

$$\min \|\mathbf{x}\|_1 = |x_1| + |x_2| = 1 \quad \text{for any } x_1, x_2 \geq 0$$

What happens if x_1 fits the data slightly better than x_2?

- $\mathbf{L}^2$ regularization produces $x_1 \approx x_2 \approx 0.5$. A smooth image with features determined by the resolution.
- $\mathbf{L}^1$ regularization produces $x_1 \approx 1$ and $x_2 \approx 0$. Good for sparse cases (few dominant components) but otherwise irregular random results.

Outline

1. **Non-destructive testing**
2. **Radome and Antenna diagnostics**
   - Inverse source problem
   - Inversion algorithm
   - Radome diagnostics
   - EMF and mm-wave exposure
3. **Compressive sensing and L^1-regularization**
4. **NDT composite panel**
   - Transmission Case
   - Reflection Case
5. **Regularization and convex optimization and bounds**
6. **Conclusions**

Non-destructive testing and inverse source problems

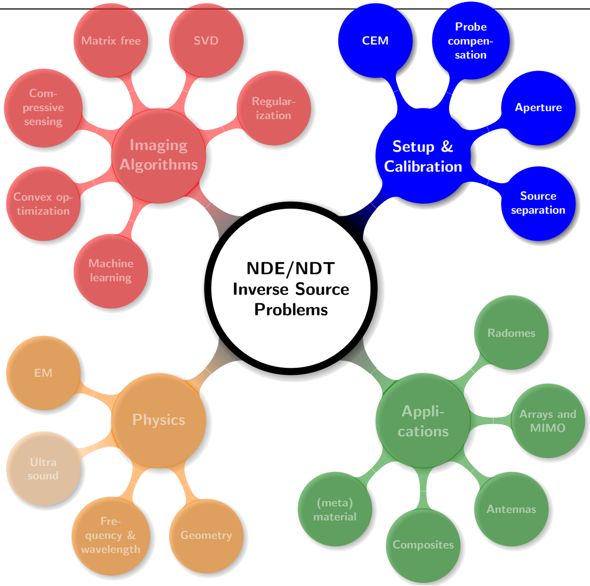

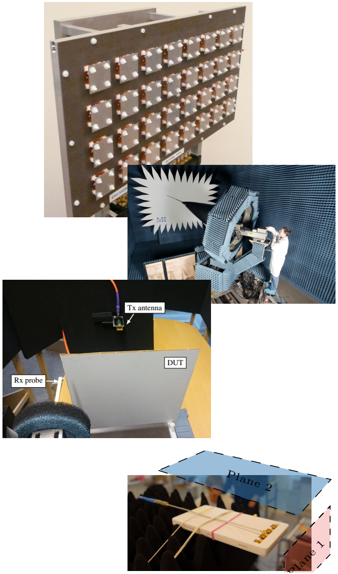

Composite panels

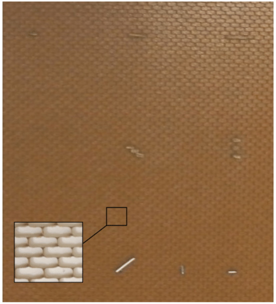

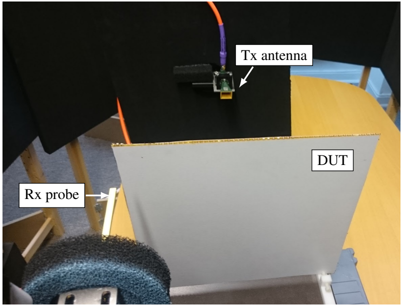

- Multilayer structure with low and high permittivity materials.
- Distinguish between regions with varying resistivities (inhomogeneities, delaminations, dielectric inclusions).
- NDT using mm-waves in transmission and reflection.

Transmission Case

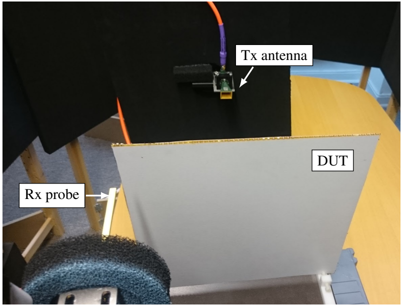

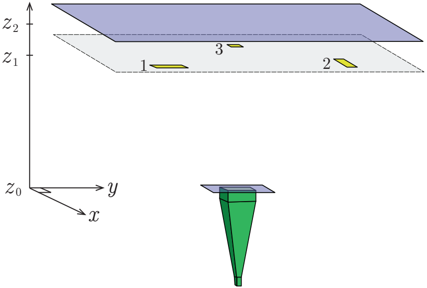

- Tx: fixed antenna illuminating the panel.
- Rx: planar near-field scan over a rectangular grid.

The received field and the field at the imaging plane are dominated by the illuminating field. Not sparse in a pixel basis and hence not suitable for CS.

(Helander et al., "Compressive Sensing Techniques for mm-Wave Nondestructive Testing of Composite Panels", 2017)

Transmission Case

How can the illuminating field be removed to produce a sparse image?

a) use measurement without the panel
b) use measurement of non-defect panel
c) simulated data from numerical model of Tx and panel
d) estimate of the illuminating field from measured data and position of Tx

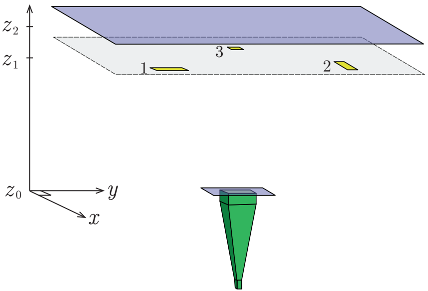

- Tx: fixed antenna illuminating the panel.
- Rx: planar near-field scan over a rectangular grid.

The received field and the field at the imaging plane are dominated by the illuminating field. Not sparse in a pixel basis and hence not suitable for CS.

(Helander et al., "Compressive Sensing Techniques for mm-Wave Nondestructive Testing of Composite Panels", 2017)

Source separation for removal of the illuminating field

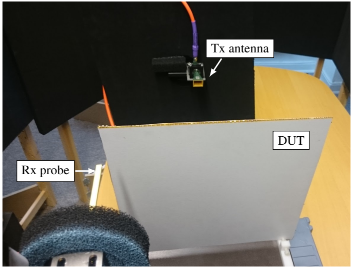

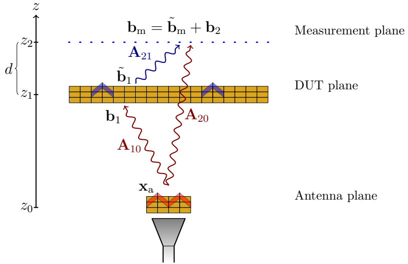

- Simplest approach based on measurements with and without the panel does not work due to strong scattering of the panel.

Source separation for removal of the illuminating field

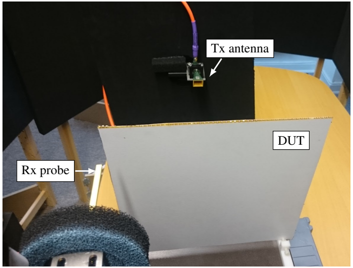

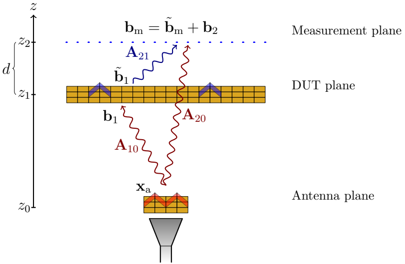

- Simplest approach based on measurements with and without the panel does not work due to strong scattering of the panel.
- Source separation: Add sources representing radiation from the Tx antenna (including transmission through the panel).

Source separation for removal of the illuminating field

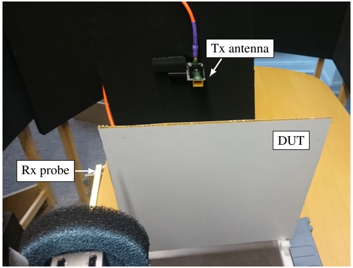

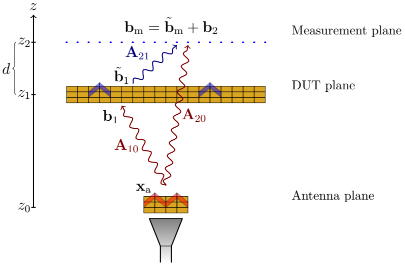

- Simplest approach based on measurements with and without the panel does not work due to strong scattering of the panel.
- Source separation: Add sources representing radiation from the Tx antenna (including transmission through the panel).
  1. Reconstruct antenna current $\mathbf{x}_\mathrm{a}$.

Source separation for removal of the illuminating field

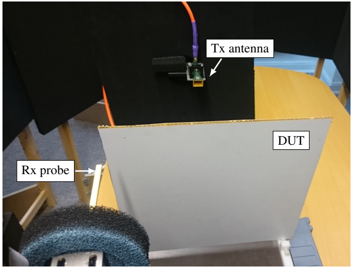

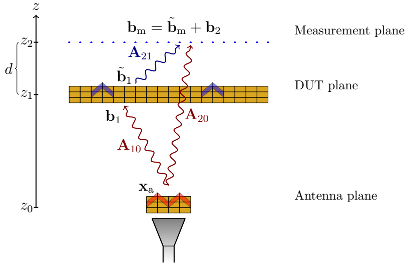

- Simplest approach based on measurements with and without the panel does not work due to strong scattering of the panel.
- Source separation: Add sources representing radiation from the Tx antenna (including transmission through the panel).
  1. Reconstruct antenna current $\mathbf{x}_\mathrm{a}$.
  2. Subtract field radiated from $\mathbf{x}_\mathrm{a}$.

Source separation for removal of the illuminating field

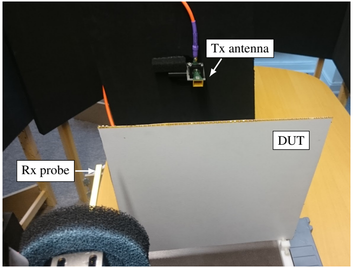

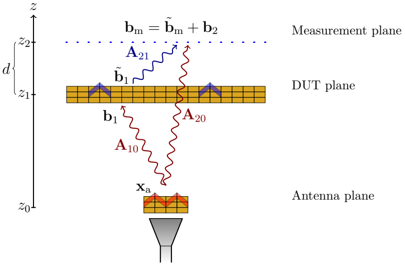

- Simplest approach based on measurements with and without the panel does not work due to strong scattering of the panel.
- Source separation: Add sources representing radiation from the Tx antenna (including transmission through the panel).
  1. Reconstruct antenna current $\mathbf{x}_{\mathrm{a}}$.
  2. Subtract field radiated from $\mathbf{x}_{\mathrm{a}}$.
  3. Reconstruct DUT current. Few defects imply sparsity in pixel bases and hence suitable for CS.

Planar scan at $60\,\mathrm{GHz}$: Synthetic data

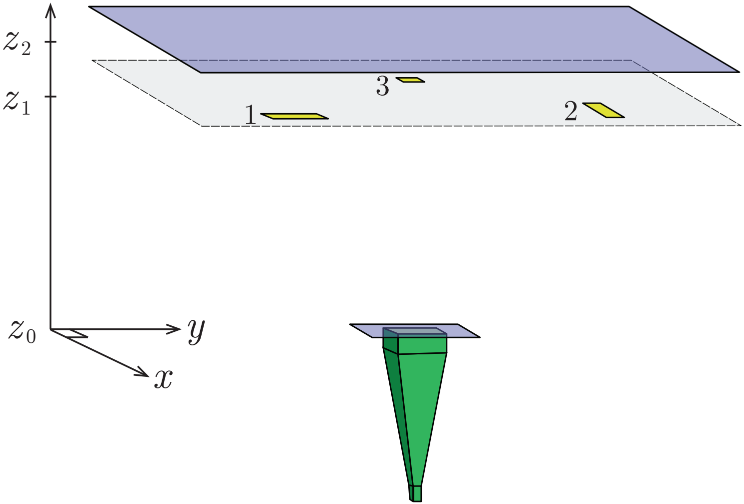

Simulation (FEKO) setup with 3 defects: side view

Planar scan at $60\,\mathrm{GHz}$: Synthetic data

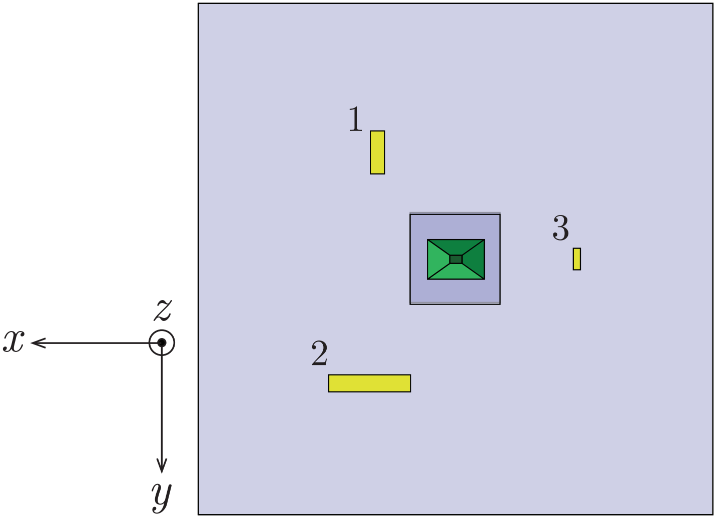

Simulation (FEKO) setup with 3 defects: top view

Planar scan at $60\,\mathrm{GHz}$: Synthetic data

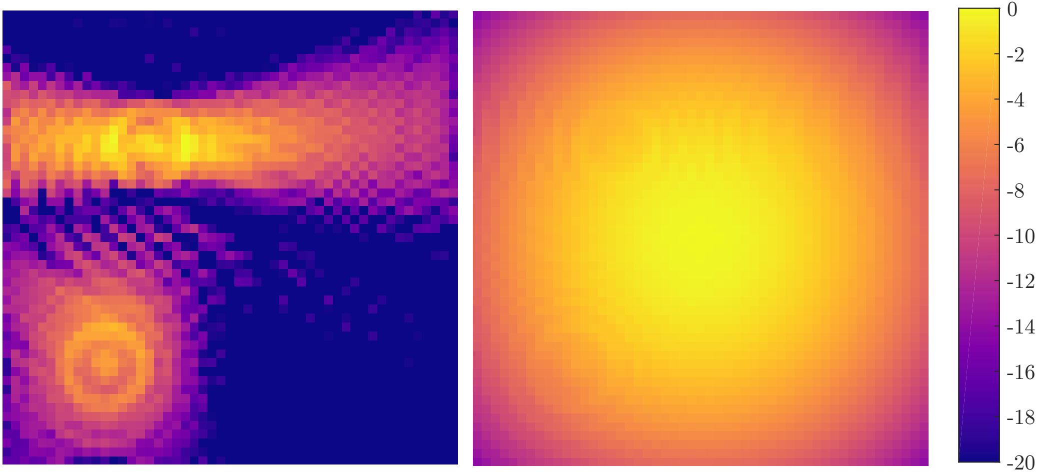

(left) scattered field (right) total field

Planar scan at $60\,\mathrm{GHz}$: Synthetic data

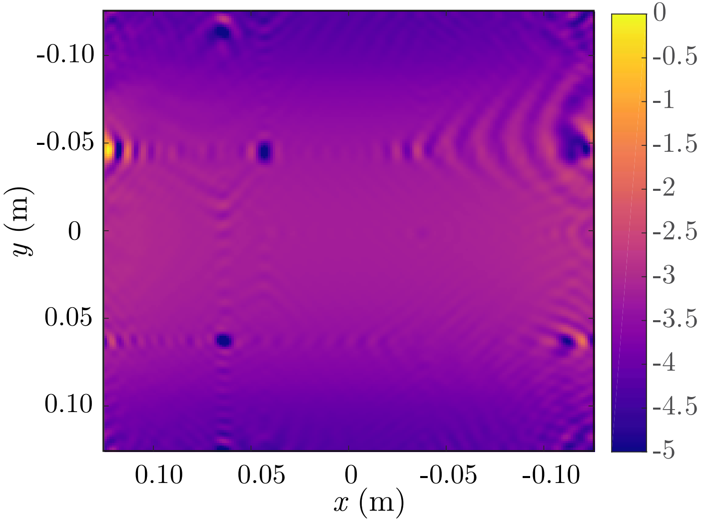

Back propagation with background subtraction. $5\,\mathrm{dB}$ range

Planar scan at $60\,\mathrm{GHz}$: Synthetic data

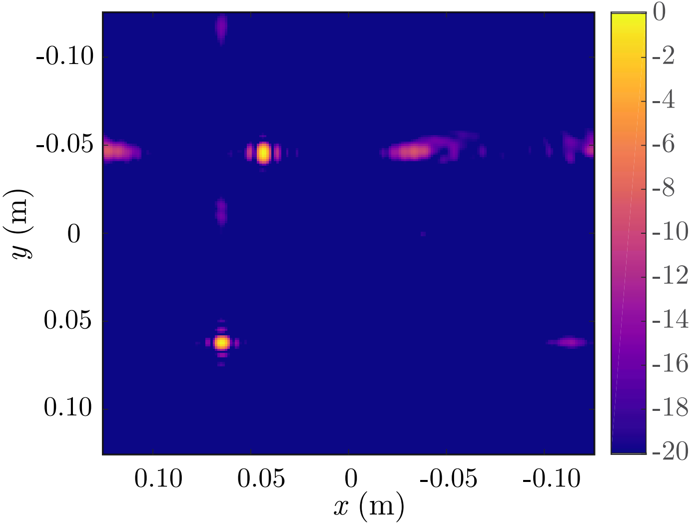

Back propagation with source separation, $20\,\mathrm{dB}$ range

Planar scan at $60\,\mathrm{GHz}$: Synthetic data

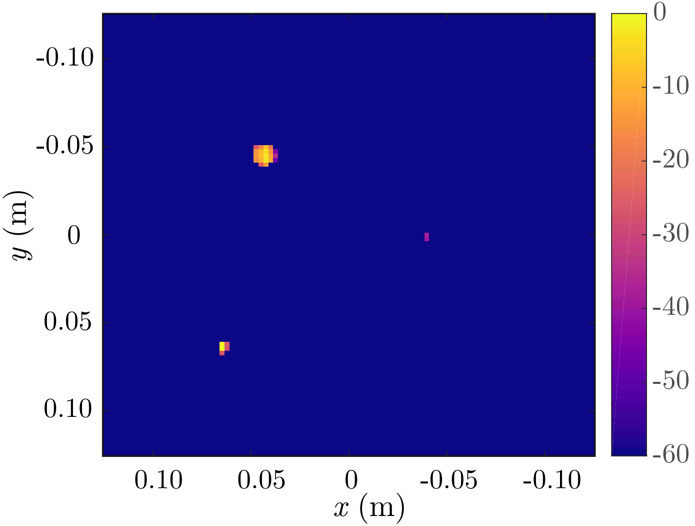

Compressive sensing with source separation, $60\,\mathrm{dB}$ range

Planar scan at $60\,\mathrm{GHz}$: Synthetic data

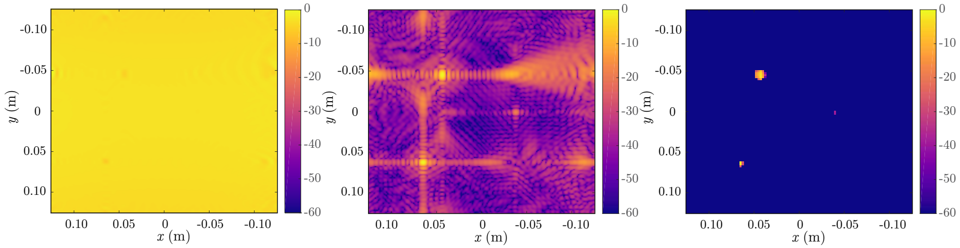

back propagation, source separation, CS

- $60\,\mathrm{dB}$ range
- back propagation dominated by scattering in panel.
- source separation removes scattering in panel.
- L^1-regularization together with source separation produce a superior image.

Planar scan at $60\,\mathrm{GHz}$ measured data

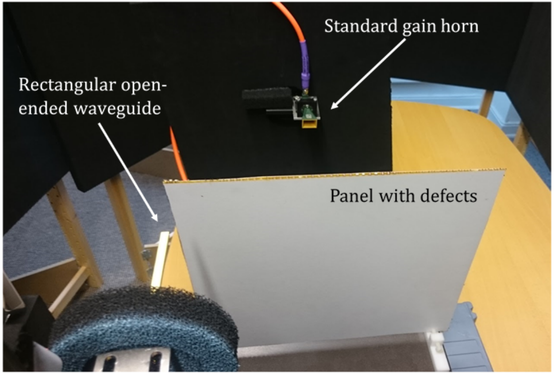

- Horn antenna (Tx) and open waveguide (Rx).
- Rx scanned over $250 \times 250\,\mathrm{mm}^2$ sampled uniformly every $5\,\mathrm{mm}$.
- $60\,\mathrm{mm}$ between Rx and DUT.

Planar scan at $60\,\mathrm{GHz}$ measured data

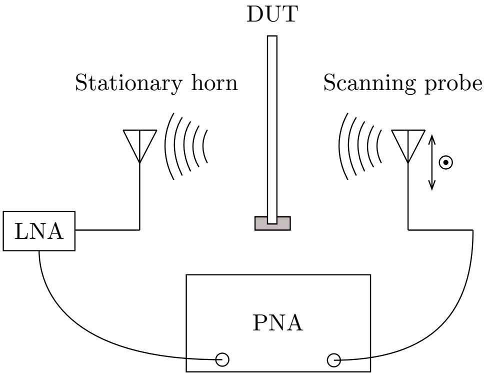

Planar scan at $60\,\mathrm{GHz}$ measured data

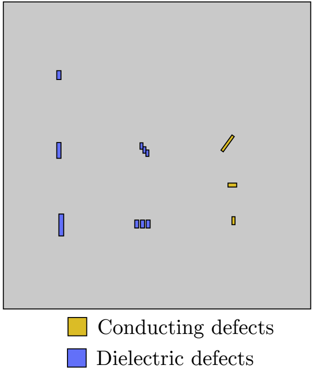

- $300 \times 300 \times 3\,\mathrm{mm}^3$ composite panel
- $2\,\mathrm{mm}$-thick low permittivity over-expanded Nomex honeycomb core sandwiched between two $0.5\,\mathrm{mm}$ sheets of TenCate EX-1515.
- Added conductive and dielectric defects inside the honeycomb core.

Planar scan at $60\,\mathrm{GHz}$ measured data

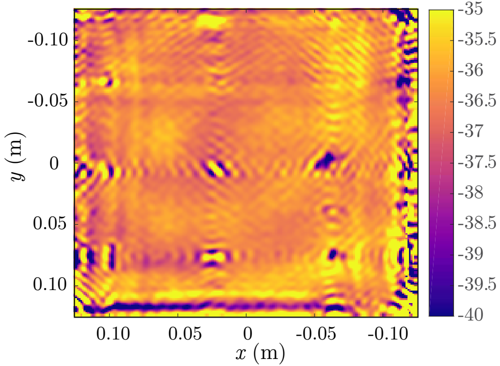

- Back propagation with background subtraction (two measurements).
- $5\,\mathrm{dB}$ range.
- Image dominated by scattering of the panel.

Planar scan at $60\,\mathrm{GHz}$ measured data

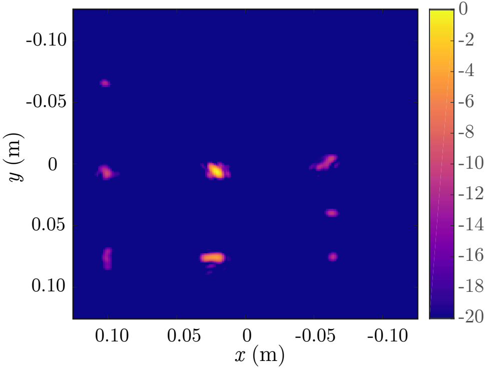

- Back propagation with source separation (one measurement).
- $20\,\mathrm{dB}$ range.
- Source separation eliminates one measurement and removes interaction with the panel.

Planar scan at $60\,\mathrm{GHz}$ measured data

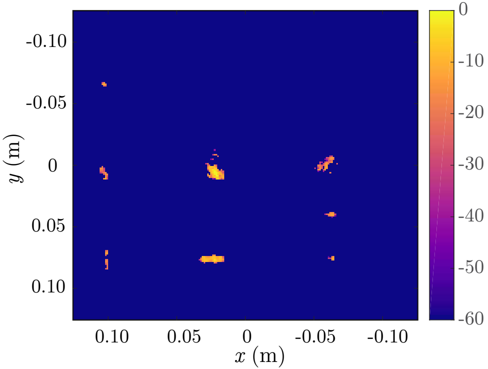

- Compressive sensing with source separation (one measurement)
- $60\,\mathrm{dB}$ range.
- L_1-regularization removes the smoothing.

Planar scan at 60 GHz measured data

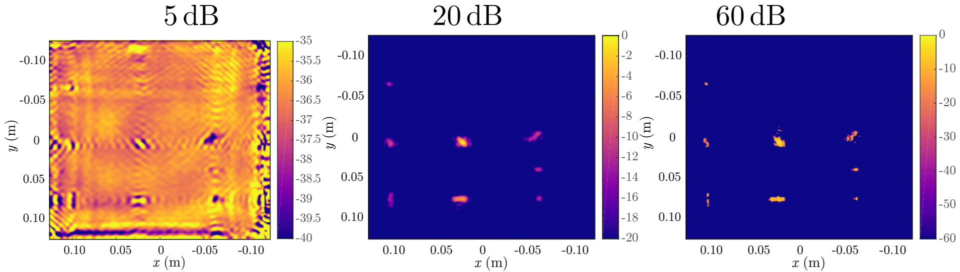

Back propagation, source separation, compressive sensing

J. Helander et al. "Compressive Sensing Techniques for mm-Wave Nondestructive Testing of Composite Panels". *IEEE Trans. Antennas Propag.* 65.10 (2017), pp. 5523–5531

Computational aspects

A $30 \times 30\,\mathrm{cm}^2$ panel at $60\,\mathrm{GHz}$ ($\lambda \approx 0.5\,\mathrm{cm}$) corresponds to $60 \times 60\lambda^2$. Discretized using $\lambda/5$ implies $N \approx 2 \times 300^2 \approx 10^5$.

The source separation compressive sensing image can often be determined in two separate steps

$$\mathbf{A}_{20}\mathbf{x}_0 \approx \mathbf{b}$$

where $\mathbf{x}_0 \in \mathbb{C}^P$ with $P \approx 100$ models the 'small' antenna aperture. Easily solved with an SVD.
The L^1 solution is determined by the optimization problem

$$\begin{aligned} \text{minimize} \quad & \|\mathbf{x}_1\|_1 \\ \text{subject to} \quad & \|\mathbf{A}_{21}\mathbf{x}_1 - \tilde{\mathbf{b}}\|_2 \leq \delta. \end{aligned}$$

This convex optimization problem is solved iteratively requiring multiple evaluations of $\mathbf{A}_{21} \in \mathbb{C}^{N,M}$ and $\mathbf{A}_{21}^{\mathsf{H}}$, where $M \approx 10^3$ (can be smaller).

Matrix-free algorithms

The computational complexity can be prohibitive for larger problems, *e.g.*, the rather coarse discretization of 100×100 unknowns corresponds to a matrix $\mathbf{A}$ with 10^8 elements. Size grows rapidly and can eventually not store the matrix explicitly but can anyway evaluate $\mathbf{Ax}$ and $\mathbf{A}^{\mathsf{H}}\mathbf{b}$ efficiently.

Often efficient to utilize (translational) symmetries and FFT based algorithms to reduce the computational complexity (Gustafsson et al., "High resolution digital transmission microscopy—a Fourier holography approach", 2004).

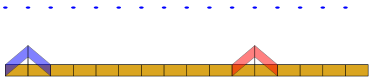

Using the same spacing for the basis functions and the data points gives a (block) Toeplitz matrix

Toeplitz matrix vector multiplication

Let $M = N$ and embed an $M \times M$ Toeplitz matrix into an $2M \times 2M$ circulant matrix such that

$$\begin{pmatrix} \mathbf{Ax} \\ \mathbf{Sx} \end{pmatrix} = \begin{pmatrix} \mathbf{A} & \mathbf{S} \\ \mathbf{S} & \mathbf{A} \end{pmatrix} \begin{pmatrix} \mathbf{x} \\ \mathbf{0} \end{pmatrix}$$

The circulant matrix $\tilde{\mathbf{A}}$ has the first row

$$\tilde{\mathbf{A}}_{1,:} = \begin{pmatrix} A_{11} & A_{21} & \cdots & A_{M1} & 0 & A_{1N} & \cdots & A_{12} \end{pmatrix}$$

Evaluate using the FFT, *i.e.*, from the first M elements of, *i.e.*,

$$\mathbf{Ax} = [\mathcal{F}^{-1}(\mathcal{F}(\tilde{\mathbf{A}}_{1,:})\mathcal{F}([\mathbf{x}\ \mathbf{0}]))]_{1:M}$$

Can reduce the dimension to $M + N - 1$

$$\tilde{\mathbf{A}}_{1,:} = \begin{pmatrix} A_{11} & A_{12} & \cdots & A_{1N} & 0 & A_{M1} & \cdots & A_{21} \end{pmatrix}$$

or $M + N + P - 1$ where $P \geq 0$ is the number of additional zeros.

Matrix-free implementation

- The translational invariance reduces memory requirements and accelerates the $\mathbf{Ax}$ multiplication ($n\log(n)$-algorithm).
- Similar approach works for 2D arrays and sub-sampling of the image.

Use anonymous functions in *e.g.*, SPGL1

```
Af = @(x,mode) Afunc(x,mode);
x = spg_bpdn(Af,b,d,opts);
```

where Afunc is a function which evaluates $\mathbf{Ax}$ and $\mathbf{A}^{\mathsf{H}}\mathbf{y}$ efficiently (chosen by mode).

Reflection Case

- Aircraft structural components often incorporate sheets of RF-impenetrable materials
- Demand for bistatic imaging systems operating in reflection rather than transmission

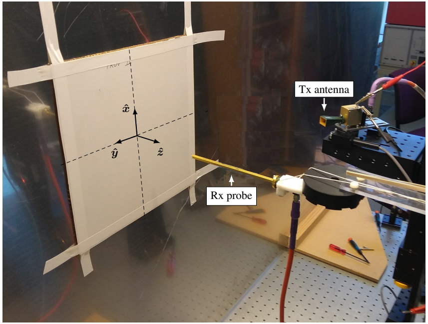

Mount the DUT on top of a ground plane to emulate/extend the underlying conducting layer

Methodology – Numerical Modeling

Experimental setup and equivalent numerical model

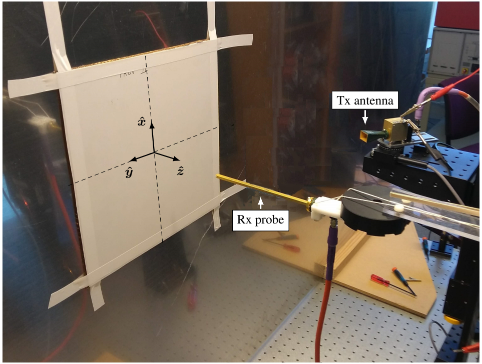

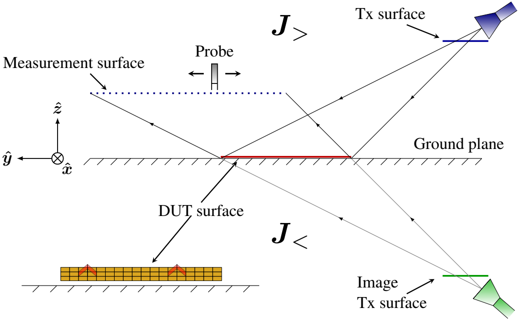

- Introduction of an image Tx surface below ground
- Discretized reconstruction surfaces (DUT, Tx and image Tx)
- User selectivity on size of the reconstruction surfaces
- Define $\mathbf{N}_{\mathrm{Tx}} = [\mathbf{N}_> \quad \mathbf{N}_<]$ and the Tx currents $\boldsymbol{J}_>$ and $\boldsymbol{J}_<$, above and below

Methodology – Source Separation

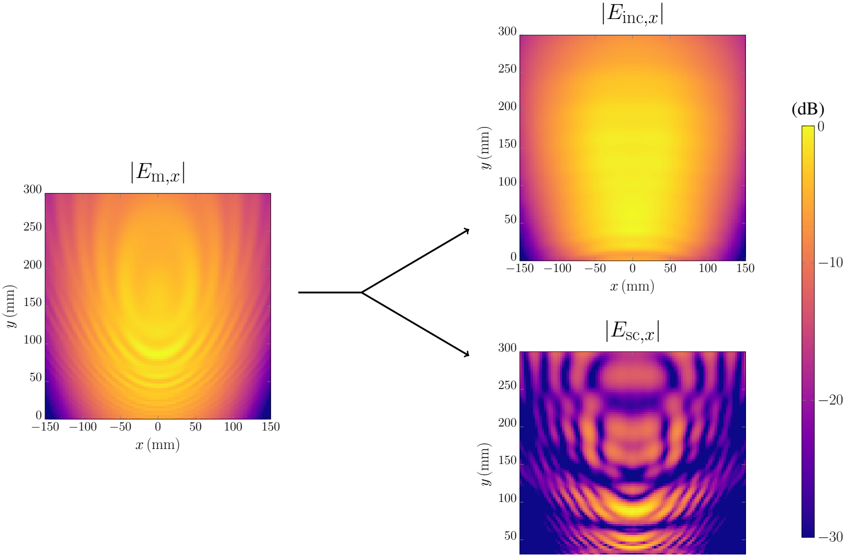

Measurements – Composite Panel

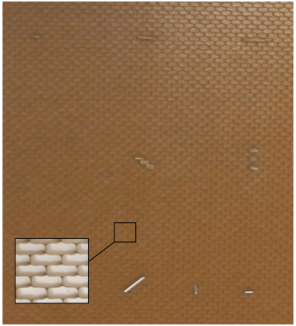

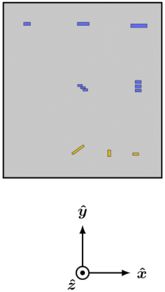

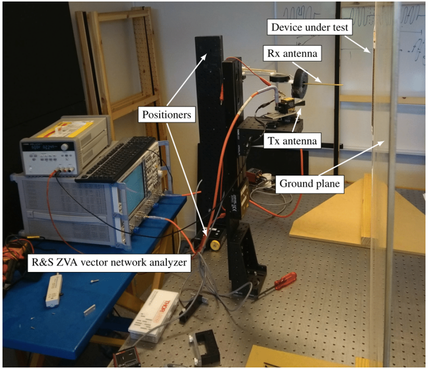

- $300\,\mathrm{mm} \times 300\,\mathrm{mm} \times 3\,\mathrm{mm}$
- Low permittivity honeycomb core
- Sheets of cyanate ester pre-preg
- Dielectric defects of assembling adhesive

- $59 - 61\,\mathrm{GHz}$
- $300\,\mathrm{mm} \times 300\,\mathrm{mm}$ measurement surface with spacing $\Delta = 3\,\mathrm{mm} \approx 3\lambda/5$
- Single TE-polarized measurement

Composite Panel – $200\,\mathrm{mm} \times 200\,\mathrm{mm}$

A $300\,\mathrm{mm} \times 300\,\mathrm{mm}$ measurement surface captures the specular reflection of a $200\,\mathrm{mm} \times 200\,\mathrm{mm}$ area of the DUT surface

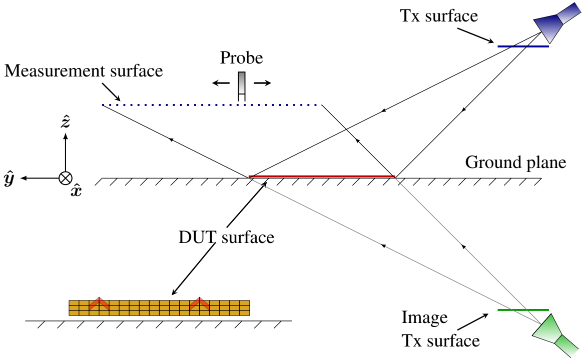

Composite Panel – $200\,\text{mm} \times 200\,\text{mm}$, $30\,\text{dB}$

A $300\,\text{mm} \times 300\,\text{mm}$ measurement surface captures the specular reflection of a $200\,\text{mm} \times 200\,\text{mm}$ area of the DUT surface

Phase conjugation

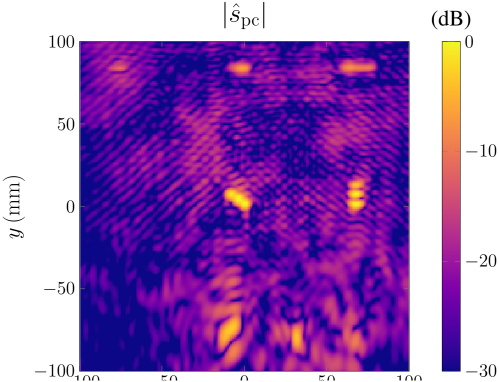

L_1-minimization

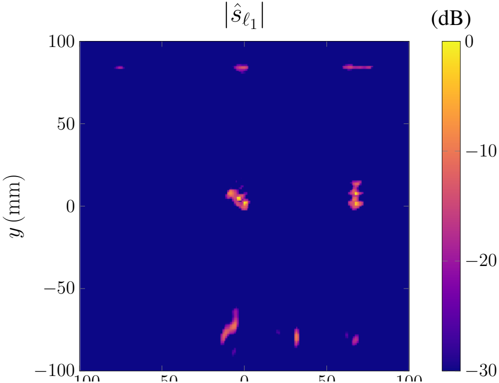

Composite Panel – $350\,\mathrm{mm} \times 350\,\mathrm{mm}$

If there's any ambiguity in how to select the DUT reconstruction surface, filtering can remove undesirable scatterers (edge diffraction)

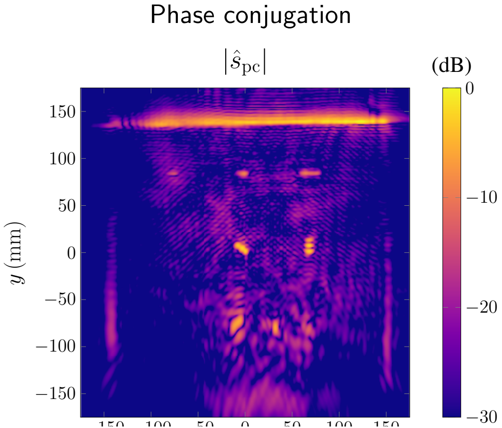

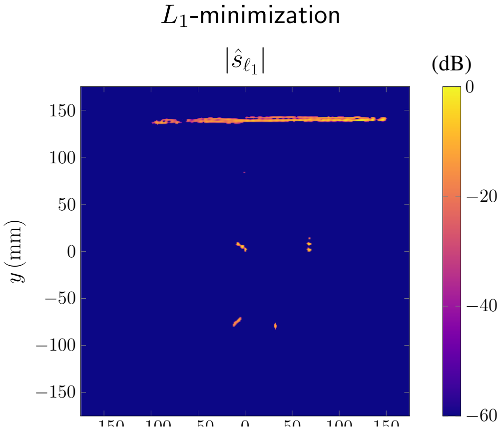

Composite Panel – $350\,\mathrm{mm} \times 350\,\mathrm{mm}$

If there's any ambiguity in how to select the DUT reconstruction surface, filtering can remove undesirable scatterers (edge diffraction)

Phase conjugation

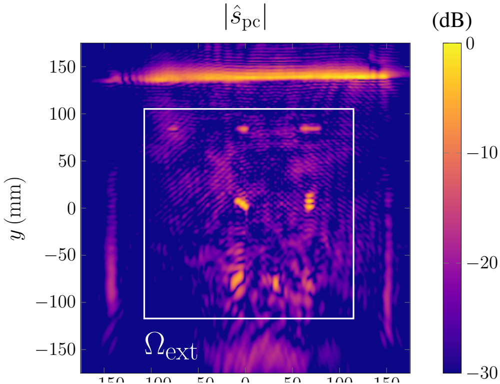

L_1-minimization

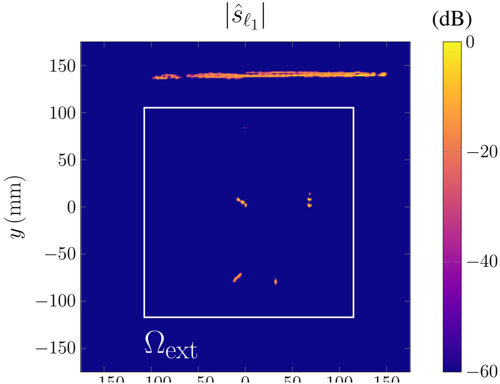

Composite Panel – $350\,\mathrm{mm} \times 350\,\mathrm{mm}$

If there's any ambiguity in how to select the DUT reconstruction surface, filtering can remove undesirable scatterers (edge diffraction)

Phase conjugation

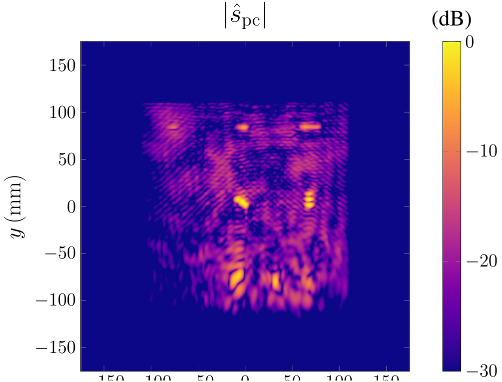

L_1-minimization

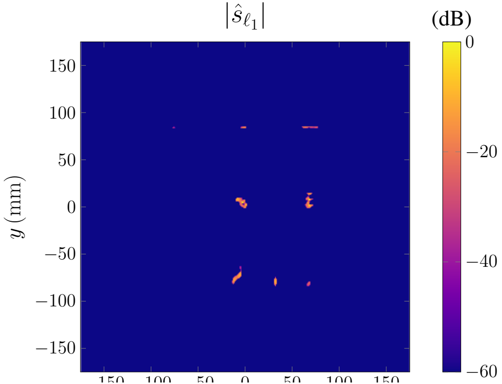

Outline

QCQP and convexity

- quadratic form $\|\boldsymbol{\Upsilon}\mathbf{I}\|_2^2 = \mathbf{I}^{\mathsf{H}}\boldsymbol{\Upsilon}^{\mathsf{H}}\boldsymbol{\Upsilon}\mathbf{I}$ often representing energy or power quantities

QCQP and convexity

- quadratic form $\|\mathbf{\Upsilon I}\|_2^2 = \mathbf{I}^\mathsf{H}\mathbf{\Upsilon}^\mathsf{H}\mathbf{\Upsilon I}$ often representing energy or power quantities
- Gramian matrix $\mathbf{\Psi} = \mathbf{\Upsilon}^\mathsf{H}\mathbf{\Upsilon}$ with elements

$$\mathbf{\Psi}_{mn} = \int_{\Omega} \boldsymbol{\psi}_m(\boldsymbol{r}) \cdot \boldsymbol{\psi}_n(\boldsymbol{r})\,\mathrm{dV}$$

  decrease mesh dependence and links $\|\mathbf{\Upsilon I}\|_2^2$ to power dissipated as material losses

QCQP and convexity

- quadratic form $\|\boldsymbol{\Upsilon}\mathbf{I}\|_2^2 = \mathbf{I}^{\mathrm{H}}\boldsymbol{\Upsilon}^{\mathrm{H}}\boldsymbol{\Upsilon}\mathbf{I}$ often representing energy or power quantities
- Gramian matrix $\boldsymbol{\Psi} = \boldsymbol{\Upsilon}^{\mathrm{H}}\boldsymbol{\Upsilon}$ with elements

$$\boldsymbol{\Psi}_{mn} = \int_{\Omega} \boldsymbol{\psi}_m(\boldsymbol{r}) \cdot \boldsymbol{\psi}_n(\boldsymbol{r}) \, \mathrm{dV}$$

  decrease mesh dependence and links $\|\boldsymbol{\Upsilon}\mathbf{I}\|_2^2$ to power dissipated as material losses
- quadratically constrained quadratic program (QCQP)

$$\begin{aligned} \text{minimize} \quad & \|\boldsymbol{\Upsilon}\mathbf{I}\|_2^2 = \mathbf{I}^{\mathrm{H}}\boldsymbol{\Psi}\mathbf{I} \\ \text{subject to} \quad & \|\mathbf{F}\mathbf{I} - \mathbf{F}_0\|_2^2 \leq \delta, \end{aligned}$$

  as finding the current density, represented by $\mathbf{I}$, in a region Ω with a prescribed radiated field and minimal losses (assuming homogeneous material parameters).

QCQP and convexity

- quadratic form $\|\boldsymbol{\Upsilon}\mathbf{I}\|_2^2 = \mathbf{I}^{\mathsf{H}}\boldsymbol{\Upsilon}^{\mathsf{H}}\boldsymbol{\Upsilon}\mathbf{I}$ often representing energy or power quantities
- Gramian matrix $\boldsymbol{\Psi} = \boldsymbol{\Upsilon}^{\mathsf{H}}\boldsymbol{\Upsilon}$ with elements

$$\boldsymbol{\Psi}_{mn} = \int_{\Omega} \boldsymbol{\psi}_m(\boldsymbol{r}) \cdot \boldsymbol{\psi}_n(\boldsymbol{r}) \, \mathrm{dV}$$

  decrease mesh dependence and links $\|\boldsymbol{\Upsilon}\mathbf{I}\|_2^2$ to power dissipated as material losses
- quadratically constrained quadratic program (QCQP)

$$\begin{aligned} &\text{minimize} && \|\boldsymbol{\Upsilon}\mathbf{I}\|_2^2 = \mathbf{I}^{\mathsf{H}}\boldsymbol{\Psi}\mathbf{I} \\ &\text{subject to} && \mathbf{I}^{\mathsf{H}}\mathbf{F}^{\mathsf{H}}\mathbf{F}\mathbf{I} - 2\,\mathrm{Re}\{\mathbf{I}^{\mathsf{H}}\mathbf{F}^{\mathsf{H}}\mathbf{F}_0\} + \mathbf{F}_0^{\mathsf{H}}\mathbf{F}_0 \leq \delta, \end{aligned}$$

  as finding the current density, represented by $\mathbf{I}$, in a region Ω with a prescribed radiated field and minimal losses (assuming homogeneous material parameters).

QCQP and convexity

- quadratic form $\|\boldsymbol{\Upsilon}\mathbf{I}\|_2^2 = \mathbf{I}^{\mathsf{H}}\boldsymbol{\Upsilon}^{\mathsf{H}}\boldsymbol{\Upsilon}\mathbf{I}$ often representing energy or power quantities
- Gramian matrix $\boldsymbol{\Psi} = \boldsymbol{\Upsilon}^{\mathsf{H}}\boldsymbol{\Upsilon}$ with elements

$$\boldsymbol{\Psi}_{mn} = \int_{\Omega} \boldsymbol{\psi}_m(\boldsymbol{r}) \cdot \boldsymbol{\psi}_n(\boldsymbol{r}) \,\mathrm{dV}$$

  decrease mesh dependence and links $\|\boldsymbol{\Upsilon}\mathbf{I}\|_2^2$ to power dissipated as material losses
- quadratically constrained quadratic program (QCQP)

$$\begin{aligned} &\text{minimize} && \|\boldsymbol{\Upsilon}\mathbf{I}\|_2^2 = \mathbf{I}^{\mathsf{H}}\boldsymbol{\Psi}\mathbf{I} \\ &\text{subject to} && \mathbf{I}^{\mathsf{H}}\mathbf{F}^{\mathsf{H}}\mathbf{F}\mathbf{I} - 2\,\mathrm{Re}\{\mathbf{I}^{\mathsf{H}}\mathbf{F}^{\mathsf{H}}\mathbf{F}_0\} + \mathbf{F}_0^{\mathsf{H}}\mathbf{F}_0 \leq \delta, \end{aligned}$$

  as finding the current density, represented by $\mathbf{I}$, in a region Ω with a prescribed radiated field and minimal losses (assuming homogeneous material parameters).

A convex QCQP similar to problems of determining physical bounds (or fundamental limits) on antennas Gustafsson and Nordebo, "Optimal Antenna Currents for Q, Superdirectivity, and Radiation Patterns Using Convex Optimization", 2013 or scatterers Gustafsson et al., "Upper bounds on absorption and scattering", 2020.

Inverse source problem and physical bounds

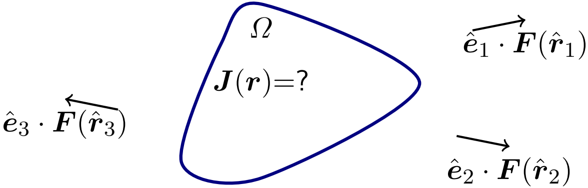

Inverse source problem

- Determine a current distribution $\boldsymbol{J}(\boldsymbol{r})$ producing a field $\hat{\boldsymbol{e}}_n \cdot \boldsymbol{F}(\hat{\boldsymbol{r}}_n)$

Physical bounds

Inverse source problem and physical bounds

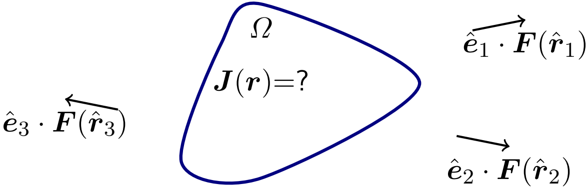

Inverse source problem

- Determine a current distribution $\boldsymbol{J}(\boldsymbol{r})$ producing a field $\hat{\boldsymbol{e}}_n \cdot \boldsymbol{F}(\hat{\boldsymbol{r}}_n)$
- Non unique $\boldsymbol{J}(\boldsymbol{r})$

Physical bounds

Inverse source problem and physical bounds

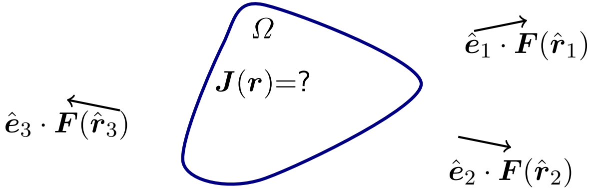

Inverse source problem

- Determine a current distribution $\boldsymbol{J}(\boldsymbol{r})$ producing a field $\hat{\boldsymbol{e}}_n \cdot \boldsymbol{F}(\hat{\boldsymbol{r}}_n)$
- Non unique $\boldsymbol{J}(\boldsymbol{r})$
- Regularization for a unique and nice solution

Physical bounds

Inverse source problem and physical bounds

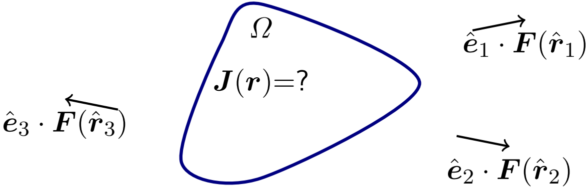

Inverse source problem

- Determine a current distribution $\boldsymbol{J}(\boldsymbol{r})$ producing a field $\hat{\boldsymbol{e}}_n \cdot \boldsymbol{F}(\hat{\boldsymbol{r}}_n)$
- Non unique $\boldsymbol{J}(\boldsymbol{r})$
- Regularization for a unique and nice solution

Physical bounds

- Determine an optimal current distribution $\boldsymbol{J}(\boldsymbol{r})$ producing the field $\hat{\boldsymbol{e}}_n \cdot \boldsymbol{F}(\hat{\boldsymbol{r}}_n)$

Inverse source problem and physical bounds

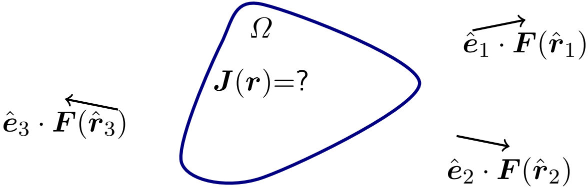

Inverse source problem

- Determine a current distribution $\boldsymbol{J}(\boldsymbol{r})$ producing a field $\hat{\boldsymbol{e}}_n \cdot \boldsymbol{F}(\hat{\boldsymbol{r}}_n)$
- Non unique $\boldsymbol{J}(\boldsymbol{r})$
- Regularization for a unique and nice solution

Physical bounds

- Determine an optimal current distribution $\boldsymbol{J}(\boldsymbol{r})$ producing the field $\hat{\boldsymbol{e}}_n \cdot \boldsymbol{F}(\hat{\boldsymbol{r}}_n)$
- Optimal in *e.g.*, minimum losses (efficiency) or minimum stored energy (Q-factor and bandwidth)

Inverse source problem and physical bounds

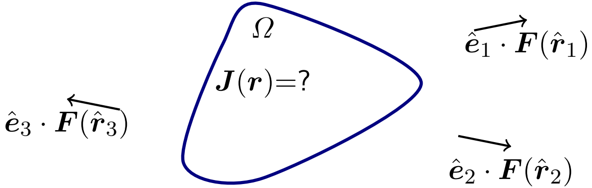

Inverse source problem

- Determine a current distribution $\boldsymbol{J}(\boldsymbol{r})$ producing a field $\hat{\boldsymbol{e}}_n \cdot \boldsymbol{F}(\hat{\boldsymbol{r}}_n)$
- Non unique $\boldsymbol{J}(\boldsymbol{r})$
- Regularization for a unique and nice solution

Physical bounds

- Determine an optimal current distribution $\boldsymbol{J}(\boldsymbol{r})$ producing the field $\hat{\boldsymbol{e}}_n \cdot \boldsymbol{F}(\hat{\boldsymbol{r}}_n)$
- Optimal in *e.g.*, minimum losses (efficiency) or minimum stored energy (Q-factor and bandwidth)

Regularizing with Gramian ($\boldsymbol{\Psi}$) is equivalent to determine physical bounds (optimal currents) for minimum losses. What about using quantities (stored energy)?

Acknowledgments

- The Swedish Research Council
- Sweden's innovation agency (VINNOVA)
- Swedish Foundation for Strategic Research (SSF)

Vetenskapsrådet

Swedish Foundation *for* Strategic Research

Collaboration with:

- Johan Lundgren, post doc LU
- Jakob Helander, PhD 2019 from LU
- Kristin Persson, PhD 2013 from LU
- Daniel Sjöberg, Gerhard Kristensson, LU
- Björn Widenberg, Christer Larsson, Torleif Martin, SAAB

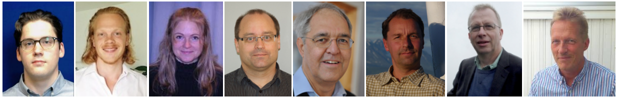

Outline

Non-destructive testing and inverse source problems

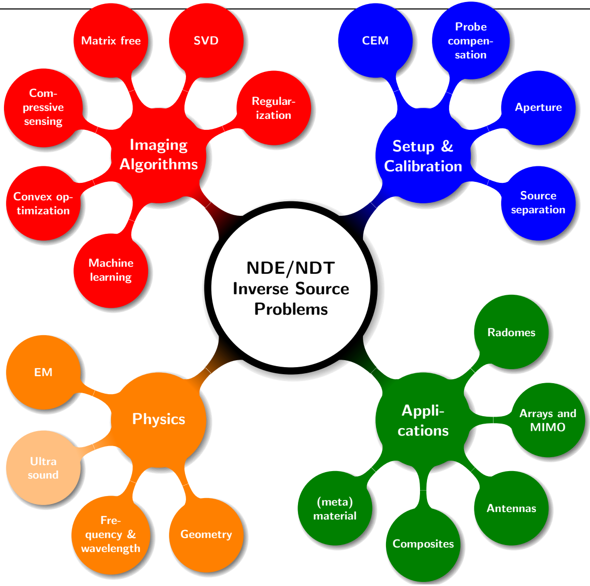

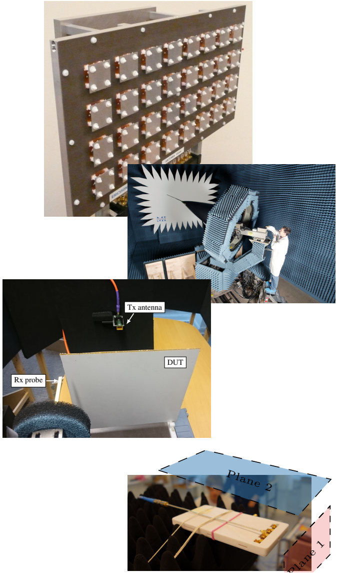

Summary

- Imaging of equivalent currents can localize defects
- Integral equations/representations for modeling
- Non-destructive testing of radomes, antennas, composite panels, EMF exposure, measurement data post processing
- Source separation to remove unwanted illumination
- L^1-norm and compressive sensing for imaging of sparse defects
- Much research remains for understanding of algorithms, regularization, and imaging quality

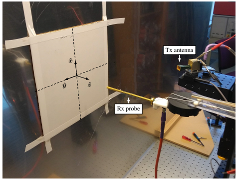

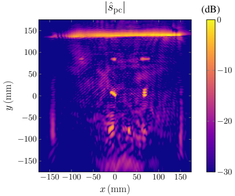

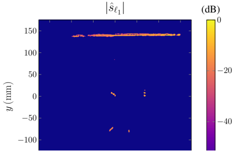

Results in this presentation mainly based on:

- J. Lundgren *etal*, 'A Near-Field Measurement and Calibration Technique –Radio-frequency electromagnetic field exposure assessment of millimeter-wave 5G devices', IEEE-APM 2021
- J. Helander *etal*, 'Reflection-Based Source Inversion for Sparse Imaging of Low-Loss Composite Panels', IEEE-TAP 2020
- J. Helander *etal*, 'Compressive Sensing Techniques for mm-Wave Nondestructive Testing of Composite Panels', IEEE-TAP 2017
- K. Persson *etal*, 'Radome Diagnostics—Source Reconstruction of Phase Objects With an Equivalent Currents Approach', IEEE-TAP 2014
- K. Persson and M. Gustafsson, 'Reconstruction of equivalent currents using a near-field data transformation-with radome applications', PIERS 2005

Some references I

[1] M. A. Abou-Khousa et al. "Comparison of X-Ray, Millimeter Wave, Shearography and Through-Transmission Ultrasonic Methods for Inspection of Honeycomb Composites". In: *AIP Conference Proceedings*. Vol. 894. 1. AIP. 2007, pp. 999–1006.

[2] S. S. Ahmed et al. "Advanced Microwave imaging". *IEEE Microw. Mag.* 13.6 (2012), pp. 26–43.

[3] J. L. A. Araque Quijano et al. "Suppression of undesired radiated fields based on equivalent currents reconstruction from measured data". *Antennas and Wireless Propagation Letters, IEEE* 10 (2011), pp. 314–317.

[4] N. Bleistein and J. K. Cohen. "Non-uniqueness in the inverse source problem in acoustics and electromagnetics". *J. Math. Phys.* 18.2 (1977), pp. 194–201.

[5] J. Blitz. *Electrical and Magnetic Methods of Non-Destructive Testing*. Vol. 3. Springer Science & Business Media, 2012.

[6] S. P. Boyd and L. Vandenberghe. *Convex Optimization*. Cambridge Univ. Pr., 2004.

[7] A. J. Devaney. *Mathematical foundations of imaging, tomography and wavefield inversion*. Cambridge University Press, 2012.

[8] T. F. Eibert and C. H. Schmidt. "Multilevel fast multipole accelerated inverse equivalent current method employing Rao-Wilton-Glisson discretization of electric and magnetic surface currents". *IEEE Trans. Antennas Propag.* 57.4 (2009), pp. 1178–1185.

[9] L. J. Foged et al. "Practical application of the equivalent source method as an antenna diagnostics tool". *IEEE Antennas Propag. Mag.* 54.5 (2012), pp. 243–249.

[10] M. Gustafsson and S. Nordebo. "Optimal Antenna Currents for Q, Superdirectivity, and Radiation Patterns Using Convex Optimization". *IEEE Trans. Antennas Propag.* 61.3 (2013), pp. 1109–1118.

[11] M. Gustafsson et al. "High resolution digital transmission microscopy—a Fourier holography approach". *Optics and Lasers in Engineering* 41.3 (2004), pp. 553–563.

[12] M. Gustafsson et al. "Upper bounds on absorption and scattering". *New Journal of Physics* 22.073013 (2020).

[13] J. E. Hansen, ed. *Spherical Near-Field Antenna Measurements*. IEE electromagnetic waves series 26. Peter Peregrinus Ltd., 1988.

[14] P. C. Hansen. *Discrete inverse problems: insight and algorithms*. Vol. 7. Society for Industrial & Applied Mathematics, 2010.

[15] J. Helander et al. "Compressive Sensing Techniques for mm-Wave Nondestructive Testing of Composite Panels". *IEEE Trans. Antennas Propag.* 65.10 (2017), pp. 5523–5531.

[16] J. Helander et al. *Reflection-Based Inverse Scattering for Sparse Image Reconstruction*. 2019.

[17] J. Helander et al. "Reflection-Based Source Inversion for Sparse Imaging of Low-Loss Composite Panels". *IEEE Trans. Antennas Propag.* 68.6 (2020), pp. 4860–4870.

Some references II

[18] E. Jörgensen et al. "Antenna diagnostics on planar arrays using a 3D source reconstruction technique and spherical Near-Field measurements". In: *Antennas and Propagation (EUCAP), Proceedings of the 6th European Conference on*. IEEE. 2012, pp. 2547–2550.

[19] S. M. Kay. *Fundamentals of Statistical Signal Processing, Estimation Theory*. Prentice-Hall, Inc., 1993.

[20] S. Kharkovsky and R. Zoughi. "Microwave and Millimeter Wave Nondestructive Testing and Evaluation - Overview and Recent Advances". *IEEE Instrum. Meas. Mag.* 10.2 (2007), pp. 26–38.

[21] F. Las-Heras et al. "Evaluating near-field radiation patterns of commercial antennas". *IEEE Trans. Antennas Propag.* 54.8 (2006), pp. 2198–2207.

[22] J. Lundgren et al. "A near-field measurement and calibration technique: Radio-frequency electromagnetic field exposure assessment of millimeter-wave 5G devices". *IEEE Antennas Propag. Mag.* 63.3 (2021), pp. 77–88.

[23] A. Massa, P. Rocca, and G. Oliveri. "Compressive Sensing in Electromagnetics-A Review". *IEEE Antennas Propag. Mag.* 57.1 (2015), pp. 224–238.

[24] G. Oliveri et al. "Compressive Sensing as Applied to Inverse Problems for Imaging: Theory, applications, current trends, and open challenges." *IEEE Antennas and Propagation Magazine* 59.5 (2017), pp. 34–46.

[25] K. Persson and M. Gustafsson. "Reconstruction of equivalent currents using a near-field data transformation – with radome applications". *Prog. Electromagn. Res.* 54 (2005), pp. 179–198.

[26] K. Persson et al. "Radome diagnostics — source reconstruction of phase objects with an equivalent currents approach". *IEEE Trans. Antennas Propag.* 62.4 (2014).

[27] K. Persson et al. "Source reconstruction by far-field data for imaging of defects in frequency selective radomes". *IEEE Antennas and Wireless Propagation Letters* 12 (2013), pp. 480–483.

[28] Y. Rahmat-Samii. "Surface diagnosis of large reflector antennas using microwave holographic metrology: an iterative approach". *Radio Sci.* 19.5 (1984), pp. 1205–1217.

[29] Y. Rahmat-Samii, L. I. Williams, and R. G. Yaccarino. "The UCLA Bi-Polar Planar-Near-Field Antenna-Measurement and Diagnostics Range". *IEEE Antennas Propag. Mag.* 37.6 (1995), pp. 16–35.

[30] A. Taaghol and T. K. Sarkar. "Near-Field to Near/Far-Field Transformation for Arbitrary Near-Field Geometry, Utilizing an Equivalent Magnetic Current". *IEEE Trans. Electromagn. Compat.* 38.3 (1996), pp. 536–542.

[31] A. Tarantola. *Inverse problem theory and methods for model parameter estimation*. Society for Industrial and Applied Mathematics, 2005.

Some references III

[32] A. D. Yaghjian. "An Overview of Near-Field Antenna Measurements". *IEEE Trans. Antennas Propag.* 34.1 (1986), pp. 30–45.

[33] R. Zoughi. *Microwave Non-Destructive Testing and Evaluation Principles*. Vol. 4. Springer Science & Business Media, 2000.